5-2015

Synthesis and Morphology of Well-Defined Mixed Homopolymer Brushes Grafted on 150 - 180 nm Silica Particles

Chunhui Bao
University of Tennessee - Knoxville, cbao@vols.utk.edu

To the Graduate Council:

I am submitting herewith a dissertation written by Chunhui Bao entitled "Synthesis and Morphology of Well-Defined Mixed Homopolymer Brushes Grafted on 150 - 180 nm Silica Particles." I have examined the final electronic copy of this dissertation for form and content and recommend that it be accepted in partial fulfillment of the requirements for the degree of Doctor of Philosophy, with a major in Chemistry.

Bin Zhao, Major Professor

We have read this dissertation and recommend its acceptance:

Jimmy Mays, Michael Best, Shanfeng Wang

Accepted for the Council:

Carolyn R. Hodges

Vice Provost and Dean of the Graduate School

(Original signatures are on file with official student records.)

Synthesis and Morphology of Well-Defined Mixed Homopolymer Brushes Grafted on 150 – 180 nm Silica Particles

A Dissertation Presented for the

Doctor of Philosophy

Degree

The University of Tennessee, Knoxville

Chunhui Bao

May 2015

Acknowledgements

The very first person I would sincerely thank is my advisor Professor Bin Zhao for his patient instructions and guidance. The most important thing I have learned during my PhD training is to learn how to work efficiently, how to organize your time wisely, and how to think critically. The lessons I learned from Prof. Zhao would be priceless treasures and will be with me for my future career.

I would like to thank Professor Jimmy Mays, Professor Michael Best, and Professor Shanfeng Wang to serve on my committee. They have given me valuable suggestions and comments on my PhD research. I greatly appreciate and value all the time they have spent with me and all the help they gave to me.

I would also greatly thank our collaborators, Professor Lei Zhu and Saide Tang from Department of Macromolecular Science and Engineering, Case Western Reserve University for all the critical help and comments on the mixed homopolymer brush project. Without their efforts and contributions, this research project may have not gone this far. Many gratitudes would also go to Professor Sheng Dai and Chengcheng Tian for the collaboration on the project of poly(4-vinylbenzenesulfonic acid) brush catalyst for the dehydration of fructose to 5-hydroxymethylfurfural in water.

I greatly thank the National Science Foundation and the Department of Chemistry at University of Tennessee Knoxville for providing funding during my five years in graduate school. I would greatly appreciate all the training that Tom Malmgren offered to me in Polymer Characterization Lab and electron microscopy training from Dr. John Dunlap.

I always feel lucky to be a member in a nice and friendly family of the Zhao research group. Many thanks go to Dr. Thomas G. O'Lenick, Dr. Jeremiah W. Woodcock, Dr. Jonathan M.

Horton, Dr. Naixiong Jin, Roger Wright, Daniel Henn, Bin Hu, Dr. Weikun Li, Dr. Wenchan Jiang, and Sisi Jiang. I greatly appreciate all the kind help and advice especially the friendship we have built up in the past five years, which will be a valuable treasure in my whole life.

I owe a huge debt for my father Guangfeng Bao and my mother Wei Huang for their encouragement, help and supporting every day in the last five years even though they are thousands of miles away. I will always remember to be a good chemist and most importantly be a good son as well.

Abstract

Mixed homopolymer brushes, composed of two distinct homopolymers randomly or alternatively immobilized by one end on a solid substrate, exhibit intriguing phase behavior. This dissertation work focuses on synthesis and morphology study of well-defined mixed brushes grafted on 150 – 180 nm silica particles. The brushes were grown from asymmetric difunctional initiator (Y-initiator)-functionalized silica particles by using two "living"/controlled polymerization techniques.

Chapter 1 is an introduction to mixed brushes. Chapter 2 presents a study on the effect of overall grafting density ($\sigma_{overall}$) [Sigma overall] on morphology of mixed poly(*tert*-butyl acrylate) (P*t*BA)/polystyrene brushes synthesized by sequential surface-initiated atom transfer radical polymerization of *t*BA and nitroxide-mediated radical polymerization (NMRP) of styrene from Y-initiator-functionalized particles. By changing the mass ratio of Y-initiator to silica particles in the initiator immobilization step, a series of brush samples with different $\sigma_{overall}$ values but similar molecular weights (MW) were synthesized. Transmission electron microscopy showed that at $\sigma_{overall} \geq 0.34$ chains/nm^2 [chains/nanometer square], the brushes formed "rippled" structures after cast from chloroform. The normalized ripple wavelength (*D*) scaled with $\sigma_{overall}^{-0.47}$ [sigma overall to the -0.47 power] in the $\sigma_{overall}$ range of 1.06 to 0.54 chains/nm^2.

Chapter 3 describes a study on the effect of MW on morphology of mixed P*t*BA/PS brushes on silica particles. A series of samples with different average MWs, from 13.8 to 33.1 kDa, but comparable $\sigma_{overall}$ were made and their morphologies were investigated. For samples cast from chloroform, *D* scaled with $MW^{0.70}$ [MW to the 0.7 power] in the studied MW range. For uniformly collapsed mixed brushes cast from water, *D* was proportional to $MW^{0.56}$ [MW to the 0.56 power].

Chapter 4 presents the synthesis of mixed brushes from Y-initiator-functionalized silica particles by surface-initiated ring-opening polymerization and NMRP. The $\sigma_{overall}$ of mixed brushes can be tuned by varying the mass ratio of Y-initiator to silica particles in the initiator immobilization step. Chapter 5 describes the synthesis of two polymer brush acid catalysts and their applications for fructose dehydration to 5-hydroxymethylfurfural in water. Both brush catalysts exhibited a higher catalytic activity than the corresponding free polymer catalysts. Chapter 6 presents conclusions and future work.

Table of Contents

List of Tables

List of Figures

List of Schemes

List of Abbreviations

AFM: Atomic force microscopy

AuNPs: Gold nanoparticles

AIBN: 2,2'-Azobis(2-methylpropionitrile)

ATRP: Atom transfer radical polymerization

CTA: Chain transfer agent

CTAB: Cetyltrimethylammonium bromide

DEAEMA: 2-(diethylamino)ethyl methacrylate

DMF: *N*,*N*-Dimethylformamide

DLS: Dynamic light scattering

DP: Degree of polymerization

DSC: Differential scattering calorimetry

EBiB: Ethyl 2-bromoisobutyrate

GPC: Gel permeation chromatography

HMF: 5-hydroxymethylfurfural

HPMA: *N*-(2-hydroxypropyl) acrylamide

HPLC: High performance liquid chromatography

^{1}H NMR: Proton nuclear magnetic resonance spectroscopy

IP: Initiator particles

^{13}C NMR: Carbon-13 nuclear magnetic resonance spectroscopy

kDa: kilodaltons

LCST: Lower critical solution temperature

MW: Molecular weight

M_n: Number average molecular weight

NMRP: Nitroxide-mediated radical polymerization

NPs: Nanoparticles

PAA: Poly(acrylic acid)

PCL: Poly(ε-caprolactone)

PDI: Polydispersity index

PMDETA: *N*, *N*, *N′*, *N′*, *N″*-Pentamethyldiethylenetriamine

PMMA: Poly(methyl methacrylate)

PEO: Poly(ethylene oxide)

PGMA: Poly(glycidyl methacrylate)

PS: Polystyrene

P(S-*r*-SF): Poly(styrene-*r*-2,3,4,5,6-pentafluorostyrene)

P*t*BA: Poly(*tert*-butyl acrylate)

P*t*BA-*b*-PS: Poly(*tert*-butyl acrylate)-*b*-polystyrene

P*t*BMA: Poly(*tert*-butyl methacrylate)

PVP: Poly(vinylpyridine)

P(VBIm$^+$-SO_3^-): Poly(3-(1-(4-vinylbenzyl)-1H-imidazol-3-ium-3-yl)propane-1-sulfonate)

P(VBIm$^+$-SO_3H/$CF_3SO_3^-$): poly(3-(3-sulfopropyl)-1-(4-vinylbenzyl)-1H-imidazol-3-ium trifluoromethanesulfonate)

PVBSA: Poly(vinylbenzenesulfonic acid)

RAFT: Reversible addition-fragmentation chain transfer (polymerization)

$\langle R_{rms} \rangle$: Chain root-mean-square end-to-end distance

ROP: Ring-opening polymerization

SEC: Size exclusion chromatography

SiP: Silica particles

STEMPO: 1-Phenyl-1-(2',2',6',6'-tetramethyl-1'-piperidinyloxy)ethane

*t*BA: *tert*-Butyl acrylate

TEM: Transmission electron microscopy

TEMPO: 2,2,6,6-tetramethylpiperidinooxy

TEOS: Tetraethyl orthosilicate

TFE: Trifluoroethanol

THF: Tetrahydrofuran

TGA: Thermogravimetric analysis

VBIm: 4-Vinylbenzyl imidazole

$VBIm^{+}$-SO_3^{-}: 3-(1-(4-Vinylbenzyl)-1H-imidazol-3-ium-3-yl)propane-1-sulfonate

YI-B-P: Y-initiator-B functionalized particles

Chapter 1. Introduction

1. Introduction to Mixed Homopolymer Brushes

Mixed homopolymer brushes, which are a type of multicomponent polymer brushes composed of two chemically distinct homopolymers randomly or alternatively end-tethered on a solid substrate, have received enormous attention in the past decades.[1] The two homopolymers can undergo spontaneous structural reorganization in a confined geometry in response to environmental changes in order to achieve the lowest free energy state (Scheme 1.1).[1] If mixed brushes are grafted on particles, it is possible to use mixed brushes to tune the behavior of particles because the grafted polymer brushes dictate how the particles interact with the environment.[1] It should be noted here that due to the covalent bonds between the mixed homopolymer brushes and the substrate, the various nanostructures formed from the same mixed brushes are fully reversible. In the following sections, I will first briefly discuss the results from theoretical and simulation studies and then the synthesis and experimental morphology study of mixed homopolymer brushes.

1.1 Theoretical and Simulation Studies of Mixed Homopolymer Brushes

Diblock copolymers, comprised of two immiscible blocks, are known to undergo microphase separation forming various nanostructures in melt and in selective solvent.[2,3] The phase behavior of diblock copolymers is determined by a number of factors: degree of polymerization (DP) of each building block (N_A and N_B), Flory-Huggins interaction parameters (χ) between two components, and volume fraction (f) of each block.[2] Different from diblock copolymers where the junction points are mobile at the interface of different microdomains, one end of each grafted polymer chain in mixed brushes is fixed on the surface of solid substrates, further restricting the phase separation of mixed brushes.[1] Thus, in addition to the factors mentioned above, the

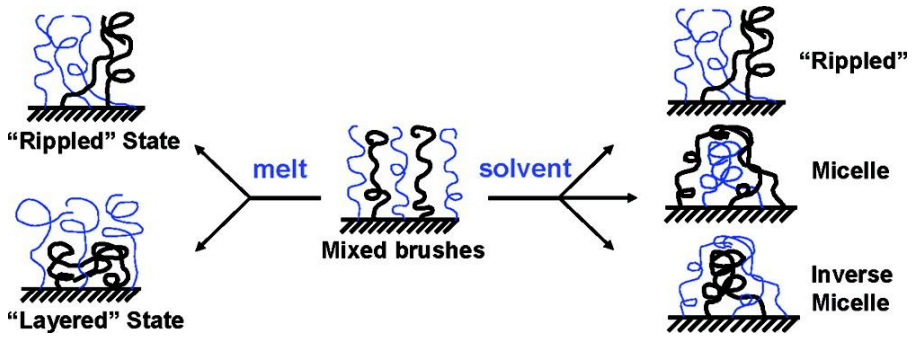

Scheme 1.1 A simplified schematic illustration of self-assembly of mixed homopolymer brushes under equilibrium melt conditions and in various solvents (Reprinted from Ref. 1, with permission from American Chemical Society).

distribution of grafting sites, grafting density, and substrate curvature and geometry also affect the phase behavior of mixed brushes. These unique characteristics afford mixed hompopolymer brushes a variety of nanostructures and properties under different environmental conditions and have attracted considerate interests in theoretical and simulation studies in the past decades.[4-23] It should be noted here that Qiu et al. recently reviewed the latest progress in theory and simulations in binary hairy particles.[23]

Marko and Witten were the first to investigate whether symmetric mixed homopolymer brushes grafted on a planar substrate phase separate "laterally" forming a "rippled" nanostructure or "vertically" producing a layered structure under equilibrium melt conditions.[4] They predicted that the "rippled" structure should be the one to appear and the lateral microphase separation occurs when the molecular weight of mixed brushes is 2.27 times that for the same species in a simple blend at its demixing threshold. The wavelength of the "rippled" nanostructure is predicted to be 1.97 times the chain root-mean-square end-to-end distance ($<R_{rms}>$). They also stated that the phase transition of mixed brushes can be controlled by tuning the relative composition and molecular weight of two grafted polymers. However, the effect of grafting density of mixed brushes on the planar surface was not discussed in their work. After the pioneering work of Marko and Witten, the lateral microphase separation of mixed homopolymer brushes in melt and in neutral solvents were also investigated by other researchers.[6,7,12] Dong studied the mixed brushes composed of two different homopolymers, A and B, in melt under strong demixing interactions, and found that the polymer chains form periodic regions comprised of pure A and B.[6] He discovered that the spatial period of the nanopatten formed by lateral microphase separation is independent of the interaction strength between A and B. For symmetric mixed brushes in good solvent, Lai observed that the chains of the same type cluster

together laterally forming the "ripple state". For asymmetric mixed brushes, layered structures appear with the minority chains stretching away from the grafting substrate.[8] Soga et al. studied the equilibrium structures of binary mixed brushes in a variety of solvent conditions.[10] They found that under strong demixing interactions, it is energetically favorable for the two polymer species to undergo lateral microphase separation. They also found that the onset of microphase separation of mixed brushes is delayed in good solvents and the onset is much more abrupt for poorer solvents.

Zhulina and Balazs investigated the nanopatterns that formed from Y-shaped binary mixed homopolymer brushes grafted on a flat surface in melt and in the presence of nonselective solvent.[12] The Y-brushes are constructed by tethering the junction point of a symmetric diblock copolymer on a planar substrate (Scheme 1.2). They assumed that the brush layer was subdivided into two horizontal sublayers with a thickness of H_1 and H_2, respectively.[12] The bottom sublayer is adjacent to the grafting surface and comprised of randomly mixed segments of two grafted polymers, A and B, while the upper layer contained microphase-separated domains of A and B forming alternating stripes. The width of each stripe is given by d, and the periodicity of the nanopattern is $2d$. They determined how various parameters such as solvent quality, grafting density of Y-brushes, and chain lengths affect the nanostructures. Quantitatively, for highly incompatible blocks A and B, they predicted that in a nonselective poor solvent, $d = N^{1/2}(s\tau^3/\chi)^{1/6}$, in which N is the number of repeat unit in A and B block, s is the area per chain (the reciprocal of the grafting density of mixed brushes), τ was a measure of the relative deviation from the θ temperature, and χ is the Flory-Huggins interaction parameter. They found that the periodicity of the ripple pattern ($2d$) formed by mixed homopolymer brushes scaled with the one-sixth power of the area per chain (s) and half-power of the DP of block A (or block B). At high grafting

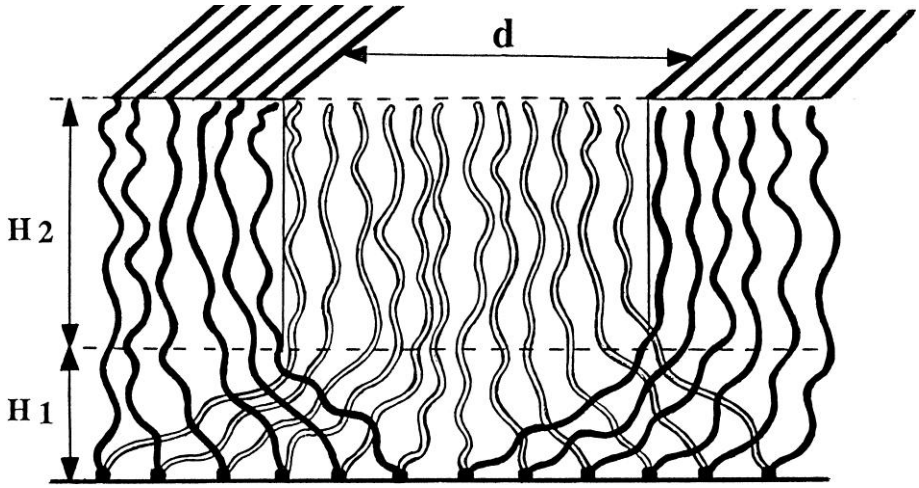

Scheme 1.2 Laterally microsegregated nanostructure formed by Y-shaped block copolymer brushes. (Reprinted from Ref. 12, with permission from American Chemical Society).

densities, a transition from a homogeneous, mixed structure at low incompatibility to a laterally segregated periodic structure at higher incompatibility could occur. At low grafting densities, the Y-brushes lose lateral homogeneity and split into separated coils in good solvents or "pinned micelles" under poor solvent conditions. A phase diagram was constructed, revealing that by varying solvent quality, a rich variety of lateral nanostructures could form. By using Monte Carlo simulations, Wenning et al. discovered that the density fluctuation of the grafting points of the grafted polymers in mixed brushes significantly enhances the formation of irregular structures of nanopattern and prevents the long-range order.[15] Even small fluctuations of the grafting points would be sufficient to pin the lateral nanostructure of the mixed homopolymer brushes. Using Single-Chain-in-Mean-Field simulations, Wang and Müller systematically investigated the effects of solvent quality and selectivity, grafting density, chemical composition and chain-length disparity on microphase separation of binary mixed homopolymer brushes on a planar surface.[18] They also found that the nanostructures formed from microphase segregation lacks a long-range periodic order.

Most theoretical work on mixed homopolymer brushes has centered on flat substrates. It can be imagined that for the mixed brushes grafted on particles with a diameter comparable to or less than the $<R_{rms}>$s of the grafted polymers, the substrate curvature would play a role in microphase separation of mixed brushes because the grafted polymer chains have more space for packing when moving away from the grafting site.[1] Roan was the first to investigate the microphase separation of mixed homopolymer brushes grafted on spherical nanoparticles (NPs). By changing the relative chain lengths and grafting densities of two homopolymers, a variety of nanostructures ranging from ordered islanded, to rippled, and layered nanostructures were observed.[16] More recently, by using numerical implementation of a self-consistent field theory,

Wang et al. studied the microphase separation of mixed homopolymer brushes grafted on a nanosphere with a radius comparable to the sizes of polymers.[20] They systematically studied the effects of overall grafting density, chemical composition, chain length asymmetry, and curvature effect. A series of island-like nanostructures with different island numbers, ranging from 2 to 12, were observed.

1.2 Synthesis and Responsive Properties of Mixed Homopolymer Brushes

Experimental study on synthesis and responsive properties of binary mixed homopolymer brushes began over a decade ago.[24] Many methods have been reported for the preparation of mixed brushes, which can be categorized into three general strategies: "grafting from",[24-37] "grafting to",[38-48] and a combination of "grafting from" and "grafting to".[49-51]

1.2.1 Synthesis and Responsive Properties of Mixed Homopolymer Brushes by "Grafting From"

"Grafting from" refers to a process where polymer chains are grown in situ from the surface of an initiator-functionalized substrate. Mixed brushes can be synthesized by either a "two-step" or a "one-step" surface-initiated polymerization process.[24-37] Sidorenko et al. were the first reporting the synthesis of binary mixed brushes composed of polystyrene (PS)/poly(2-vinylpyridine) (PVP) by a "grafting from" method.[24] Silicon wafers were first surface-functionalized with an azo free radical initiator, followed by a two-step conventional free radical polymerization process to grow two polymers; the second polymer was grown from the residual surface azo initiator that did not decompose in the synthesis of the first polymer. The obtained mixed brushes showed responsive properties to environmental variations. Specifically, upon

treatment with toluene, a selective good solvent for PS, the grafted PS chains were stretched while PVP collapsed, producing a hydrophobic surface. When exposed to a HCl solution, the PVP chains occupied the outermost layer making the surface hydrophilic. It should be noted here that the surface-initiated conventional radical polymerization lacks control of molecular weights and molecular weight distributions of the resultant brushes.

Unlike conventional free radical polymerization, "living"/controlled radical polymerizations, including atom transfer radical polymerization (ATRP),[52] nitroxide-mediated radical polymerization (NMRP),[53] and reversible-addition fragmentation chain transfer polymerization (RAFT),[54] can produce well-defined polymers with predetermined molecular weight and narrow polydispersities. These controlled radical polymerization methods have been widely used in the synthesis of well-defined polymer brushes with high grafting densities.[55] Our group has developed a two-step "grafting from" method to synthesize well-defined mixed brushes by using two different "living"/controlled radical polymerizations: ATRP and NMRP.[25-30,32,33,35-37] An asymmetric difunctional initiator (Y-initiator) bearing an ATRP initiating moiety and an alkoxyamine for NMRP was designed to ensure that the two initiators are well mixed at the molecular level in the initiator layer on the substrate (Scheme 1.3), which is necessary for synthesizing well-mixed binary homopolymer brushes.[25,27,29,30,32,33,35-37] The use of Y-initiator minimizes the fluctuation of the grafting points of two polymers in the mixed brushes. The alkoxyamine moiety in the Y-initiator was confirmed to be stable under typical ATRP conditions.[25] With the addition of corresponding free initiators in both ATRP and NMRP processes, the surface-initiated polymerizations were well controlled, affording well-defined mixed brushes. Compared with silicon wafers, silica particles as substrates for mixed brushes have many advantages because of the relatively higher surface area. The brushes can be cleaved

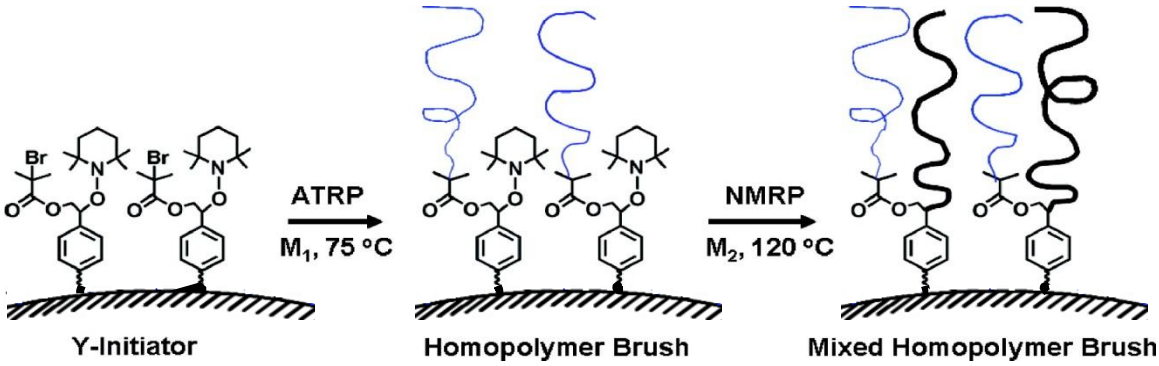

Scheme 1.3 Synthesis of mixed homopolymer brushes by sequential surface-initiated atom transfer radical polymerization and nitroxide-mediated radical polymerization from asymmetric difunctional initiator (Y-Initiator)-functionalized silica particles in a two-step process (Adapted from Ref. 1, with permission from American Chemical Society).

off from the particles and analyzed by ^{1}H NMR spectroscopy and size exclusion chromatography (SEC). Traditional block copolymer characterization techniques such as differential scanning calorimetry (DSC) and transmission electron microscopy (TEM) can be used to study mixed brushes grafted on silica particles directly. Our lab synthesized poly(*tert*-butyl acrylate) (P*t*BA)/PS brushes from Y-initiator functionalized silica particles with a diameter of 180 nm by surface-initiated ATRP of *t*BA first and then NMRP of styrene.[25] Cleavage experiments using HF to etch silica core showed that the molecular weights and molecular weight distributions of the grafted polymers were essentially the same as those of the corresponding free polymers formed from the free initiators.[25] Amphiphilic mixed poly(acrylic acid) (PAA)/PS brush-grafted silica particles were obtained after the removal of *tert*-butyl groups of P*t*BA from mixed P*t*BA/PS brush-grafted particles. The responsive properties of mixed PAA/PS in different solvents were convincingly demonstrated by ^{1}H NMR spectroscopy analysis.[25] As can be seen in Figure 1.1, in *N*,*N*-dimethylformamide-d_7 (DMF-d_7), which is a nonselective good solvent for both PAA and PS, the peaks from both PAA and PS were visible in the ^{1}H NMR spectrum, indicating that both polymers were in the swollen states. In $CDCl_3$, a selective good solvent for PS, while the characteristic peak from PAA chains at around 2.5 ppm disappeared, the aromatic peaks of PS were still visible, indicating that PAA collapsed and PS chains were stretched. In CD_3OD, a selective solvent for PAA, the PAA chains were stretched, but PS collapsed, as evidenced by the peak at ~ 2.5 ppm from PAA and the disappearance of the aromatic peaks of PS.

Mixed brushes have also been prepared by other "grafting from" methods.[31,34] By taking advantage of different mechanisms and the compatibility of cationic ring-opening polymerization and NMRP, Wang et al. synthesized binary mixed poly(2-phenyl-2-oxazoline)/PS brushes on

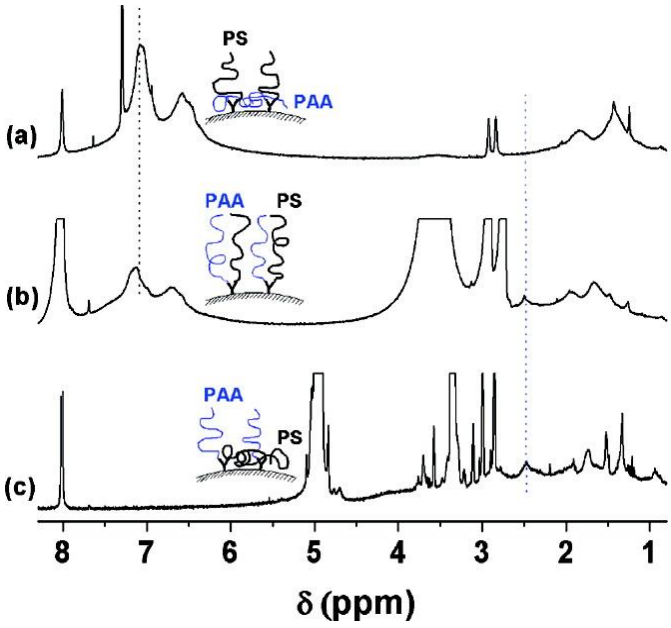

Figure 1.1 ^{1}H NMR spectra of mixed PAA/PS brush-grafted silica particles in (a) $CDCl_3$, (b) DMF-d_7, and (c) CD_3OD. A drop of DMF-d_7 was added into the particles prior to $CDCl_3$ and CD_3OD to facilitate the dispersion of hairy particles. Mixed PAA/PS brush-grafted particles were synthesized from P*t*BA/PS brush-grafted particles with P*t*BA M_n of 24.2 kDa and PS M_n of 23 kDa. The grafting densities of P*t*BA and PS were 2.5 and 2.7 nm^2/chain, respectively (reproduced from Ref. 25, with permission from American Chemical Society).

silicon wafers via a one-step "grafting from" method.[31] The mixed brushes exhibited reversible surface property changes when subjected to different solvents. More recently, Huang et al. reported the synthesis of mixed brushes from mesoporous silica particles by using surface-initiated ATRP and RAFT from a bifunctional hetero-initiator.[34] Specifically, they conducted surface-initiated RAFT polymerization of 2-(diethylamino)ethyl methacrylate (DEAEMA) first. After the removal of the RAFT chain transfer agent from the chain end of poly(DEAEMA) using 4,4'-azobis(4-cyanovaleric acid) through radical reaction, the surface-initiated ATRP of *N*-(2-hydroxypropyl) acrylamide (HPMA) was carried out to grow the second polymer from the surface of silica particles.

1.2.2 Synthesis and Responsive Properties of Mixed Homopolymer Brushes by "Grafting To"

"Grafting to" is also widely used to prepare polymer brushes, where polymers are grafted onto a solid substrate via a reaction with functional group on the surface.[38-48] This method is straightforward, and polymers with predetermined molecular weights, well-defined end groups, and controlled chemical compositions and architectures can be used. Mixed polymer brushes can be prepared by a two-step or one-step "grafting to" process using two end-functionalized polymers (Scheme 1.4)[39,42,48] or a one-step surface reaction employing block copolymers (Scheme 1.5).[38,40,41,43-47] For instance, Minko et al. reported the synthesis of binary mixed PS/PVP brushes by grafting carboxyl-terminated PS and PVP onto the silicon wafers that were functionalized with 3-glycidoxypropyltrimethoxysilane.[39] Chiu et al. prepared mixed PS/PVP brush-grafted gold nanoparticles (Au NPs) by one-step grafting of PS with a molecular weight

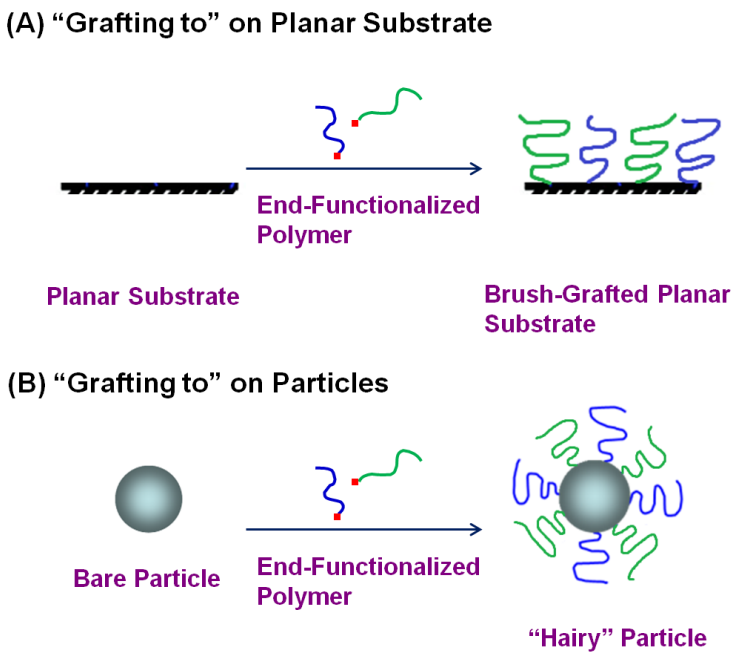

Scheme 1.4. Schematic illustration of synthesis of mixed homopolymer brushes by grafting two end-functionalized polymers onto (A) a planar substrate and (B) particles

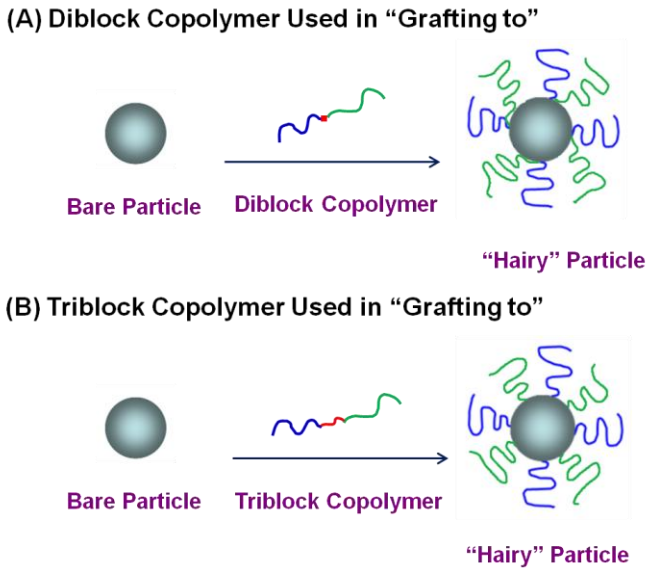

Scheme 1.5 Schematic illustration of synthesis of mixed brushes by a one-step "grafting to" process using (A) a diblock copolymer with a functional group at the junction point (red) and (B) an ABC triblock copolymer with a short central block (red) via the reaction of the red functional group or block with the substrate.

(MW) of 1.3 kDa and PVP with a MW of 1.5 kDa.[42] They found binary mixed brush-grafted Au NPs exhibited different behavior when dispersed in a PS-*b*-PVP lamellar diblock copolymer compared with either pure PS- or pure PVP-coated NPs. Boyer et al. reported the synthesis of doubly thermosensitive mixed brush-grafted gold NPs.[48] The thermoresponsive polymers used in their work are polyacrylates with a short oligo(ethylene glycol) pendant on each repeating unit. The thermoresponsive properties of mixed brushes grafted on Au NPs were investigated by fluorescence spectroscopy using pyrene as probe. When pyrene is sequestered into a hydrophobic environment, there is a drop in the intensity ratio of the first (I_1) to the third (I_3) vibration band. Two transitions were clearly observed from the plot of I_1/I_3 versus temperature, which corresponded to the lower critical solution temperature (LCST) transitions of two grafted thermosensitive polymers.

Block copolymers with appropriate functional groups have also been used to make mixed brushes by "grafting to", as illustrated in Scheme 1.5.[38,40,41,43,47] Wang et al. prepared mixed poly(methyl methacrylate) (PMMA)/PS brushes on silicon wafers by using PS-*b*-poly(4-hydroxystyrene)-*b*-PMMA through a one-step reaction of the central block with the surface of silicon wafers.[38] Julthongpiput et al. fabricated Y-shaped mixed brushes by grafting PS-*b*-P*t*BA diblock copolymers onto silicon wafers through the reaction between the carboxylic acid group at the junction point of the two blocks of PS-*b*-P*t*BA and the silanol groups on the surface of silicon wafers.[40,41] Zubarev et al. grafted diblock copolymers with a carboxylic acid group at the junction point of the two blocks to 4-mercaptophenol-functionalized Au NPs through an *N*,*N'*-dicyclohexylcarbodiimide-catalyzed coupling reaction.[43,44] Mixed PS/poly(ethylene oxide) (PEO) brush-grafted Au NPs with PS M_n of 4 kDa and PEO M_n of 2.2 kDa have been shown to self-assemble into well-defined rod-like nanoassemblies with a diameter of 18 nm and ~100 nm

in length (Figure 1.2) after dialysis of a THF/H_2O (1 : 3, v/v) solution against deionized water.[43] The radius of the nanorods was in agreement with the length of PS chains in the fully extended conformation. Wang et al. prepared mixed PS/PVP brushes on silicon wafers using a diblock copolymer PS-*b*-PVP containing a methylhydridosilane linking group capable of chemically grafting onto a substrate functionalized with an 8-trichlorosilyloctene monolayer via a simple one-step hydrosilylation reaction.[45] Motornov et al. synthesized amphiphilic mixed brush-grafted particles by reacting a triblock copolymer PS-*b*-PVP-*b*-PEO with 11-bromoundodecyltrimethoxysilane-functionalized silica particles.[46] The mixed brush-grafted particles showed responsive properties to different solvents and pH values in water. Cheng et al. reported the use of a "grafting to" method to anchor poly(*tert*-butyl methacrylate)-*b*-poly(glycidyl methacrylate)-*b*-PS (P*t*BMA-*b*-PGMA-*b*-PS) onto the surface of nanodiamond through the reaction between the carboxyl groups on nanodiamond and the epoxy groups of PGMA.[47]

1.2.3 Synthesis of Mixed Homopolymer Brushes by Combining "Grafting To" and "Grafting From"

More recently, Wang et al. developed a new method for the synthesis of mixed homopolymer brushes on Au NPs by combining "grafting to" and "grafting from" (Scheme 1.6).[50] Mixed PEO/PMMA brush-grafted Au NPs were synthesized by incubating initiator 11-mercaptoundecyl 2-bromo-2-methylpropionate-coated Au NPs with a thiol-terminated PEO and subsequent surface-initiated ATRP of MMA. Duan et al. synthesized mixed brushes on gold nanocrystals by co-assembling a thiol-terminated 5 kDa PEO with a disulfide-containing ATRP initiator onto the

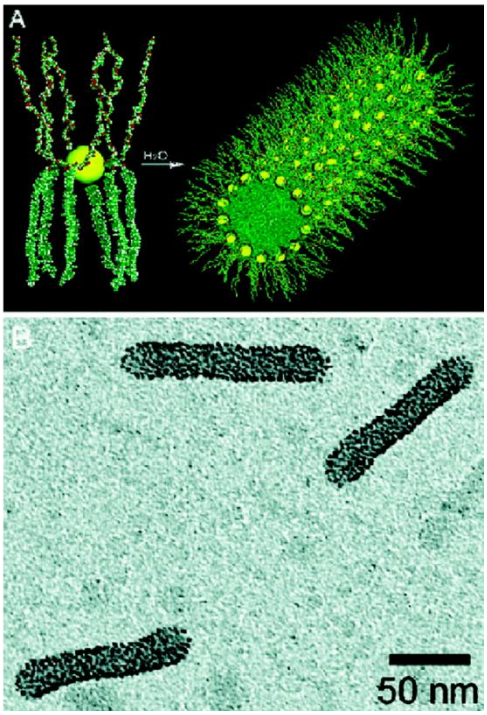

Figure 1.2 (A) Schematic representation of the self-assembly of mixed PS/PEO brush-grafted Au nanoparticles in water. (B) TEM image of a sample prepared from an aqueous solution of mixed PS/PEO brush-grafted nanoparticles after dialysis of a THF/H_2O (1 : 3 v/v) solution against DI water (reproduced from Ref. 43, with permission from American Chemical Society).

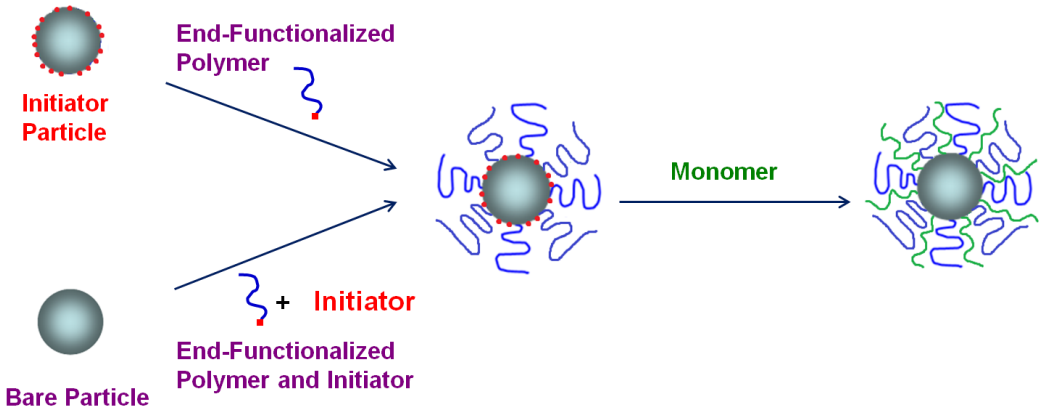

Scheme 1.6 Schematic illustration of synthesis of mixed homopolymer brushes via combination of "grafting to" and "grafting from"

surface of gold nanocrystals followed by surface-initiated polymerization.[51] Wang et al. reported the preparation of Janus Au NPs that were surface-functionalized with two different types of polymers on the opposite sides of Au NPs by combining "grafting from" and "solid-state grafting to".[49] Au NPs were first immobilized onto the thiol-terminated PEO single crystals, followed by a ligand exchange reaction to functionalize the "exposed" side of Au NPs. Janus AuNPs were obtained after the surface-initiated ATRP from the NP surface and subsequent dissolution of the PEO single crystals.

1.3 Experimental Studies of Morphology of Mixed Homopolymer Brushes

Although considerate progress has been made on theoretical study of phase morphology of mixed homopolymer brushes, experimental work lags far behind largely because of the difficulty in the synthesis of well-defined mixed brushes. Minko et al. investigated the morphologies of mixed PMMA/poly(styrene-*r*-2,3,4,5,6-pentafluorostyrene) (PMMA/P(S-*r*-SF) brushes grafted on planar substrates upon exposure to various solvents using atomic force microscopy (AFM) and X-ray photoemission microscopy.[13] They reported that the two incompatible grafted polymers segregated into a "ripple" structure when treated with a nonselective solvent. When a selective solvent was used, a "dimple" structure appeared, in which the unfavored component formed clusters. They also studied the inner structure of mixed PS/PMMA brushes grafted on silicon wafers, synthesized by a two-step surface-initiated conventional free radical polymerization process, through a combination of step-by-step oxygen plasma etching and AFM.[56] Three-dimensional structures of the mixed brushes were reconstructed using nanotomography data.

Although efforts had been made to elucidate the morphology of mixed brushes, the nanostructures formed from self-assembly of mixed brushes had not been directly visualized by using transmission electron microscopy (TEM), one of the most powerful methods for studying the morphology of multicomponent polymer systems. Our group has been interested in using traditional block copolymer characterization techniques, particularly, TEM, to elucidate the morphology formed from microphase separation of mixed brushes grafted on particles.[32-33,57-58] TEM allows direct visualization of the morphologies of mixed brushes on silica particles. For mixed P*t*BA/PS brushes, RuO_4 can be used to selectively stain PS nanodomains, which appear dark under TEM, making it possible to analyze the nanostructures of mixed brushes. For example, for mixed P*t*BA/PS brushes grafted on 180 nm silica particles with P*t*BA M_n of 24.2 kDa and PS M_n of 23.0 kDa (the high MW sample), random and worm-like "rippled" nanostructures were clearly observed under TEM with alternating dark (PS) and white stripes after the sample was cast from chloroform, a nonselective good solvent (Figure 1.3).[57] For the sample with the P*t*BA M_n of 10.4 kDa and PS M_n of 11.9 kDa (the low MW sample), no microphase separation was observed (Figure 1.3), suggesting that the critical molecular weight for microphase separation of mixed P*t*BA/PS brushes was between ~ 11 kDa and ~ 23 kDa. DSC study further confirmed the TEM observation; two distinct glass transition temperatures, corresponding to those of P*t*BA and PS, were observed for the high MW sample, while there was only one broad glass transition temperature for the low MW sample, indicating that no microphase separation occurred.[57]

As discussed earlier, mixed brushes can undergo self-reorganization in response to environmental variations. As shown in Figure 1.4, after cast from *n*-octane, a good solvent for P*t*BA but a poor solvent for PS, the high MW mixed P*t*BA/PS brush sample exhibited a different

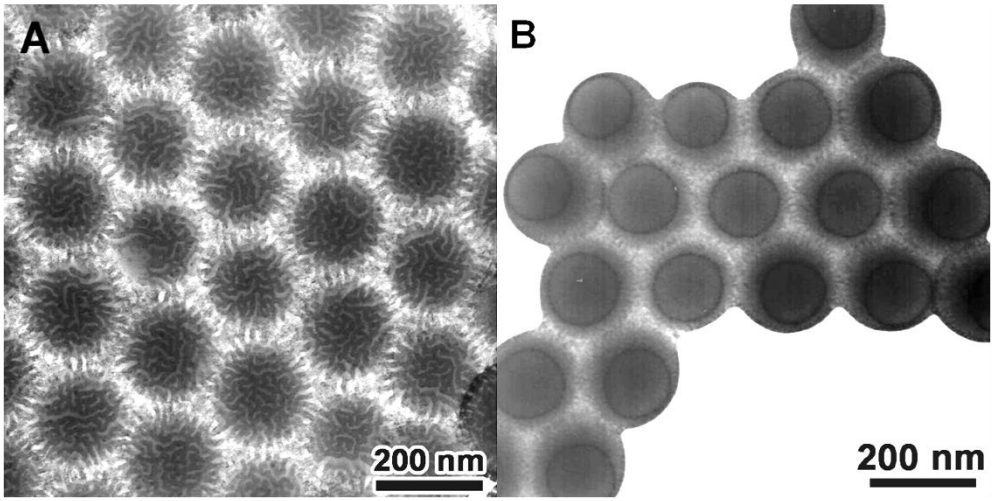

Figure 1.3 Top-view bright field TEM micrograph of (a) mixed brush sample with P*t*BA M_n of 24.2 kDa and grafting density of 2.5 nm^2/P*t*BA chain and PS M_n of 23.0 kDa and grafting density of 2.7 nm^2/PS chain and (b) mixed brush sample with P*t*BA M_n of 10.4 kDa and grafting density of 3.1 nm^2/P*t*BA chain and PS M_n of 11.9 kDa and grafting density of 2.9 nm^2/PS chain. Samples were cast from chloroform and stained with RuO_4 for 30 min (Reproduced from Ref. 58, with permission from American Chemical Society).

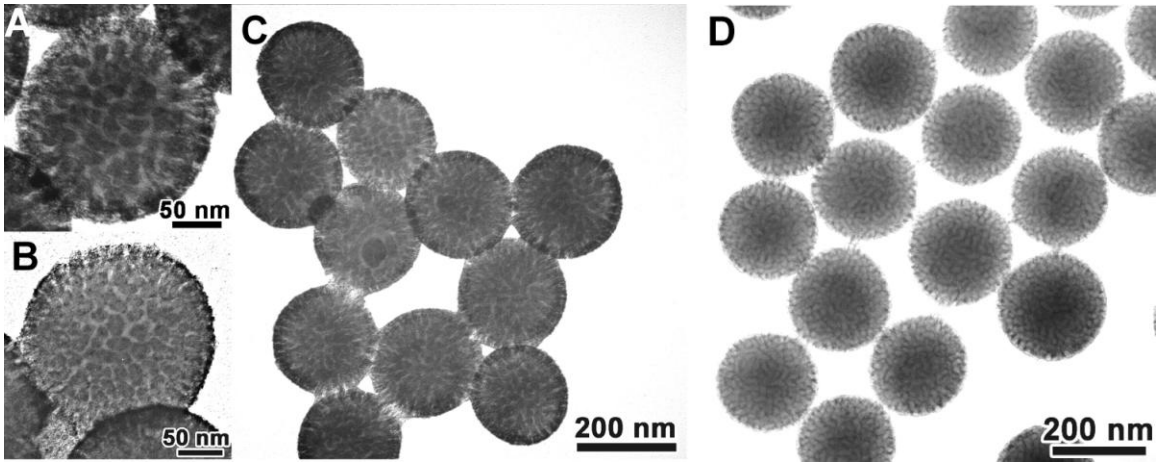

Figure 1.4 TEM micrographs of the high MW mixed P*t*BA/PS brush-grafted particles that were cast from *n*-octane, a selective solvent for P*t*BA (A−C), and mixed PAA/PS brush-grafted particles cast from water, a selective solvent for PAA (D). Micrographs (A) and (B) are magnified images showing the (dark) isolated PS microdomains in the (bright) continuous P*t*BA matrix. The mixed P*t*BA/PS brush samples were stained with RuO_4 vapor for 30 min. The mixed PAA/PS brush-grafted particles were stained with uranyl acetate. The mixed PAA/PS brush-grafted particles were synthesized from the high MW mixed P*t*BA/PS brush sample (P*t*BA M_n of 24.2 kDa and PS M_n of 23.0 kDa) by the removal of *tert*-butyl groups of P*t*BA (reproduced from Ref. 58, with permission from American Chemical Society).

morphology.[58] Surface micellar structures composed of isolated dark PS domains buried inside the P*t*BA matrix were observed. Apparently, the PS chains collapsed into a dense core, which was shielded by the stretched P*t*BA chains to minimize the contact between PS and *n*-octane. Micellar nanostructures were also observed under TEM for mixed PAA/PS brush particles, which were cast from water, a selective solvent for PAA, and stained with uranyl acetate.

The morphology of mixed brushes is affected by many factors, such as relative chain length, molecular weights of grafted polymers, overall and relative grafting density, and substrate curvature.[1] Jiang et al. investigated the effect of chain length disparity on microphase separation of mixed P*t*BA/PS brushes.[32,33] Silica particles with a size of 160 nm were surface-modified with a monochlorosilane-terminated Y-initiator.[32] By taking advantage of the "living" nature of NMRP, a series of mixed brush-grafted particle samples with the same MW for P*t*BA but different MWs for PS were synthesized from P*t*BA brush-grafted silica particles. The overall grafting density ($\sigma_{overall}$) of these mixed brush samples was 0.6 ~ 0.7 chains/nm^2, falling into the intermediate grafting density regime. With the increase of PS MW from below to above that of P*t*BA, the phase morphology of mixed brushes changed from isolated and nearly spherical PS domains buried inside the P*t*BA matrix, to short PS cylinders, to worm-like, nearly bicontinous nanostructures, and a two-layered structure comprised of a thin PS top layer and a microphase-separated bottom layer (Figure 1.5). Jiang et al. further synthesized a set of high grafting density asymmetric mixed P*t*BA/PS brushes with overall grafting densities of 0.9 ~ 1.2 chains/nm^2 from silica particles with a diameter of 172 nm that were functionalized with a triethoxysilane-terminated Y-initiator.[33] The initiator immobilization involved an ammonia-catalyzed process on the surface of silica particles. Similar morphological evolution was observed using TEM, however, the feature size was significantly smaller compared with intermediate grafting density

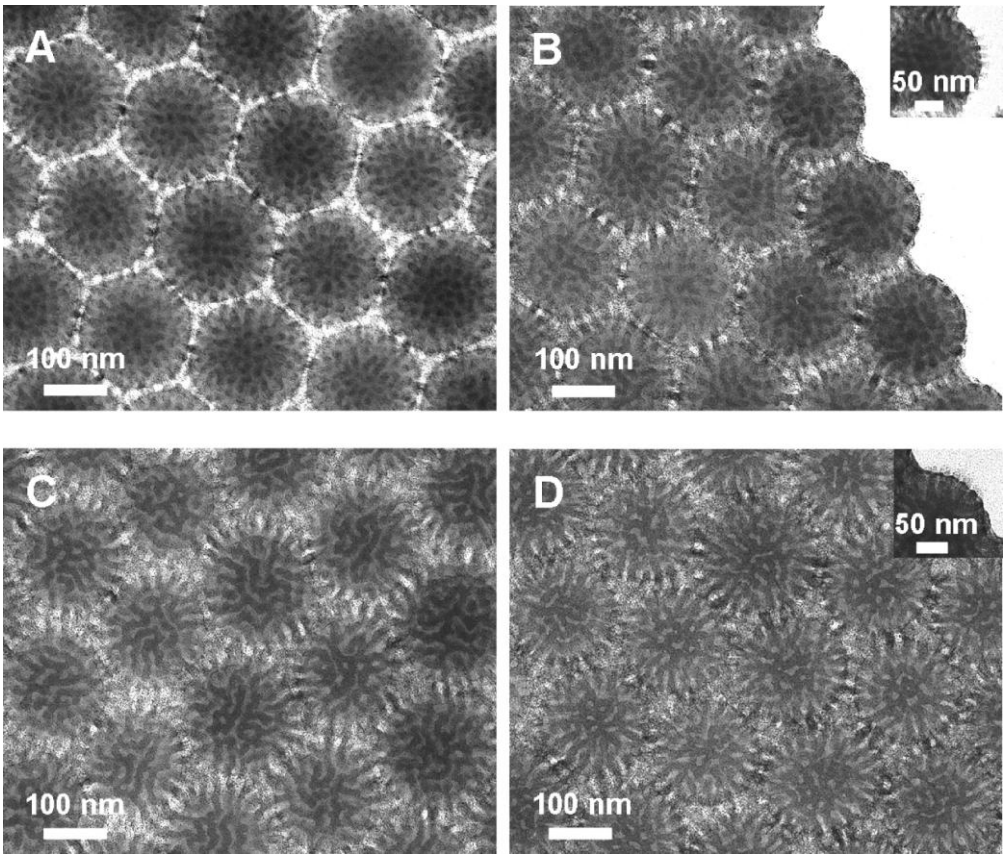

Figure 1.5 Top-view TEM micrographs of (A) mixed brush-grafted silica particle with P*t*BA $M_{n,SEC}$ of 24.5 kDa and PS M_n of 14.8 kDa, (B) mixed brush-grafted particle with P*t*BA $M_{n,SEC}$ of 24.5 kDa and PS M_n of 18.7 kDa, (C) mixed brush-grafted particle with P*t*BA $M_{n,SEC}$ of 24.5 kDa and PS M_n of 24.9 kDa, and (D) mixed brush-grafted particle with P*t*BA $M_{n,SEC}$ of 24.5 kDa and PS M_n of 30.4 kDa after being cast from $CHCl_3$, a nonselective good solvent for both P*t*BA and PS, and thermally annealed at 120 ℃ in vacuum for 3 h. The samples were stained with RuO_4 vapor. (Reprinted from Ref. 32, with permission from American Chemical Society).

mixed brushes ($\sigma_{overall}$ = 0.6 ~ 0.7 chains/nm^2). This is believed to be a result of enthalpy and entropy competition in the microphase separation. DSC studies indicated that all intermediate and high grafting density mixed brush samples were clearly microphase separated, evidenced by the appearance of two distinct glass transitions corresponding to the glass transitions of P*t*BA and PS.

2. Dissertation Overview

Although progress has been made in the understanding of self-assembly of mixed homopolymer brushes, many issues remained unsolved. This dissertation work is devoted to the synthesis and morphology study of well-defined mixed homopolymer brushes grafted on silica particles. In particular, we investigated the effects of overall grafting density and average molecular weight on microphase separation of mixed homopolymer brushes.

Chapter 2 presents a systematic study on the effect of overall grafting density ($\sigma_{overall}$) on microphase separation of well-defined mixed P*t*BA/PS brushes, which were grown from Y-initiator-functionalized, 173 nm silica particles by sequential surface-initiated ATRP of *t*BA and NMRP of styrene. By changing the mass ratio of Y-initiator to silica particles in the initiator immobilization step, the overall grafting density of mixed brushes can be systematically tuned while the individual grafting densities of two polymers remained comparable. A series of mixed P*t*BA/PS brushes with molecular weights of ~ 23 kDa for both P*t*BA and PS and $\sigma_{overall}$ from 1.06 to 0.12 chains/nm^2 were prepared. The samples were cast from chloroform, stained with RuO_4 and studied by TEM. The ripple wavelength (*D*) increased with decreasing $\sigma_{overall}$; the normalized *D* scaled with $\sigma_{overall}^{-0.47}$ in the $\sigma_{overall}$ range of 1.06 to 0.54 chains/nm^2. With further

decreasing the grafting density, the phase separation became weaker, and no microphase separation was observed in the sample with $\sigma_{overall}$ of 0.122 chain/nm^2.

Chapter 3 presents a systematic study on the effect of molecular weight on microphase separation of mixed P*t*BA/PS brushes grafted on 172 nm silica particles. The MWs of the two polymers in each sample were controlled to be similar to each other. A series of mixed P*t*BA/PS brush samples with different average MWs, ranging from 13.8 to 33.1 kDa, but comparable overall grafting densities, were prepared. The TEM samples were prepared by drop casting the dispersions of mixed P*t*BA/PS brush-grafted particles in $CHCl_3$ and also in water (stabilized by a surfactant). All samples underwent lateral microphase separation, forming nearly bicontinuous rippled nanopatterns. The average ripple wavelength *D* increased with increasing the MW. For samples directly cast from chloroform dispersions, *D* scaled with $MW^{0.70}$ in the studied molecular weight range. For uniformly collapsed mixed brushes cast from water, *D* was proportional to $MW^{0.56}$ in the MW range of 17.9 to 33.1 kDa. The microphase separation behavior of mixed P*t*BA/PS brushes grafted on silica particles was compared with that of diblock copolymers. It was found that the phase separation of mixed brushes on silica particles was weaker than that of diblock copolymers.

Chapter 4 describes the synthesis of mixed homopolymer brushes grafted on 157 nm silica particles composed of poly(ε-caprolactone) (PCL) and PS by sequential surface-initiated ring-opening polymerization (ROP) of ε-caprolactone and NMRP of styrene. The surface-initiated ROP and NMRP polymerizations were carried out in the presence of a corresponding free initiator. The overall grafting density of mixed PCL/PS brushes can be tuned by varying the mass ratio of Y-initiator-terminated triethoxysilane to bare silica particles in the initiator immobilization step.

Chapter 5 presents the synthesis and characterization of polymer brush-supported acid catalysts grafted on silica particles and the use of these catalysts for the dehydration of fructose into 5-hydroxymethylfurfural in water. The brush catalysts exhibited a higher activity than the corresponding free homopolymer catalysts.

Chapter 6 provides a summary of this dissertation work. Possible future work is suggested.

References

1. Zhao, B.; Zhu, L. *Macromolecules* **2009**, *42*, 9369-9383.
2. Bates, F. S.; Fredrickson, G. H. *Phys. Today* **1999**, *52*, 32.
3. Mai, Y.; Eisenberg, A. *Chem. Soc. Rev.* **2012**, *41*, 5969-5985.
4. Marko, J. F.; Witten, T. A. *Phys. Rev. Lett.* **1991**, *66*, 1541-1544.
5. Marko, J. F.; Witten, T. A. *Macromolecules* **1992**, *25*, 296-307.
6. Dong, H. *J. Phys. II France* **1993**, *3*, 999-1020.
7. Brown, G.; Chakrabarti, A.; Marko, J. F. *Europhys. Lett.* **1994**, *25*, 239.
8. Lai, P. Y. *J. Chem. Phys.* **1994**, *100*, 3351-3357.
9. Chen, C.; Dan, N.; Dhoot, S.; Tirrell, M.; Mays, J.; Watanabe, H. *Israel J. Chem.* **1995**, *35*, 41-47.
10. Soga, K. G.; Zuckermann, M. J.; Guo, H. *Macromolecules* **1996**, *29*, 1998-2005.
11. Singh, C.; Pickett, G. T.; Balazs, A. C. *Macromolecules* **1996**, *29*, 7559-7570.
12. Zhulina, E.; Balazs, A. C. *Macromolecules* **1996**, *29*, 2667-2673.
13. Minko, S.; Müller, M.; Usov, D.; Scholl, A.; Froeck, C.; Stamm, M. *Phys. Rev. Lett.* **2002**, *88*, 035502.
14. Müller, M. *Phys. Rev. E* **2002**, *65*, 030802.
15. Wenning, L.; Müller, M.; Binder, K. *Europhys. Lett.* **2005**, *71*, 639.
16. Roan, J.-R. *Phys. Rev. Lett.* **2006**, *96*, 248301.
17. Merlitz, H.; He, G.-L.; Sommer, J.-U.; Wu, C.-X. *Macromolecules* **2008**, *42*, 445-451.
18. Wang, J.; Müller, M. *J. Phys. Chem. B* **2009**, *113*, 11384-11402.
19. Uhlmann, P.; Merlitz, H.; Sommer, J.-U.; Stamm, M. *Macromol. Rapid Commun.* **2009**, *30*, 732-740.

20. Wang, Y.; Yang, G.; Tang, P.; Qiu, F.; Yang, Y.; Zhu, L. *J. Chem. Phys.* **2011**, *134*, 134903-10.

21. Ma, X.; Yang, Y.; Zhu, L.; Zhao, B.; Tang, P.; Qiu, F. *J. Chem. Phys.* **2013**, *139*, 214902.

22. Ma, X.; Chen, C.; Yang, Y.; Qiu, F. *Soft Matter* **2014**, *10*, 6005-6013.

23. Chen, C.; Tang, P.; Qiu, F. *J. Polym. Sci. Part B: Polym. Phys.* **2014**, *52*, 1583-1599.

24. Sidorenko, A.; Minko, S.; Schenk-Meuser, K.; Duschner, H.; Stamm, M. *Langmuir* **1999**, *15*, 8349-8355.

25. Li, D.; Sheng, X.; Zhao, B. *J. Am. Chem. Soc.* **2005**, *127*, 6248-6256.

26. Zhao, B. *Polymer* **2003**, *44*, 4079-4083.

27. Zhao, B.; He, T. *Macromolecules* **2003**, *36*, 8599-8602.

28. Zhao, B. *Langmuir* **2004**, *20*, 11748-11755.

29. Zhao, B.; Haasch, R. T.; MacLaren, S. *J. Am. Chem. Soc.* **2004**, *126*, 6124-6134.

30. Zhao, B.; Haasch, R. T.; MacLaren, S. *Polymer* **2004**, *45*, 7979-7988.

31. Wang, Y.; Brittain, W. J. *Macromol. Rapid Commun.* **2007**, *28*, 811-815.

32. Jiang, X.; Zhong, G.; Horton, J. M.; Jin, N.; Zhu, L.; Zhao, B. *Macromolecules* **2010**, *43*, 5387-5395.

33. Jiang, X.; Zhao, B.; Zhong, G.; Jin, N.; Horton, J. M.; Zhu, L.; Hafner, R. S.; Lodge, T. P. *Macromolecules* **2010**, *43*, 8209-8217.

34. Huang, X.; Hauptmann, N.; Appelhans, D.; Formanek, P.; Frank, S.; Kaskel, S.; Temme, A.; Voit, B. *Small* **2012**, *8*, 3579-3583.

35. Horton, J. M.; Tang, S.; Bao, C.; Tang, P.; Qiu, F.; Zhu, L.; Zhao, B. *ACS Macro Lett.* **2012**, *1*, 1061-1065.

36. Bao, C.; Tang, S.; Horton, J. M.; Jiang, X.; Tang, P.; Qiu, F.; Zhu, L.; Zhao, B. *Macromolecules* **2012**, *45*, 8027-8036.

37. Bao, C.; Tang, S.; Wright, R. A. E.; Tang, P.; Qiu, F.; Zhu, L.; Zhao, B. *Macromolecules* **2014**, *47*, 6824-6835.

38. Wang, J.; Kara, S.; Long, T. E.; Ward, T. C. *J. Polym. Sci. Part A: Polym. Chem.* **2000**, *38*, 3742-3750.

39. Minko, S.; Patil, S.; Datsyuk, V.; Simon, F.; Eichhorn, K.-J.; Motornov, M.; Usov, D.; Tokarev, I.; Stamm, M. *Langmuir* **2002**, *18*, 289-296.

40. Julthongpiput, D.; Lin, Y.-H.; Teng, J.; Zubarev, E. R.; Tsukruk, V. V. *Langmuir* **2003**, *19*, 7832-7836.

41. Julthongpiput, D.; Lin, Y.-H.; Teng, J.; Zubarev, E. R.; Tsukruk, V. V. *J. Am. Chem. Soc.* **2003**, *125*, 15912-15921.

42. Chiu, J. J.; Kim, B. J.; Kramer, E. J.; Pine, D. J. *J. Am. Chem. Soc.* **2005**, *127*, 5036-5037.

43. Zubarev, E. R.; Xu, J.; Sayyad, A.; Gibson, J. D. *J. Am. Chem. Soc.* **2006**, *128*, 15098-15099.

44. Zubarev, E. R.; Xu, J.; Sayyad, A.; Gibson, J. D. *J. Am. Chem. Soc.* **2006**, *128*, 4958-4959.

45. Wang, Y.; Zheng, J. X.; Brittain, W. J.; Cheng, S. Z. D. *J. Polym. Sci. Part A: Polym. Chem.* **2006**, *44*, 5608-5617.

46. Motornov, M.; Sheparovych, R.; Lupitskyy, R.; MacWilliams, E.; Minko, S. *J. Colloid Interface Sci.* **2007**, *310*, 481-488.

47. Cheng, J.; He, J.; Li, C.; Yang, Y. *Chem Mater.* **2008**, *20*, 4224-4230.

48. Boyer, C.; Whittaker, M. R.; Luzon, M.; Davis, T. P. *Macromolecules* **2009**, *42*, 6917-6926.

49. Wang, B.; Li, B.; Zhao, B.; Li, C. Y. *J. Am. Chem. Soc.* **2008**, *130*, 11594-11595.

50. Wang, B.; Li, B.; Dong, B.; Zhao, B.; Li, C. Y. *Macromolecules* **2010**, *43*, 9234-9238.

51. Cheng, L.; Liu, A.; Peng, S.; Duan, H. *ACS Nano* **2010**, *4*, 6098-6104.

52. Matyjaszewski, K.; Xia, J. *Chem. Rev.* **2001**, *101*, 2921-2990.

53. Hawker, C. J.; Bosman, A. W.; Harth, E. *Chem. Rev.* **2001**, *101*, 3661-3688.

54. Moad, G.; Rizzardo, E.; Thang, S. H. *Acc. Chem Res* **2008**, *41*, 1133-1142.

55. Barbey, R.; Lavanant, L.; Paripovic, D.; Schüwer, N.; Sugnaux, C.; Tugulu, S.; Klok, H.-A. *Chem. Rev.* **2009**, *109*, 5437-5527.

56. Usov, D.; Gruzdev, V.; Nitschke, M.; Stamm, M.; Hoy, O.; Luzinov, I.; Tokarev, I.; Minko, S. *Macromolecules* **2007**, *40*, 8774-8783.

57. Zhao, B.; Zhu, L. *J. Am. Chem. Soc.* **2006**, *128*, 4574-4575.

58. Zhu, L.; Zhao, B. *J. Phys. Chem. B* **2008**, *112*, 11529-11536.

Chapter 2. Effect of Overall Grafting Density on Microphase Separation of Mixed Homopolymer Brushes Synthesized from Y-Initiator-Functionalized Silica Particles

Abstract

This chapter presents a systematic study on the effect of overall grafting density ($\sigma_{overall}$) on microphase separation of mixed poly(*tert*-butyl acrylate) (P*t*BA)/polystyrene (PS) brushes synthesized from asymmetric difunctional initiator (Y-initiator)-functionalized silica particles. The initiator particles were made by the immobilization of a triethoxysilane-terminated Y-initiator on the surface of 173 nm silica particles via an ammonia-catalyzed hydrolysis/condensation process in ethanol. Mixed P*t*BA/PS brushes were then grown from initiator particles by surface-initiated atom transfer radical polymerization of *t*BA at 75 °C and nitroxide-mediated radical polymerization of styrene at 120 °C. By changing the mass ratio of Y-initiator to silica particles in the initiator immobilization step, we found that the overall grafting density of mixed brushes can be systematically tuned while the individual grafting densities of two polymers remained comparable. A series of mixed P*t*BA/PS brushes with molecular weights of ~ 23 kDa for both P*t*BA and PS and $\sigma_{overall}$ from 1.06 to 0.122 chains/nm^2 were prepared. Their microphase separation behavior was studied by transmission electron microscopy (TEM) after the samples were drop cast from chloroform onto carbon-coated TEM grids, annealed with $CHCl_3$ vapor, and stained with ruthenium tetraoxide (RuO_4). $CHCl_3$ is a good solvent for both grafted polymers. When the $\sigma_{overall}$ was 0.34 chains/nm^2 and above, the mixed P*t*BA/PS brushes underwent lateral microphase separation, forming "rippled" nanostructures. The ripple wavelength (*D*) increased with decreasing $\sigma_{overall}$; the normalized *D* scaled with $\sigma_{overall}^{-0.47}$ in the $\sigma_{overall}$ range of 1.06 to 0.54 chains/nm^2. With further decreasing the grafting density, the phase separation became weaker, and no microphase separation was observed in the sample with $\sigma_{overall}$ of 0.122 chain/nm^2.

2.1 Introduction

Binary mixed homopolymer brushes are composed of two chemically distinct homopolymers randomly or alternately immobilized by one end on a solid substrate.[1-3] These brushes are an intriguing class of environmentally responsive nanostructured materials and have received tremendous interest in both fundamental and application studies in the past years.[1-15] Marko and Witten were the first to investigate whether symmetric mixed homopolymer brushes on a flat substrate phase separate laterally forming a "rippled" nanostructure or vertically yielding a "layered" structure under equilibrium melt conditions.[1] They predicted that the lateral microphase separation preempted vertical microphase segregation and the "rippled" nanostructure should be the one to appear. Since this seminal work, the lateral phase separation of mixed brushes under melt or near melt conditions and in nonselective or nearly nonselective solvents was repeatedly observed by many researchers in theoretical and simulation studies.[2,4-8] In addition, the two grafted polymers in the brush layer can undergo spontaneous chain reorganization in response to environmental changes, making mixed brushes exhibit different morphologies under different conditions. Because the polymer chains are covalently end-grafted on the substrate, the different nanostructures formed from the same mixed brushes are fully reversible. Since Sidorenko et al. reported the first synthesis of mixed brushes,[9] the responsive properties of mixed homopolymer brushes have been extensively investigated,[10-12] and the mixed brush-based "smart" materials have shown promise in many applications.

Our group has been particularly interested in the fundamental understanding of how various parameters, e.g., chain length disparity and grafting densities of two polymers, affect the phase behavior and responsive properties of mixed brushes.[3,12,14,15] The effects of overall grafting density and relative grafting densities of two tethered polymers on phase morphology of mixed

brushes have been theoretically investigated.[4,6-8] In general, decreasing the grafting density leads to the weakening of the demixing interaction between two polymers in the brush layer.[4] Because the grafting density determines the degree of stretching of polymer chains in the brush layer, it can be imagined that if the grafting densities are too low, the entropy loss due to the associated stretching in the phase segregation may not be compensated by the energy gain. In the limit where the two polymers are highly incompatible and their grafting densities are high, Zhulina and Balazs found, by scaling arguments, that in nonselective poor solvents the periodicity of the ripple pattern scales with the one sixth power of the area per chain,[4] i.e., the ripple wavelength decreases with the increase of overall grafting density. Relative grafting densities of two polymers in the brush layer also have a profound effect on the phase structures of mixed brushes, which have been revealed in a number of computer simulation studies.[6-8] For instance, Wang and Müller observed that the morphology of mixed brushes on a flat substrate evolves from isolated domains of polymer A in a matrix of polymer B to rippled nanostructures to isolated domains of B in a matrix of A with the increase of the ratio of individual grafting densities of A to B.[6] Roan and Wang et al. studied the effect of relative grafting densities on the phase morphology of mixed brushes grafted on nanospheres, and found that the morphology of mixed brushes varies from layered to various ordered polyhedral, and rippled nanostructures with the change of relative grafting densities of two polymers.[7,8]

There had been no systematic experimental study on the effect of overall grafting density on phase morphology of mixed brushes, largely because of the challenge in the tuning of overall grafting density of mixed brushes while keeping individual grafting densities of two polymers similar. Our group previously reported the synthesis of a set of high grafting density mixed poly(*tert*-butyl acrylate) (P*t*BA)/polystyrene (PS) brushes with a fixed P*t*BA M_n of 18.6 kDa and

PS M_n varying from 8.7 to 28.0 kDa on silica particles by sequential atom transfer radical polymerization (ATRP) of *t*BA and nitroxide-mediated radical polymerization (NMRP) of styrene and the morphological evolution of these mixed brushes with the change of chain length disparity of two grafted polymers.[15b] The silica particles were functionalized with a triethoxysilane-terminated asymmetric difunctional initiator (Y-initiator) via an ammonia-catalyzed hydrolysis/condensation process. The overall grafting densities ($\sigma_{overall}$) of the obtained mixed brushes were in the range of 0.9 – 1.2 chains/nm^2. Transmission electron microscopy (TEM) studies showed that the feature sizes of the nanopatterns formed from lateral microphase separation of mixed brushes were significantly smaller than those formed from intermediate grafting density mixed P*t*BA/PS brushes ($\sigma_{overall}$ = ~ 0.6 chains/nm^2) prepared from silica particles that were surface modified with a monochlorosilane-terminated Y-initiator.[15a]

The work presented in this Chapter was inspired by the theoretical prediction of Zhulina and Balazs[4] and the aforementioned observations reported in the previous publications from our group;[15] we sought to elucidate the effect of overall grafting density on the ripple wavelength of the nanopattern formed from lateral microphase separation of mixed brushes through a systematic study. By varying the mass ratio of a triethoxysilane-terminated Y-initiator to bare silica particles (Scheme 2.1) in the initiator immobilization step, we found that the overall grafting density of mixed brushes synthesized from initiator particles can be systematically tuned while the individual grafting densities of two polymers remained comparable. Transmission electron microscopy was then employed to study the nanostructures after the mixed brush-grafted particles were cast onto carbon-coated TEM grids, annealed with $CHCl_3$ vapor, and stained with RuO_4 vapor. $CHCl_3$ is a good solvent for both P*t*BA and PS. The ripple wavelength (*D*) was found to gradually increase with the decrease of $\sigma_{overall}$, and a scaling relationship

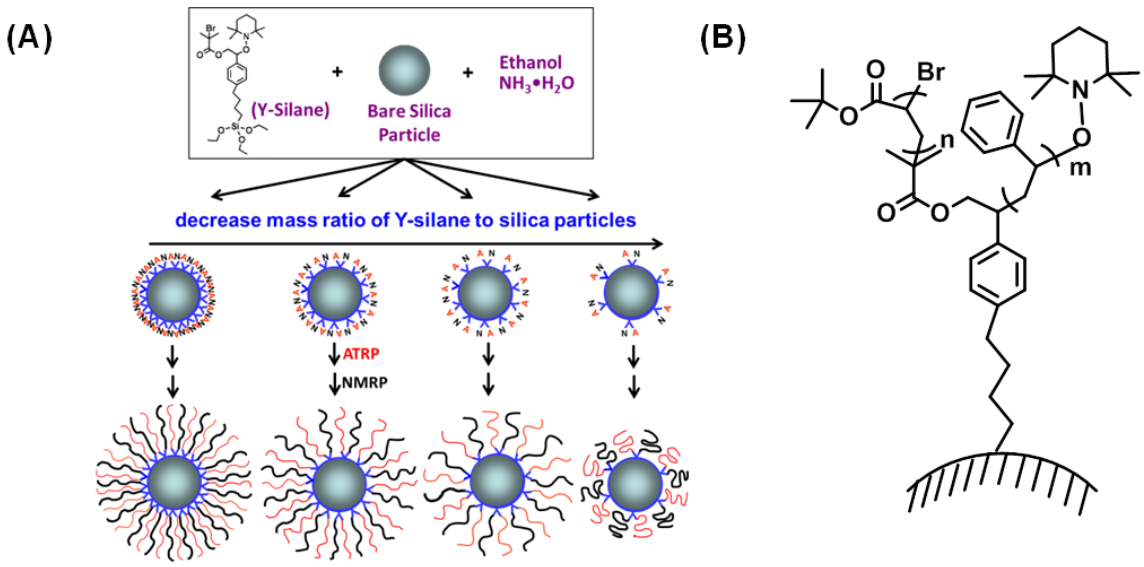

Scheme 2.1 (A) Synthesis of mixed homopolymer brushes with various overall grafting densities by changing the mass ratio of Y-initiator to silica particles in the initiator immobilization step via an ammonia-catalyzed hydrolysis/condensation process (B) Schematic illustration of mixed poly(*tert*-butyl acrylate) (P*t*BA)/polystyrene (PS) mixed brushes on silica particles

between D and $\sigma_{overall}$ was obtained. In addition, when the grafting density was sufficiently low, no microphase separation was observed.

2.2 Experimental Section

2.2.1 Materials

Tetraethyl orthosilicate (98%), ammonium hydroxide (25% in water), triethoxysilane (95%), and 2,2,6,6-tetramethylpiperidinooxy (TEMPO) were purchased from Acros Organics and used as received. Platinum-divinyltetramethyldisiloxane complex in xylene (2.1~2.4% Pt concentration in xylene) was obtained from Gelest, Inc. 2-[4-(But-3-enyl)phenyl]-2-(2',2',6',6'-tetramethyl-1'-piperidinyloxy)ethyl 2-bromo-2-methylpropanoate (Y-silane precursor) was prepared according to a procedure described in a previous publication from our group.[12f] Styrene (99%, Aldrich) and *tert*-butyl acrylate (*t*-BA, 99%, Aldrich) were dried with CaH_2, distilled under reduced pressure, and passed through a basic alumina column to remove the inhibitor. The purified monomers were stored in solvent storage flasks in a refrigerator prior to use. CuBr (98%, Aldrich) was stirred in glacial acetic acid overnight, filtered, and washed with absolute ethanol and ethyl ether. The salt was then collected, dried under vacuum, and stored in a desiccator. *N*, *N*, *N'*, *N'*, *N''*-Pentamethyldiethylenetriamine (99 %, Aldrich) and ethyl 2-bromoisobutyrate were dried with calcium hydride, distilled under a reduced pressure, and stored in a desiccator. 1-Phenyl-1-(2',2',6',6'-tetramethyl-1'-piperidinyloxy)ethane (STEMPO), an initiator for NMRP, was prepared by following a procedure from the literature.[16] All other chemical reagents were purchased from either Aldrich or Fisher and used without further purification.

2.2.2 General Characterization

Size exclusion chromatography (SEC) was carried out at ambient temperature using PL-GPC 20 (an integrated SEC system from Polymer Laboratories, Inc.) with a refractive index detector, one PLgel 5 μm guard column (50 × 7.5 mm), and two PLgel 5 μm mixed-C columns (each 300 × 7.5 mm, linear range of molecular weight from 200 to 2,000,000 according to Polymer Laboratories, Inc.). THF was used as the carrier solvent at a flow rate of 1.0 mL/min. Polystyrene standards (Polymer Laboratories, Inc.) were employed for calibration. The data were processed using Cirrus GPC/SEC software (Polymer Laboratories, Inc.). ^{1}H NMR spectra were recorded on a Varian Mercury 300 MHz NMR spectrometer. Thermogravimetric analysis (TGA) was performed in air at a heating rate of 20 ℃/min from room temperature to 800 ℃ using TA Q-series Q50. The particle samples for TGA were dried at 45 ℃ in vacuum for at least 5 h.

2.2.3 Synthesis of Bare Silica Particles

Ammonium hydroxide (25 % in water, 19.909 g) and tetraethyl orthosilicate (TEOS, 10.504 g) were each mixed with 10 mL of ethanol. The two solutions were then added into a 500 mL one-necked flask that contained 280 mL of ethanol under the stirring condition. The concentrations of NH_3, TEOS, and water in the solution were 0.43 M, 0.15 M, 2.92 M, respectively. The mixture was stirred vigorously at room temperature for 5.5 h. The particles were isolated by centrifugation (Eppendorf 5804 Centrifuge, 8000 rpm), redispersed in ethanol, and centrifugated again. This washing process was repeated with ethanol an additional two times, water two times, and ethanol again. The particles were dried with a stream of air flow (3.20 g). The average diameter of silica particles, measured by transmission electron microscopy, was 173 nm. The bare silica particles were used to prepare Y-initiator-functionalized silica particles.

2.2.4 Synthesis of Y-Initiator-Functionalized Silica Particles

The triethoxysilane-terminated Y-initiator (Y-silane, Scheme 2.1) was immobilized onto the surface of silica particles via a hydrolysis/condensation process. The following is the procedure for the preparation of Y-initiator-functionalized silica particles, Y-Particle-4 (Table 2.1), which were used for the synthesis of mixed P*t*BA/PS brush-grafted particles with an overall grafting density of 0.68 chains/nm^2 (MB-4). Other initiator particles were made by using the same procedure except different amounts of Y-initiator (i.e., different mass ratios of Y-initiator to bare silica particles).

2-[4-(But-3-enyl)phenyl]-2-(2',2',6',6'-tetramethyl-1'-piperidinyloxy)ethyl 2-bromo-2-methylpropanoate (Y-silane precursor, 65.9 mg, 0.138 mmol) was added into a 25 mL two-necked flask and dried at room temperature in vacuum for 1 h. Triethoxysilane (1.8 mL, 9.8 mmol) was added by a disposable plastic syringe into the flask under the N_2 atmosphere, followed by the injection of Pt complex in xylene (50 μL) using a microsyringe. The mixture was stirred at 45 °C under the nitrogen atmosphere; the hydrosilylation reaction was monitored by ^{1}H NMR spectroscopy analysis. Once the reaction was complete, excess triethoxysilane was removed under high vacuum at 45 °C, and the product,Y-silane, was used directly in the next step for the preparation of Y-initiator-functionalized silica particles (Y-Particle-4).

Bare silica particles (0.151 g) were dispersed in ethanol (14.0 mL) by ultrasonication to form a homogenous, stable dispersion. A solution of ammonia (25% in water, 1.098 g) in ethanol (5.2 mL) was added dropwise into the particle dispersion. After the mixture was stirred at 40 °C for 2 h, a solution of Y-silane freshly synthesized from 65.9 mg of Y-silane precursor in ethanol (3.0 mL) was added dropwise into the dispersion. After the reaction mixture was stirred at 40 °C for 19 h, the particles were isolated by centrifugation and re-dispersed in THF. This process was

repeated for a total of five times. The obtained Y-initiator particles were then dried with a stream of N_2 flow and used for the preparation of mixed homopolymer brush-grafted silica particles (MB-4).

2.2.5 Synthesis of P*t*BA Brush-Grafted Silica Particles

The Y-initiator particles (Y-Particle-4, 51.8 mg) were added into a 25 mL two-necked flask and dried under high vacuum at 35 °C overnight. The initiator particles were then dispersed in anisole (3.5 mL) by ultrasonication to form a stable dispersion. CuBr (22.5 mg, 0.157 mmol), *tert*-butyl acrylate (*t*BA, 12.006 g, 93.7 mmol), *N*,*N*,*N*′,*N*′,*N*″-pentamethyldiethylenetriamine (27.5 mg, 0.157 mmol), and ethyl 2-bromoisobutyrate (EBiB, 30.1 mg, 0.154 mmol) were added into a 50 mL three-necked flask and stirred under a N_2 atmosphere. The particle dispersion was then transferred into the 50 mL flask using a syringe, and the mixture was degassed immediately by three freeze−pump−thaw cycles. The flask was then placed into a 75 ℃ oil bath, and the polymerization was monitored by SEC and ^{1}H NMR spectroscopy analysis. After 64 h, the flask was removed from the oil bath and opened to air. THF (~10 mL) was added into the flask to dilute the mixture. The particles were isolated by centrifugation, and the supernatant was passed through a column of neutral, activated aluminum oxide to remove the copper catalyst. The particles were redispersed in THF. The dispersion was left to stand still at ambient conditions overnight, and the green precipitate was removed. The P*t*BA brush-grafted silica particles were separated by centrifugation again. This washing process was repeated with THF five times, followed by drying of the hairy particles with a stream of air flow. The $M_{n,SEC}$ and polydispersity index (PDI) of the free P*t*BA formed from free initiator EBiB in the polymerization were 22.9 kDa and 1.09, respectively, determined from SEC using PS as standards.

2.2.6 Preparation of Mixed P*t*BA/PS Brush-Grafted Silica Particles from P*t*BA Brush-Grafted Silica Particles with P*t*BA $M_{n,SEC}$ of 22.9 kDa

The P*t*BA brush-grafted silica particles (P*t*BA $M_{n,SEC}$ = 22.9 kDa, 19.1 mg) were dispersed in anisole (10.0 mL) in a 25 mL two-necked flask using an ultrasonic water bath. The particle dispersion was then transferred into a 50 mL three-necked flask that contained free initiator 1-phenyl-1-(2',2',6',6'-tetramethyl-1'-piperidinyloxy)ethane (STEMPO, 49.1 mg, 0.188 mmol) and 2,2,6,6,-tetramethylpiperidinooxy (TEMPO, 3.2 mg), followed by the addition of styrene (15.017 g, 144.2 mmol). After the mixture was degassed by three freeze-pump-thaw cycles, the flask was placed into a 120 °C oil bath. The polymerization was monitored by ^{1}H NMR spectroscopy and SEC. When the molecular weight of the free polystyrene reached the desired value, the polymerization was stopped by removing the flask from the oil bath and diluting the mixture with THF. The mixed P*t*BA/PS brushed-grafted particles were isolated by centrifugation, redispersed in THF, and centrifugated again. This washing process was repeated four times to remove the physically adsorbed polymer. The particles were then dried with a stream of N_2 flow. The $M_{n,SEC}$ and PDI of the free polystyrene, measured by SEC, were 22.2 kDa and 1.16, respectively. Other mixed P*t*BA/PS brush-grafted silica particle samples and the corresponding P*t*BA brush-grafted silica particles were synthesized by using similar procedures.

2.2.7 Transmission Electron Microscopy (TEM) Study of Mixed P*t*BA/PS Brush-Grafted Silica Particles

Chloroform, a good solvent for both P*t*BA and PS, was used to prepare the particle dispersions. For each sample, ~ 1 mg of mixed P*t*BA/PS brush-grafted silica particles was dispersed in 1 mL of chloroform in a small vial by ultrasonication in an ultrasonic water bath for 5 min. The particle dispersion was drop cast onto a carbon-coated, copper TEM grid using a

glass pipette and was allowed to dry at ambient conditions. The TEM samples were annealed with $CHCl_3$ vapor at room temperature as detailed below. The sample-loaded TEM grids were placed in a small glass dish with a diameter of 2". The dish was then transferred into a glass jar that contained ~ 2 mL of $CHCl_3$. The jar was covered with a watch glass. After being annealed by $CHCl_3$ vapor at room temperature for at least 3 h, the samples were removed from the jar, allowed to dry at ambient conditions for 30 min, and then stained with RuO_4 at room temperature for 20 min. TEM experiments were performed on FEI Tecnai T12 at an accelerating voltage of 100 kV and bright field images were taken with a bottom-mounted Gatan CCD camera. The image analysis was performed using Nano Measurer 1.2 software.

2.3 Results and Discussion

2.3.1 Synthesis of Mixed P*t*BA/PS Brushes with Various Overall Grafting Densities

To systematically study the effect of overall grafting density ($\sigma_{overall}$) on microphase separation of mixed brushes and to reveal the relation between $\sigma_{overall}$ and ripple wavelength of the nanopattern, it is necessary to synthesize a series of mixed brushes with different overall grafting densities but similar molecular weights and comparable individual grafting densities for the two homopolymers. Our group previously reported the synthesis of high grafting density mixed P*t*BA/PS brushes ($\sigma_{overall}$ = ~ 1.1 chains/nm^2) by using a triethoxysilane-terminated Y-initiator to functionalize silica particles.[15b] This method of immobilizing the Y-initiator onto the surface of silica particles is similar to that reported by Ohno et al. for the fixation of an ATRP initiator.[17] The key is the ammonia-catalyzed hydrolysis and condensation of the initiator-terminated triethoxysilane on the surface of bare silica particles in ethanol, yielding a high density initiator layer and hence high grafting density polymer brushes.

It is worth noting here that in that work a large amount of Y-initiator, 108.8 wt % with respect to silica particles with an average size of 172 nm, was used for the synthesis of high grafting density mixed P*t*BA/PS brushes.[15b] We reasoned that by gradually changing the mass ratio of Y-initiator to silica particles with the same or a similar size in the initiator immobilization step, the Y-initiator density on the surface of silica particles would be different, which would lead to different overall grafting densities for mixed brushes. Therefore, we set out to make a series of Y-initiator particles from the same batch of bare silica particles with an average diameter of 173 nm by using different mass ratios of Y-initiator to silica particles. The other reaction conditions were kept identical. The bare silica particles were synthesized by the standard Stöber process, which is known to produce silica particles with a relatively uniform size distribution.[18] The mass ratio of Y-silane precursor to bare silica particles ranged from ~ 86% to ~ 8% (Y-Particle-2 to -7, Table 2.1). The triethoxysilane-terminated Y-initiator was prepared by a platinum-catalyzed hydrosilylation reaction of 2-[4-(but-3-enyl)phenyl]-2-(2',2',6',6'-tetramethyl-1'-piperidinyloxy)ethyl 2-bromo-2-methylpropanoate (the Y-silane precursor) with triethoxysilane ($HSi(OC_2H_5)_3$). For all initiator particles, the immobilization of Y-initiator onto the surface of silica particles was carried out at 40 °C for 19 h. The initiator particles were then isolated and repeatedly washed. For comparison, we also included in Table 2.1 the preparation of Y-initiator particles (Y-Particle-1) from 172 nm bare silica particles for the synthesis of high grafting density mixed brushes reported in Ref. 15b.

The Y-initiator particles were then used to grow mixed P*t*BA/PS brushes with molecular weights of ~ 23 kDa for both polymers by following the established protocol from our laboratory.[12f,15] P*t*BA was grown first by surface-initiated ATRP of *tert*-butyl acrylate in anisole at 75 ℃ using CuBr/*N*, *N*, *N'*, *N'*, *N''*-pentamethyldiethylenetriamine (PMDETA) as catalyst and

Table 2.1 Characterization Data for a Series of Mixed P*t*BA/PS Brush-Grafted Particle Samples with Different Overall Grafting Densities and Reaction Conditions for the Preparation of Corresponding Y-initiator-Functionalized Silica Particles

Initiator Particle	Mass Ratio of Y-Initiator to Particles[a]	Mixed Brushes	$M_{n,SEC}$ and PDI of P*t*BA[b]	$M_{n,SEC}$ and PDI of PS[b]	σ_{PtBA}, σ_{PS}, and $\sigma_{overall}$ (chains/nm^2)[c]
Y-Particle-1[d]	108.8 %	MB-1	18600, 1.09	19400,1.14	0.63, 0.43, 1.06
Y-Particle-2	85.8 %	MB-2	23600, 1.09	23500, 1.17	0.63, 0.40, 1.03
Y-Particle-3	86.6 %	MB-3	25200, 1.09	21900, 1.14	0.45, 0.50, 0.95
Y-Particle-4	43.7 %	MB-4	22900, 1.09	22200, 1.16	0.36, 0.32, 0.68
Y-Particle-5	32.1 %	MB-5	21300, 1.10	20700, 1.25	0.31, 0.23, 0.54
Y-Particle-6	15.6 %	MB-6	23000, 1.09	21900, 1.14	0.14, 0.20, 0.34
Y-Particle-7	8.13 %	MB-7	22100, 1.10	23500, 1.15	0.10, 0.022, 0.122
NA[e]	NA	MB-8	24500, 1.11	24900, 1.17	0.36, 0.27, 0.63

[a] The mass ratio of Y-silane precursor to bare silica particles used in the preparation of corresponding Y-initiator-functionalized silica particles. [b] The values of number average molecular weight ($M_{n,SEC}$) and polydispersity index (PDI) were determined by size exclusion chromatography (SEC) using polystyrene standards for calibration. [c] σ_{PtBA}, σ_{PS}, and $\sigma_{overall}$ are P*t*BA grafting density, PS grafting density, and overall grafting density ($\sigma_{overall} = \sigma_{PtBA} + \sigma_{PS}$). The grafting densities were calculated by using TGA data and molecular weights of P*t*BA and PS. [d] The synthesis of Y-particle-1 and the corresponding mixed P*t*BA/PS brushes MB-1 was detailed in Ref. 15b. The average size of bare silica particles used to prepare Y-particle-1 was 172 nm, essentially the same as bare particles for Y-particle-2 to -7. [e] The Y-initiator-functionalized 160 nm silica particles used to synthesize MB-8 were made by using a monochlorosilane-terminated Y-initiator.[15a]

ethyl 2-bromoisobutyrate (EBiB) as free initiator. The TEMPO group in the Y-initiator was previously confirmed to be stable under this ATRP condition.[12f] The addition of a free initiator into the polymerization mixtures allowed the surface-initiated polymerizations to be controlled by the solution polymerizations. In addition, the polymerizations can be conveniently monitored by taking samples from the reaction mixtures. The polymerizations were stopped when the molecular weights of the free P*t*BA reached the desired values. The P*t*BA brush-grafted silica particles were then repeatedly washed to remove the physically absorbed free polymer and characterized by thermogravimetric analysis (TGA).

Mixed P*t*BA/PS brushes were obtained by growing PS from P*t*BA brush-grafted silica particles via surface-initiated nitroxide-mediated polymerizations, which were carried out in anisole at 120 °C. Again, a free initiator, 1-phenyl-1-(2',2',6',6'-tetramethyl-1'-piperidinyloxy)ethane (STEMPO), was added into the reaction mixtures to facilitate the control of surface-initiated polymerizations. The mixed P*t*BA/PS brush-grafted silica particle samples were purified and analyzed by TGA to determine the polymer contents. Figure 2.1 shows the TGA data of six mixed P*t*BA/PS brush-grafted silica particle samples (MB-2 to -7 in Table 2.1) along with the corresponding Y-initiator particles and P*t*BA brush-grafted silica particles. It has been established that the molecular weight and molecular weight distribution of polymer brushes on silica particles synthesized by surface-initiated "living"/controlled radical polymerization, including high density homopolymer brushes (σ = 0.65 – 0.90 chains/nm^2) and mixed homopolymer brushes, are essentially identical to those of the free polymer formed from the free initiator.[12f,17] By using the size of silica particles (173 nm), TGA data, and the molecular weights of P*t*BA and PS, and assuming that the density of silica particles was identical to that of bulk SiO_2 (2.07 g/cm^3), the grafting densities of P*t*BA (σ_{PtBA}) and PS (σ_{PS}) on silica particles were

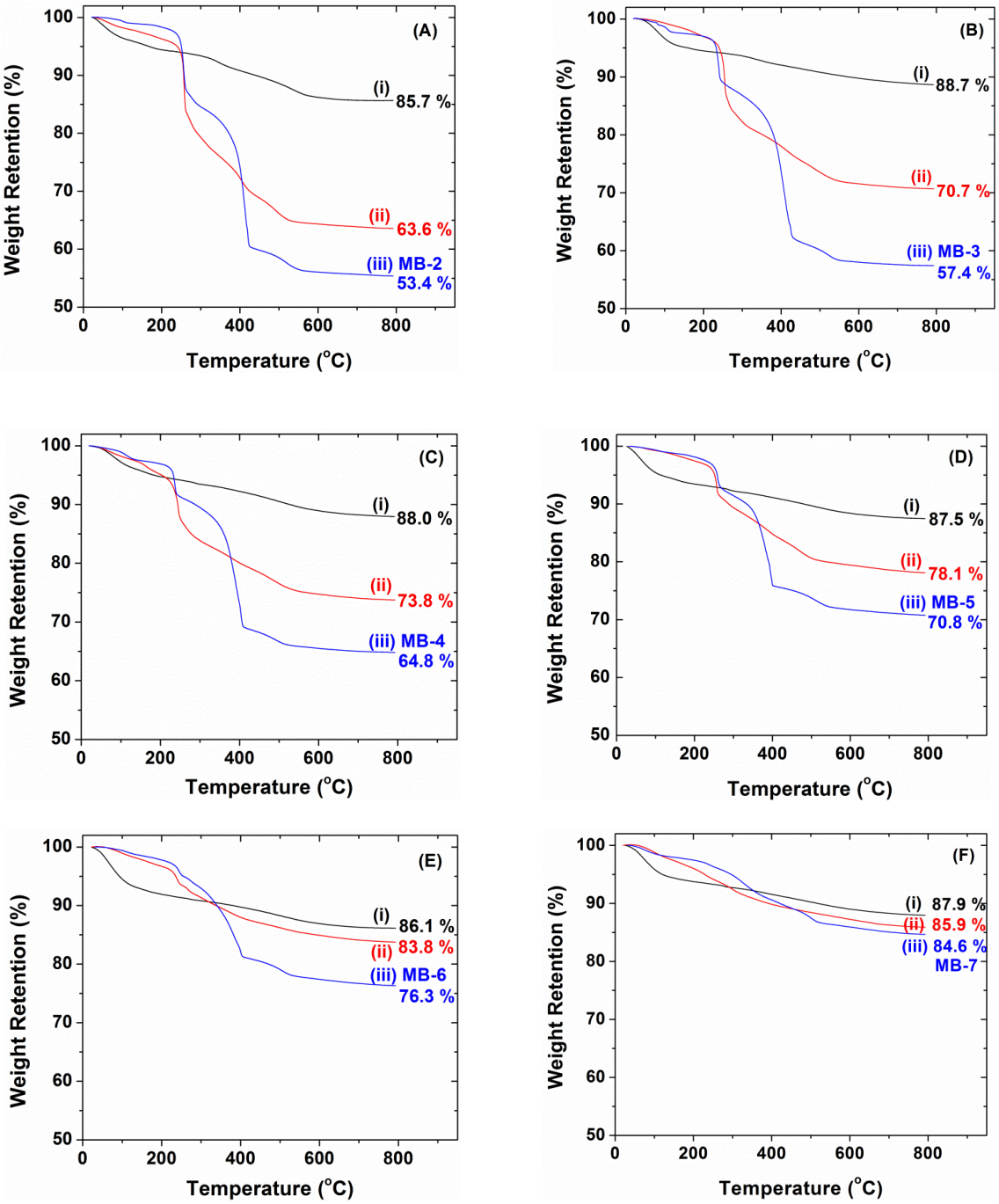

Figure 2.1 Thermogravimetric analysis (TGA) of (i) Y-initiator-functionalized silica particles, (ii) P*t*BA brush-grafted silica particles, and (iii) mixed P*t*BA/PS brush-grafted silica particles obtained in the preparation of mixed brush-grafted particle sample (A) MB-2, (B) MB-3, (C) MB-4, (D) MB-5, (E) MB-6, and (F) MB-7.

calculated and summarized in Table 2.1.[19] The overall grafting density ($\sigma_{overall}$) for each sample, which is the sum of grafting densities of two polymers ($\sigma_{PtBA} + \sigma_{PS}$), is also included.

Figure 2.2 shows the plots of overall grafting density of mixed brushes ($\sigma_{overall}$) and individual grafting densities of P*t*BA and PS (σ_{PtBA} and σ_{PS}) versus mass ratio of Y-initiator to silica particles used in the preparation of Y-initiator-functionalized silica particles. Clearly, there is a correlation between $\sigma_{overall}$ of mixed brushes and mass ratio of Y-initiator to silica particles; the higher the ratio, the higher the overall grafting density. From Table 2.1 and Figure 2.2, one can also find that the σ_{PtBA} and σ_{PS} are similar in most of mixed brush particle samples. For MB-1 and -2, σ_{PtBA} is larger than σ_{PS} by ~ 0.20 chains/nm^2, which could be due to the steric hindrance presented by the existing P*t*BA chains in the growth of PS chains. For the lowest overall grafting density sample (MB-7), the disparity between σ_{PtBA} (0.10 chains/nm^2) and σ_{PS} (0.022 chains/nm^2) may partly come from the inherent uncertainty in TGA analysis. We cleaved the grafted mixed P*t*BA/PS brushes from sample MB-7 by HF and collected the polymer mixture. ^{1}H NMR spectroscopy analysis showed that the molar ratio of P*t*BA to PS units was 100 to 64.3, which corresponded to the molar ratio of P*t*BA and PS chains of 100 to 54.5 (= ratio of grafting densities of P*t*BA and PS). If the overall grafting density is still 0.122 chains/nm^2, the individual grafting densities of P*t*BA and PS would be 0.079 and 0.043 chains/nm^2, respectively. Since our focus in this work is the effect of overall grafting density on ripple wavelength of the nanopattern formed from lateral microphase separation of mixed brushes, the small difference in the grafting densities of two polymers should not affect the ripple wavelength much because many simulation works have shown that the lateral microphase separation can tolerate small variations in grafting densities and molecular weights of two end-tethered homopolymers.[6]

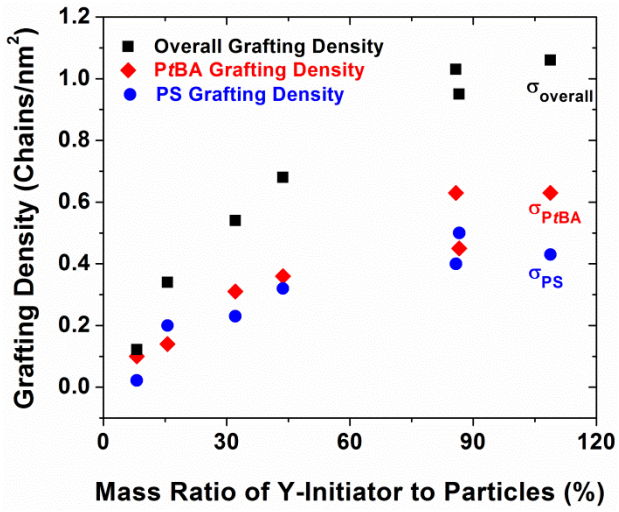

Figure 2.2 Plots of overall grafting density of mixed P*t*BA/PS brushes ($\sigma_{overall}$, black solid square), grafting density of P*t*BA (σ_{PtBA}, red solid diamond), and grafting density of PS (σ_{PS}, blue solid circle) on silica particles versus mass ratio of Y-initiator to silica particles used in the process of immobilizing the Y-initiator onto the surface of bare silica particles.

2.3.2 TEM Study of Mixed P*t*BA/PS Brushes with Various Overall Grafting Densities

For TEM study of microphase separation, mixed P*t*BA/PS brush-grafted silica particle samples were dispersed in $CHCl_3$, a good solvent for both P*t*BA and PS, and drop cast onto carbon-coated TEM copper grids. The TEM samples were then annealed with $CHCl_3$ vapor in a closed container for at least 3 h and stained with RuO_4 vapor at room temperature for 20 min. Note that RuO_4 vapor selectively stains PS, making PS and P*t*BA nanodomains appear dark and bright, respectively, under TEM.[14] It was previously showed that without staining with RuO_4 the nanostructures formed from microphase separation of mixed P*t*BA/PS brushes cannot be seen.[14a] Figure 2.3 shows representative top-view bright field TEM micrographs of six mixed P*t*BA/PS brush samples (MB-2 to -7) and a TEM image of MB-1 from Ref. 15b,[20] which are arranged in the order of decreasing the overall grafting density of mixed brushes. Clearly, in samples of MB-2 to -5, mixed P*t*BA/PS brushes were microphase separated, forming rippled nanostructures composed of dark PS and bright P*t*BA nanostripes. This is consistent with the previous observations that nearly symmetric mixed brushes underwent lateral microphase separation[15] and also with the results from computer simulations.[6] By looking through the TEM micrographs in Figure 2.3, one can easily recognize that the feature size gradually increases with the decrease of overall grafting density, which is qualitatively in agreement with the prediction of Zhulina and Balazs.[4] The nanopatterns formed by MB-2 and -3 (Figures 2.3B and C) are similar to that of MB-1, the sample that has the highest overall grafting density. On the other hand, the feature size of MB-5 with $\sigma_{overall}$ of 0.54 chains/nm^2 in Figure 2.3E is apparently larger with a typical ripple wavelength of ~ 19 nm. This is very similar to the nanopattern formed by intermediate grafting density mixed P*t*BA/PS brushes on 160 nm silica particles ($\sigma_{overall}$ = ~ 0.60 chains/nm^2) that our

Figure 2.3 Top-view bright field TEM micrographs of (A) MB-1 (P*t*BA M_n = 18.6 kDa, σ_{PtBA} = 0.63 chains/nm^2; PS M_n = 19.4 kDa, σ_{PS} = 0.43 chains/nm^2; $\sigma_{overall}$ = 1.06 chains/nm^2), (B) MB-2 (P*t*BA M_n = 23.6 kDa, σ_{PtBA} = 0.63 chains/nm^2; PS M_n = 23.5 kDa, σ_{PS} = 0.40 chains/nm^2; $\sigma_{overall}$ = 1.03 chains/nm^2), (C) MB-3 (P*t*BA M_n = 25.2 kDa, σ_{PtBA} = 0.45 chains/nm^2; PS M_n = 21.9 kDa, σ_{PS} = 0.50 chains/nm^2; $\sigma_{overall}$ = 0.95 chains/nm^2), (D) MB-4 (P*t*BA M_n = 22.9 kDa, σ_{PtBA} = 0.36 chains/nm^2; PS M_n = 22.2 kDa, σ_{PS} = 0.32 chains/nm^2; $\sigma_{overall}$ = 0.68 chains/nm^2), (E) MB-5 (P*t*BA M_n = 21.3 kDa, σ_{PtBA} = 0.31 chains/nm^2; PS M_n = 20.7 kDa, σ_{PS} = 0.23 chains/nm^2; $\sigma_{overall}$ = 0.54 chains/nm^2), (F) MB-6 (P*t*BA M_n = 23.0 kDa, σ_{PtBA} = 0.14 chains/nm^2; PS M_n = 21.9 kDa, σ_{PS} = 0.20 chains/nm^2; $\sigma_{overall}$ = 0.34 chains/nm^2), and (G) MB-7 (P*t*BA M_n = 22.1 kDa, σ_{PtBA} = 0.10 chains/nm^2; PS M_n = 23.5 kDa, σ_{PS} = 0.022 chains/nm^2; $\sigma_{overall}$ = 0.122 chains/nm^2) after being cast from $CHCl_3$ dispersions and annealed with $CHCl_3$ vapor for at least 3 h. The samples were stained with RuO_4 vapor at room temperature for 20 min.

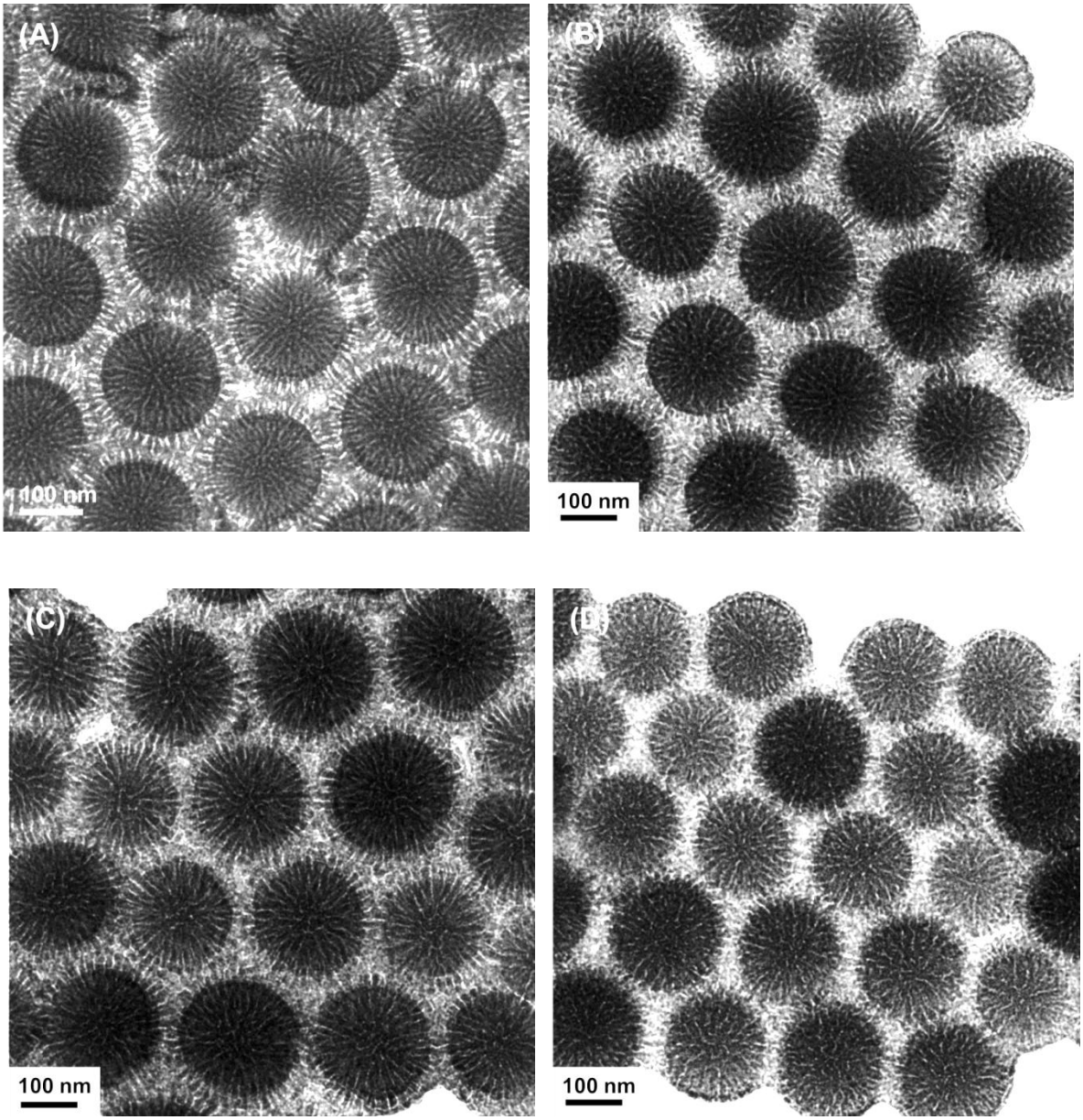

(Figure 2.3 continued)

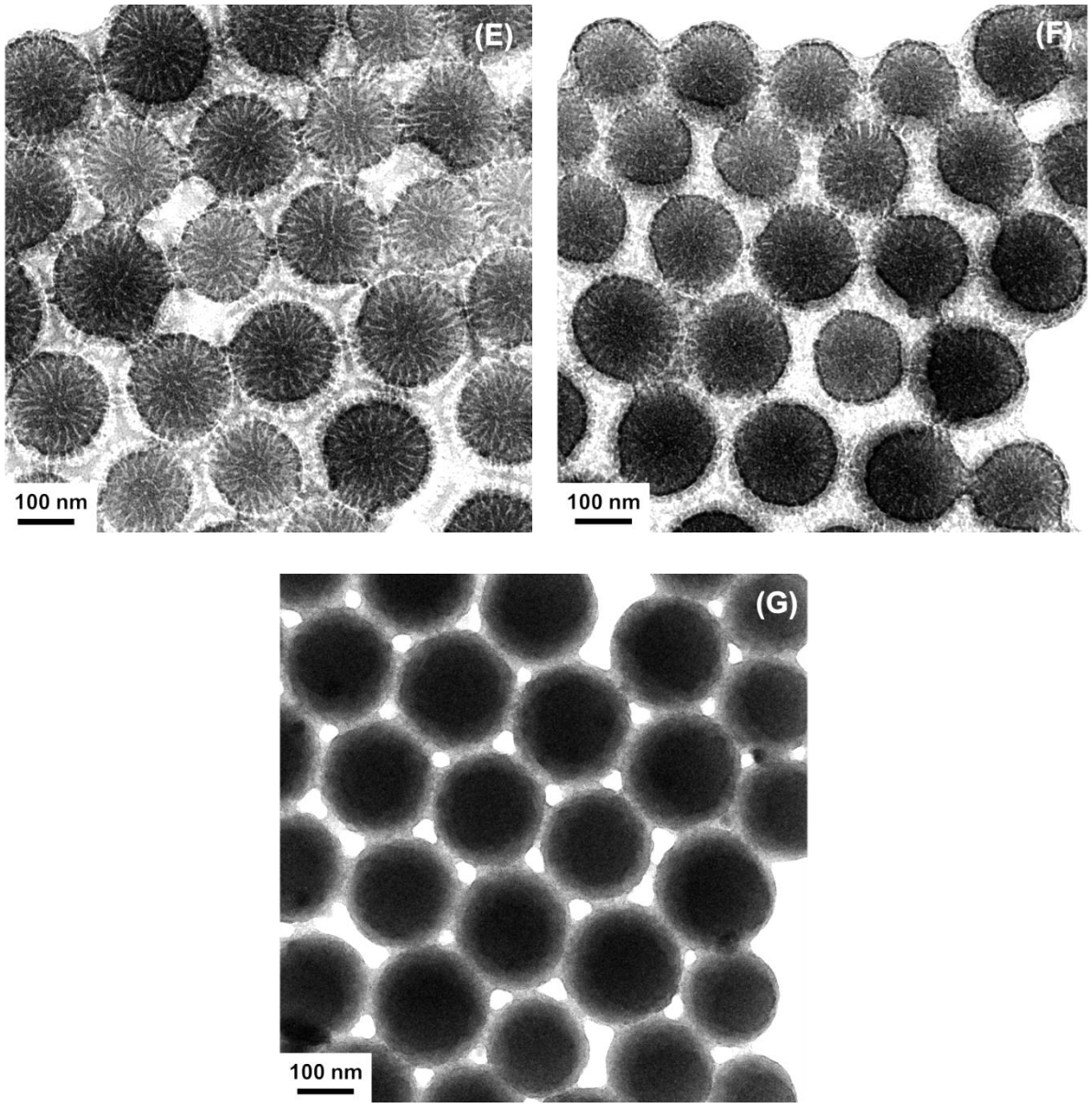

(Figure 2.3 continued)

group reported before.[15a] Thus, these new results corroborate the previous observations on lateral microphase separation of high and intermediate grafting density mixed P*t*BA/PS brushes.[15]

Although in MB-6 dark and bright domains are still discernible (Figure 2.3F), the nanopattern is not as clear as in MB-5 (Figure 2.3E); the driving force for phase separation in MB-6 appears to become weaker. Interestingly, while the polymer brushes can be clearly seen between and among particles, no microphase separated nanostructures are observed in MB-7 (Figure 2.3G); the two grafted polymers were in the miscible state. We believe that the low $\sigma_{overall}$ and the fluctuation of grafting sites should be responsible for these observations. With the decrease of $\sigma_{overall}$ to a certain degree, the microphase separation may become unfavorable because phase separation involves further stretching of polymer chains. The entropy loss associated with lateral phase separation may not be compensated by the enthalpy gain. Consequently, the miscible state is the one having the lowest Gibbs free energy. This should be the case for MB-7.[21] On the other hand, the increased fluctuation of grafting sites may also contribute to the weakened lateral microphase separation of MB-6 and no phase segregation of MB-7. With the decrease of the amount of Y-initiator used in the preparation of Y-initiator-functionalized silica particles (only 15.6 wt % and 8.13 wt % of Y-initiator were used for MB-6, and -7, respectively), the fluctuation of Y-initiator density on the surface of silica particles may not be negligible, i.e., the Y-initiator and thus the grafted P*t*BA and PS chains may not be uniformly distributed on the surface of particles. With the departure from the symmetric composition, a higher interaction strength is required for microphase separation, which can be seen from the shape of the phase diagram of diblock copolymers.[22] The simulation work of Wenning et al. suggested that the density and composition fluctuations of grafting points enhance the formation of irregular nanostructures and prevent the appearance of long-range order.[5e]

Using software Nano Measurer 1.2, we conducted image analysis of TEM micrographs A-E in Figure 2.3 by selecting the features in the area between the half radius ($R/2$) and the periphery (R) from the particle center (i.e., the edge view of the particles). As can be seen from Figure 2.3A to E, the features in this area tend to be clearer, which would make the analysis more accurate. The results are presented in Figure 2.4 as plots of counts versus ripple wavelength (sum of widths of neighboring P*t*BA and PS stripes). As expected, the average ripple wavelength increases with the decrease of $\sigma_{overall}$, from 12.8 nm for MB-1, to 14.6 nm for MB-2, to 15.9 nm for MB-3, to 17.4 nm for MB-4, and 18.5 nm for MB-5.

The molecular weights of P*t*BA and PS in mixed brush samples MB-1 to -5 are not exactly the same. Theoretical studies have shown that the ripple wavelength of the nanopattern formed from lateral phase separation of mixed brushes is proportional to the square root of molecular weight.[4] Therefore, to better compare the ripple wavelength and extract the scaling relationship between ripple wavelength and $\sigma_{overall}$, we normalized the average ripple wavelengths from TEM image analysis by using the molecular weights of P*t*BA and PS of mixed brushes MB-4 as reference. That is, normalized ripple wavelength = average ripple wavelength/$\{[(M_{n,SEC\text{-}PtBA} + M_{n,SEC\text{-}PS})/(M_{n,SEC\text{-}PtBA\text{-}4} + M_{n,SEC\text{-}PS\text{-}4})]^{1/2}\}$. The results are included in Table 2.2. To help obtain the relation between ripple wavelength and $\sigma_{overall}$, we also analyzed a TEM image of an intermediate grafting density mixed P*t*BA/PS brush sample (MB-8 in Table 2.1, the TEM picture is included in the Appendix A) from Ref. 15b. As can be seen from Table 2.2, the normalized average wavelength (D_N) also increased with the decrease of overall grafting density.

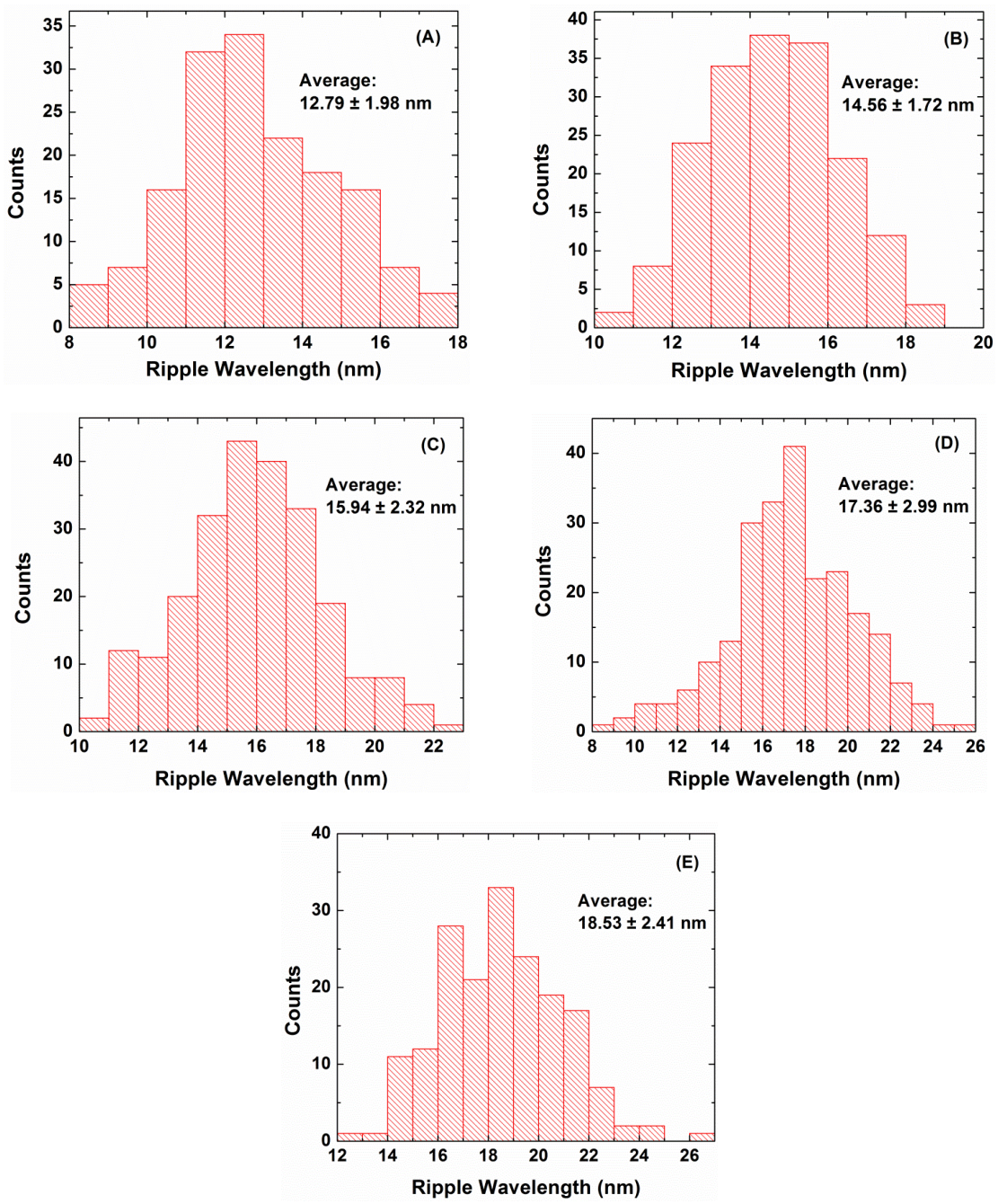

Figure 2.4 Distributions of ripple wavelengths of features (sum of widths of neighboring P*t*BA and PS stripes) obtained from TEM image analysis of (A) Figure 2.3A, MB-1, (B) Figure 2.3B, MB-2, (C) Figure 2.3C, MB-3, (D) Figure 2.3D, MB-4, and (E) Figure 2.3E, MB-5.

Table 2.2 Average Ripple Wavelengths of Nanopatterns Formed by Lateral Microphase Separation of MB-1 to -5 and MB-8 from TEM Image Analysis and Average Ripple Wavelengths Normalized Against the Molecular Weights of MB-4

Mixed Brushes	$M_{n,SEC}$ of P*t*BA	$M_{n,SEC}$ of PS	$\sigma_{overall}$(chains/nm^2)	Average Ripple Wavelength (D), nm[a]	Normalized Ripple Wavelength (D_N), nm[b]
MB-1	18600	19400	1.06	12.8	13.9
MB-2	23600	23500	1.03	14.6	14.3
MB-3	25200	21900	0.95	15.9	15.6
MB-4	22900	22200	0.68	17.4	17.4
MB-5	21300	20700	0.54	18.5	19.2
MB-8[c]	24500	24900	0.63	19.5	18.6

[a] Average ripple wavelength obtained from image analysis of TEM micrographs (Figure 4).
[b] Normalized ripple wavelength = average ripple wavelength/{[($M_{n,SEC\text{-}PtBA} + M_{n,SEC\text{-}PS}$)/($M_{n,SEC\text{-}PtBA\text{-}4} + M_{n,SEC\text{-}PS\text{-}4}$)]$^{1/2}$}. [c] Mixed P*t*BA/PS brush-grafted silica particles (silica particle size = 160 nm) synthesized from silica particles functionalized by using a monochlorosilane-terminated Y-initiator (P*t*BA M_n = 24.5 kDa, PDI = 1.11, σ_{PtBA} = 0.36 chains/nm^2; PS M_n = 24.9 kDa, PDI = 1.17, σ_{PS} = 0.27 chains/nm^2).

Figure 2.5 shows the plot of D_N versus overall grafting density $\sigma_{overall}$ on a double logarithmic scale. A linear dependence of $\log D_N$ on $\log\sigma_{overall}$ with a slope of -0.47 was observed (linear fit R = 0.983), suggesting that in the range of overall grafting density of 0.54 – 1.06 chains/nm^2 the ripple wavelength scales with -0.47 power of overall grafting density, i.e., $D_N \sim \sigma_{overall}^{-0.47}$. This means that our experimentally observed D_N has a stronger dependence on $\sigma_{overall}$ than that predicted by Zhulina and Balazs ($D \sim \sigma_{overall}^{-1/6}$),[4] though the general trend is the same. The experimentally observed ripple wavelength appears to be approximately proportional to the distance between neighboring chains in the overall grafting density range of 0.54 – 1.06 chains/nm^2 for our system. The discrepancy observed here could arise from the different conditions used in our experiments and in the theoretical consideration. In our experiments, the mixed P*t*BA/PS brush-grafted particles were cast from a dispersion in $CHCl_3$, a good solvent for both polymers, and annealed with $CHCl_3$ vapor. In the theoretical study of Zhulina and Balazs,[4] the scaling relationship was obtained from perfect symmetric mixed brushes in nonselective poor solvents in the limit where the two polymers are highly incompatible and their grafting densities are high. In addition, our samples are not perfect Y-shaped mixed brushes. Nevertheless, our experimental results have revealed the basic feature of how the ripple wavelength of the nanopattern formed from lateral microphase separation of mixed homopolymer brushes changes with $\sigma_{overall}$.

2.4 Conclusions

A systematic study on the effect of overall grafting density on microphase separation of mixed P*t*BA/PS brushes grafted on 173 nm silica particles was carried out. By varying the mass ratio of Y-initiator to bare silica particles in the initiator immobilization step, a series of mixed

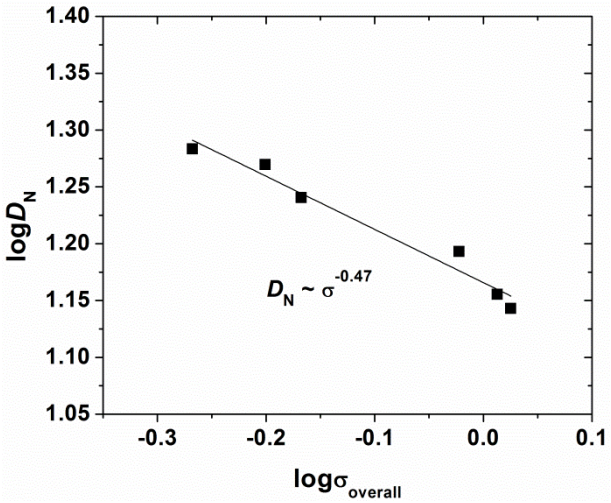

Figure 2.5 Plot of logD_N versus log$\sigma_{overall}$, where D_N is the normalized ripple wavelength and $\sigma_{overall}$ is the overall grafting density of mixed brushes. The straight solid line is a linear fit with R = 0.983 and a slope of -0.47.

P*t*BA/PS brushes with different overall grafting densities but similar molecular weights and similar individual grafting densities for the two polymers were obtained. The mixed brushes were grown by sequential ATRP of *t*BA and NMRP of styrene. TEM studies showed that the feature size of the nanopattern formed from lateral microphase separation increased with the decrease of overall grafting density. The normalized ripple wavelength was found to scale with $\sigma_{overall}^{-0.47}$ in the $\sigma_{overall}$ range of 0.54 – 1.06 chains/nm^2. When the grafting density was very low, no microphase separation was observed, presumably because at a very low grafting density the entropy loss from phase separation cannot be compensated by the enthalpy gain, resulting in the miscible state being favored. This is the first time that the effect of overall grafting density on lateral microphase separation of mixed homopolymer brushes was investigated. The results could provide a guide for potential applications of mixed homopolymer brushes.

References

1. Marko, J. F.; Witten, T. A. *Phys. Rev. Lett.* **1991,** *66*, 1541-1544.
2. (a) Marko, J. F.; Witten, T. A. *Macromolecules* **1992,** *25*, 296-307. (b) Dong, H. *J. Phys. II Fr.* **1993,** *3*, 999-1020. (c) Brown, G.; Chakrabarti, A.; Marko, J. F. *Europhys. Lett.* **1994,** *25*, 239-244. (d) Luzinov, I.; Minko, S.; Tsukruk, V. V. *Soft Matter* **2008**, *4*, 714-725.
3. Zhao, B.; Zhu, L. *Macromolecules* **2009**, *42*, 9369-9383.
4. Zhulina, E.; Balazs, A. C. *Macromolecules* **1996,** *29*, 2667-2673.
5. (a) Lai, P. Y. *J. Chem. Phys.* **1994,** *100*, 3351-3357. (b) Soga, K. G.; Zuckermann, M. J.; Guo, H. *Macromolecules* **1996,** *29*, 1998-2005. (c) Müller, M. *Phys. Rev. E* **2002,** *65*, 030802. (d) Minko, S.; Müller, M.; Usov, D.; Scholl, A.; Froeck, C.; Stamm, M. *Phys. Rev. Lett.* **2002,** *88*, 035502. (e) Wenning, L.; Müller, M.; Binder, K. *Europhys. Lett.* **2005**, *71*, 639-645. (f) Merlitz, H.; He, G. L.; Sommer, J. U.; Wu, C. X. *Macromolecules* **2009**, *42*, 445-451. (g) Egorov, S.A. *Soft Matter* **2012**, *8*, 3971-3979.
6. Wang, J.; Müller, M. *J. Phys. Chem. B.* **2009**, *113*, 11384-11402.
7. Roan, J.-R. *Phys. Rev. Lett.* **2006**, *96*, 248301.
8. Wang, Y. Q.; Yang, G. A.; Tang, P.; Qiu, F.; Yang, Y. L.; Zhu, L. *J. Chem. Phys.* **2011**, *134*, 134903.
9. Sidorenko, A.; Minko, S.; Schenk-Meuser, K.; Duschner, H.; Stamm, M. *Langmuir* **1999,** *15*, 8349-8355.
10. (a) Minko, S.; Usov, D.; Goreshnik, E.; Stamm, M. *Macromol. Rapid Commun.* **2001,** *22*, 206-211. (b) Lemieux, M.; Usov, D.; Minko, S.; Stamm, M.; Shulha, H.; Tsukruk, V. V. *Macromolecules* **2003,** *36*, 7244-7255. (c) Usov, D.; Gruzdev, V.; Nitschke, M.; Stamm, M.; Hoy, O.; Luzinov, I.; Tokarev, I.; Minko, S. *Macromolecules* **2007**, *40*, 8774-8783. (d)

Santer, S.; Kopyshev, A.; Yang, H. K.; Rühe, J. *Macromolecules* **2006,** *39*, 3056-3064. (e) Tsujii, Y.; Ohno, K.; Yamamoto, S.; Goto, A.; Fukuda, T. *Adv. Polym. Sci.* **2006**, *197*, 1-45.

11. (a) Minko, S.; Müller, M.; Motornov, M.; Nitschke, M.; Grundke, K.; Stamm, M. *J. Am. Chem. Soc.* **2003,** *125*, 3896-3900. (b) Ionov, L.; Minko, S.; Stamm, M.; Gohy, J. F.; Jerome, R.; Scholl, A. *J. Am. Chem. Soc.* **2003,** *125*, 8302-8306. (c) Ionov, L.; Sidorenko, A.; Stamm, M.; Minko, S.; Zdyrko, B.; Klep, V.; Luzinov, I. *Macromolecules* **2004**, *37*, 7421-7423. (d) LeMieux, M. C.; Julthongpiput, D.; Bergman, K. N.; Cuong, P. D.; Ahn, H. S.; Lin, Y. H.; Tsukruk, V. V. *Langmuir* **2004,** *20*, 10046-10054. (e) Julthongpiput, D.; Lin, Y. H.; Teng, J.; Zubarev, E. R.; Tsukruk, V. V. *Langmuir* **2003,** *19*, 7832-7836. (f) Filimon, M.; Kopf, I.; Ballout, F.; Schmidt, D. A.; Bründermann, E.; Rühe, J.; Santer, S.; Havenith, M. *Soft Matter*, **2010**, *6*, 3764-3768. (g) Estillore, N. C.; Advincula, R. C. *Langmuir* **2011**, *27*, 5997-6008. (h) Ochsmann, J. W.; Lenz, S.; Lellig, P.; Emmerling, S. G. J.; Golriz, A. A.; Reichert, P.; You, J.; Perlich, J.; Roth, S. V.; Beger, R.; Gutmann, J. S. *Macromolecules* **2012**, *45*, 3129-3136. (i) Zhang, P.; Jiang, K.; Ye, C.; Zhao, Y. L. *Chem Commun.* **2011**, *47*, 9504-9506. (j) Price, A. D.; Hur, S.-M.; Fredrickson, G. H.; Frischknecht, A. L.; Huber, D. L. *Macromolecules* **2012**, *45*, 510-524. (k) Xiong, D. A.; Liu, G. J.; Duncan, E. J. S. *ACS Appl. Mater. Interfaces* **2012**, *4*, 2445–2454.(l) Li, G. L.; Wan, D.; Neoh, K. G.; Kang, E. T. *Macromolecules* **2010**, *43*, 10275-10282. (m) Ye, P. L.; Dong, H. C.; Zhong, M. J.; Matyjaszewski, K. *Macromolecules* **2011**, *44*, 2253-2260.

12. (a) Zhao, B. *Polymer* **2003,** *44*, 4079-4083. (b) Zhao, B. *Langmuir* **2004,** *20*, 11748-11755. (c) Zhao, B.; He, T. *Macromolecules* **2003,** *36*, 8599-8602. (d) Zhao, B.; Haasch, R. T.; MacLaren, S. *J. Am. Chem. Soc.* **2004,** *126*, 6124-6134. (e) Zhao, B.; Haasch, R. T.;

MacLaren, S. *Polymer* **2004,** *45*, 7979-7988. (f) Li, D. J.; Sheng, X.; Zhao, B. *J. Am. Chem. Soc.* **2005**, *127*, 6248−6256. (g) Santer, S.; Kopyshev, A.; Donges, J.; Rühe, J.; Jiang, X. G.; Zhao, B.; Müller, M. *Langmuir* **2007,** *23*, 279-285.

13. (a) Chiu, J. J.; Kim, B. J.; Kramer, E. J.; Pine, D. J. *J. Am. Chem. Soc.* **2005**, *127*, 5036-5037. (b) Shan, J.; Nuopponen, M.; Jiang, H.; Viitala, T.; Kauppinen, E.; Kontturi, K.; Tenhu, H. *Macromolecules* **2005**, *38*, 2918-2926. (c) Zubarev, E. R.; Xu, J.; Sayyad, A.; Gibson, J. D. *J. Am. Chem. Soc.* **2006**, *128*, 4958-4959. (d) Guo, Y.; Moffitt, M. G. *Macromolecules* **2007**, *40*, 5868-5878. (e) Cheng, J.; He, J.; Li, C.; Yang, Y. *Chem. Mater.* **2008**, *20*, 4224-4230. (f) Motornov, M.; Sheparovych, R.; Lupitskyy, R.; MacWilliams, E.; Hoy, O.; Luzinov, I.; Minko, S. *Adv. Funct. Mater.* **2007**, *17*, 2307-2314.

14. (a) Zhao, B.; Zhu, L. *J. Am. Chem. Soc.* **2006,** *128*, 4574-4575. (b) Zhu, L; Zhao, B. *J. Phys. Chem. B* **2008**, *112*, 11529-11536.

15. (a) Jiang, X. M.; Zhong, G. J.; Horton, J. M.; Jin, N. X.; Zhu, L.; Zhao, B. *Macromolecules* **2010**, *43*, 5387-5395. (b) Jiang X. M.; Zhao, B.; Zhong, G. J.; Jin, N. X.; Horton, J. M.; Zhu, L.; Hafner, R. S.; Lodge, T. P. *Macromolecules* **2010**, *43*, 8209-8217.

16. Matyjaszewski, K.; Woodworth, B. E.; Zhang, X.; Gaynor, S. G.; Metzner, Z. *Macromolecules* **1998**, *31*, 5955-5957.

17. (a) Ohno, K.; Morinaga, T.; Koh, K.; Tsujii, Y.; Fukuda, T. *Macromolecules* **2005**, *38*, 2137-2142. (b) Ohno, K.; Morinaga, T.; Takeno, S.; Tsujii, Y.; Fukuda, T. *Macromolecules* **2006**, *39*, 1245-1249.

18. (a) Stöber, W.; Fink, A.; Bohn, E. *J. Colloid & Interface Sci.* **1968**, *26*, 62-69. (b) Horton, J. M.; Bao, C. H.; Bai, Z. F.; Lodge, T. P.; Zhao, B. *Langmuir* **2011**, *27*, 13324-13334.

19. The molecular weights of P*t*BA measured by SEC against PS standards were used in the calculation of P*t*BA grafting densities. We previously observed that the P*t*BA molecular weights from SEC were very close to those calculated from the monomer-to-initiator ratio and monomer conversion. See references 12f and 15. The difference between weight retentions of Y-initiator-functionalized particles and polymer brush-grafted silica particles at 100 °C is presumably caused by the water content, though all samples were dried under high vacuum at 45 °C for at least 5 h. This difference was taken into consideration in the calculation of grafting density of polymer brushes by vertically shifting the curves to the same position – the highest weight retention at 100 °C among three curves as described in reference 18b. The calculation of grafting densities of P*t*BA and PS in MB-5 is presented in the Appendix A.
20. More TEM micrographs can be found in the Appendix A.
21. To further confirm that there is no microphase separation when the overall grafting density of mixed brushes is sufficiently low, we synthesized two additional samples using 181 nm silica particles. The molecular weights of polymers are similar (~ 21 kDa) and the overall grafting densities of two samples are 0.17 and 0.09 chains/nm^2. TEM studies showed no microphase separation. The details are included in the Appendix A.
22. Bates, F. S.; Fredrickson, G. H. *Phys. Today* **1999**, *52*, 32-38.
23. The work presented in this Chapter has been published in *Macromolecules* as an article (*Macromolecules* **2012**, *45*, 8027-8036).

Appendix A

for

Chapter 2. Effect of Overall Grafting Density on Microphase Separation of Mixed Homopolymer Brushes Synthesized from Y-Initiator-Functionalized Silica Particles

A1. Calculation of Grafting Densities of P*t*BAand PS on Silica Particles.

The following is a description of the calculation of grafting densities of P*t*BA and PS in sample MB-5. The grafting densities of other hairy particles were calculated in the same way.

We assume that $m_{Y\text{-}initiator\text{-}particles}$(800 ℃) = $m_{PtBA\text{-}Particles}$(800 ℃) = $m_{PtBA\text{-}PS\text{-}Particles}$(800 ℃), where $m_{Y\text{-}initiator\text{-}particles}$, $m_{PtBA\text{-}Particles}$, and $m_{PtBA\text{-}PS\text{-}Particles}$ represent the mass of a single Y-initiator-functionalized silica particle, a P*t*BA brush-grafted silica particle, and a single mixed P*t*BA/PS brush-grafted silica particle, respectively, at 800 ℃ in TGA analysis. To correct the differences in weight retentions at 100 ℃ of Y-initiator-functionalized silica particles, P*t*BA brush-grafted silica particles, and mixed PtBA/PS brush-grafted silica particles, which are due to the loss of adsorbed water on silica particles, we vertically shifted the TGA curves of initiator particles and P*t*BA brush-grafted particles so that their weight retentions at 100 ℃ are identical to that of mixed P*t*BA/PS brush-grafted silica particles at the same temperature. Therefore, the corrected weight retentions of Y-initiator particles and P*t*BA brush-grafted particles at 800 °C are 91.38 % and 78.19 %, respectively.

We then calculated the ratio of the volatile portion to the silica residue at 800 ℃ for initiator particles, P*t*BA brush-grafted particles, and mixed P*t*BA/PS brush-grafted particles, and they are 9.43 : 100, 27.89 : 100, and 41.28 : 100, respectively. Therefore, the ratio of the amount of the grafted P*t*BA to the silica residue at 800 ℃ is 18.46 : 100, and the ratio of the amount of the grafted PS to the silica residue at 800 ℃ is 13.39 : 100.

Assuming that the silica particles are spherical and the density is 2.07 g/cm^3, a calculation shows that the mass of a single silica particle with a diameter of 173 nm is 5.61×10^{-15}g. Therefore, the amount of the grafted P*t*BA in one hairy particle is 1.04×10^{-15}g. It was previously observed that the P*t*BA molecular weights from SEC were very close to those

calculated from the monomer-to-initiator ratio and monomer conversion (*J. Am. Chem. Soc.* **2005**, *127*, 6248−6256; *Macromolecules* **2010**, *43*, 5387-5395; *Macromolecules* **2010**, *43*, 8209-8217). Therefore, we used the molecular weight of P*t*BA from SEC analysis ($M_{n,SEC}$ = 21300 g/mol) for the calculation of the number of polymer chains grafted on one particle. The number of grafted P*t*BA chains in one P*t*BA brush-grafted silica particle is (1.04×10^{-15}g/21300 g/mol) × $6.022 \times 10^{23} = 2.94 \times 10^{4}$ chains. The surface area of one bare silica particle is $\pi D^2 = 9.40 \times 10^{4}$nm^2. Thus, the grafting density of P*t*BA brushes on silica particles is 0.31 chains/nm^2.

Similarly, we calculated the amount of the grafted PS in one mixed P*t*BA/PS brush-grafted silica particle; it is 7.51×10^{-16}g. The polystyrene molecular weight from SEC using PS standards is 20700 g/mol. Therefore the number of grafted PS chains in one mixed P*t*BA/PS brush-grafted silica particle is (7.51×10^{-16} g/20700 g/mol) × $6.022 \times 10^{23} = 2.19 \times 10^{4}$ chains. The grafting density of PS is [(2.19×10^{4} chains)/(9.40×10^{4} nm^2)] = 0.23 chains/nm^2. The overall grafting density of this sample = $\sigma_{PtBA} + \sigma_{PS}$ = 0.54 chains/nm^2.

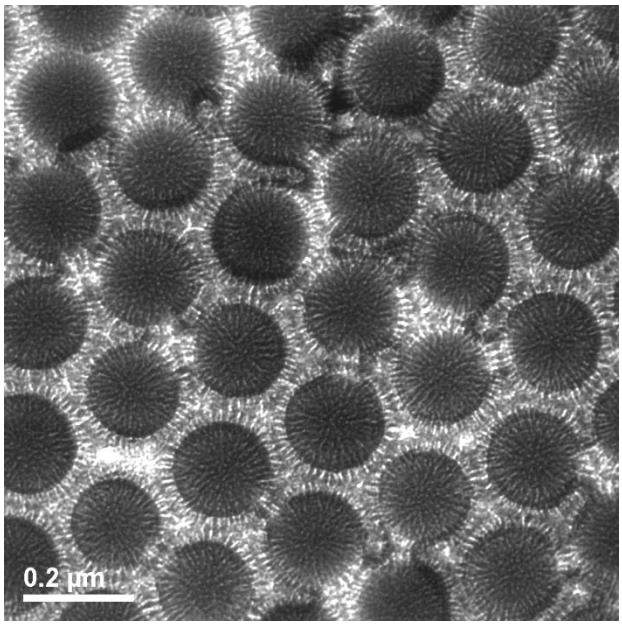

Figure A1. A top-view bright field TEM micrograph of MB-1 (P*t*BA M_n = 18.6 kDa, σ_{PtBA} = 0.63 chains/nm^2; PS M_n = 19.4 kDa, σ_{PS} = 0.43 chains/nm^2; $\sigma_{overall}$ = 1.06 chains/nm^2) after being cast from a $CHCl_3$ dispersion, annealed with $CHCl_3$ vapor for at least 3 h, and stained with RuO_4 vapor at room temperature for 20 min. $CHCl_3$ is a good solvent for both P*t*BA and PS.

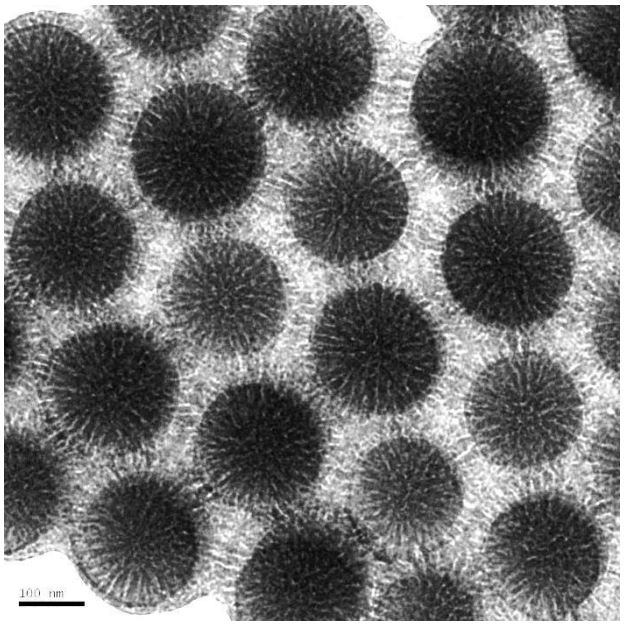

Figure A2. A top-view bright field TEM micrograph of MB-2 (P*t*BA M_n = 23.6 kDa, σ_{PtBA} = 0.63 chains/nm^2; PS M_n = 23.5 kDa, σ_{PS} = 0.40 chains/nm^2; $\sigma_{overall}$ = 1.03 chains/nm^2) after being cast from a $CHCl_3$ dispersion, annealed with $CHCl_3$ vapor for at least 3 h, and stained with RuO_4 vapor at room temperature for 20 min. $CHCl_3$ is a good solvent for both P*t*BA and PS.

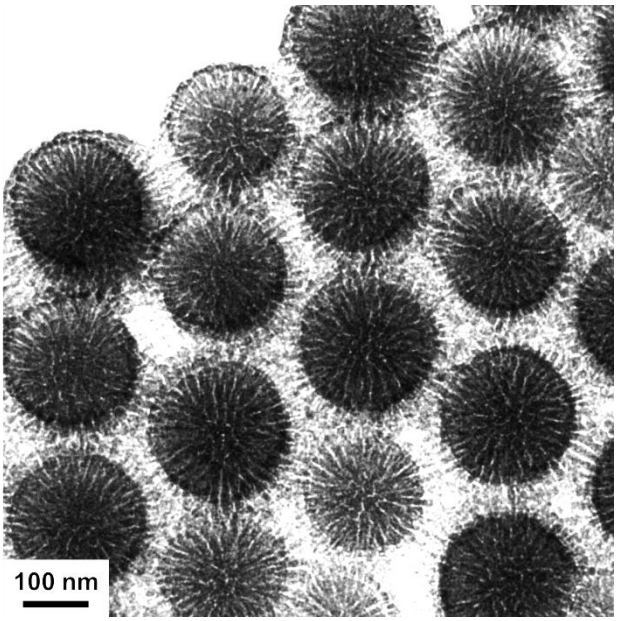

Figure A3. A top-view bright field TEM micrograph of MB-3 (P*t*BA M_n = 25.2 kDa, σ_{PtBA} = 0.45 chains/nm^2; PS M_n = 21.9 kDa, σ_{PS} = 0.50 chains/nm^2; $\sigma_{overall}$ = 0.95 chains/nm^2) after being cast from a $CHCl_3$ dispersion, annealed with $CHCl_3$ vapor for at least 3 h, and stained with RuO_4 vapor at room temperature for 20 min. $CHCl_3$ is a good solvent for both P*t*BA and PS.

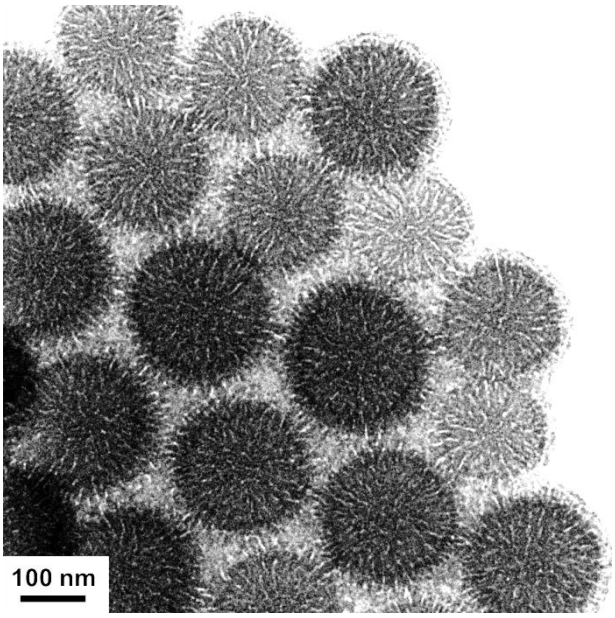

Figure A4. A top-view bright field TEM micrograph of MB-4 (P*t*BA M_n = 22.9 kDa, σ_{PtBA} = 0.36 chains/nm^2; PS M_n = 22.2 kDa, σ_{PS} = 0.32 chains/nm^2; $\sigma_{overall}$ = 0.68 chains/nm^2) after being cast from a $CHCl_3$ dispersion, annealed with $CHCl_3$ vapor for at least 3 h, and stained with RuO_4 vapor at room temperature for 20 min. $CHCl_3$ is a good solvent for both P*t*BA and PS.

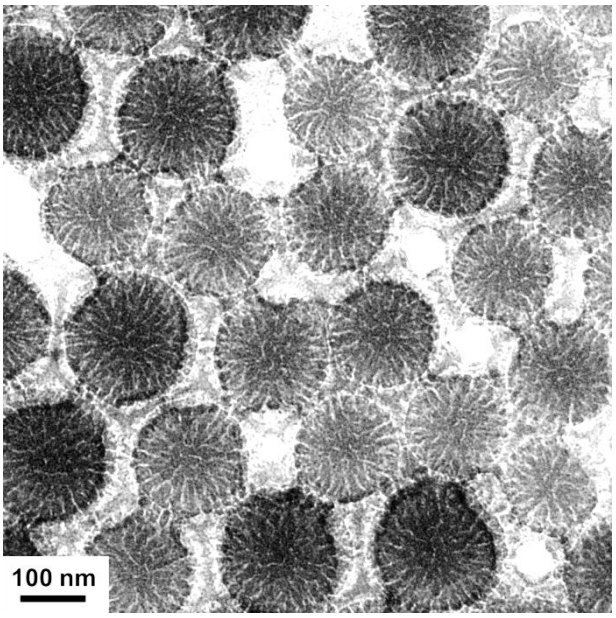

Figure A5. A top-view bright field TEM micrograph of MB-5 (P*t*BA M_n = 21.3 kDa, σ_{PtBA} = 0.31 chains/nm^2; PS M_n = 20.7 kDa, σ_{PS} = 0.23 chains/nm^2; $\sigma_{overall}$ = 0.54 chains/nm^2) after being cast from a $CHCl_3$ dispersion, annealed with $CHCl_3$ vapor for at least 3 h, and stained with RuO_4 vapor at room temperature for 20 min. $CHCl_3$ is a good solvent for both P*t*BA and PS.

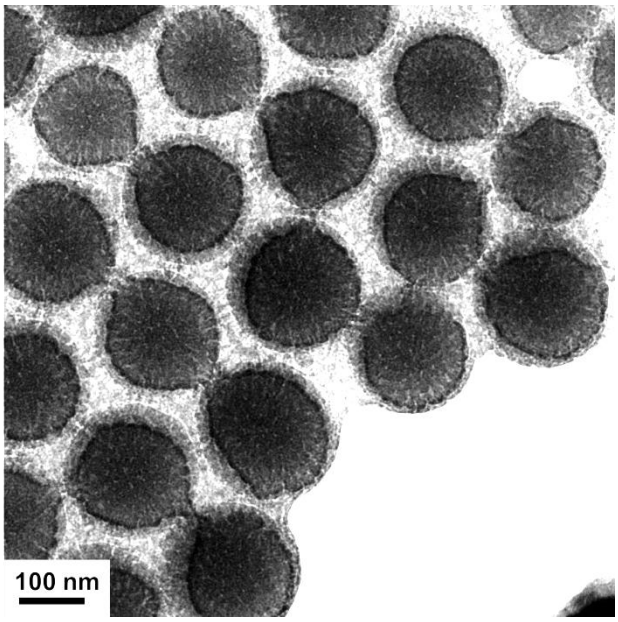

Figure A6. A top-view bright field TEM micrograph of MB-6 (P*t*BA M_n = 23.0 kDa, σ_{PtBA} = 0.14 chains/nm^2; PS M_n = 21.9 kDa, σ_{PS} = 0.20 chains/nm^2; $\sigma_{overall}$ = 0.34 chains/nm^2) after being cast from a $CHCl_3$ dispersion, annealed with $CHCl_3$ vapor for at least 3 h, and stained with RuO_4 vapor at room temperature for 20 min. $CHCl_3$ is a good solvent for both P*t*BA and PS.

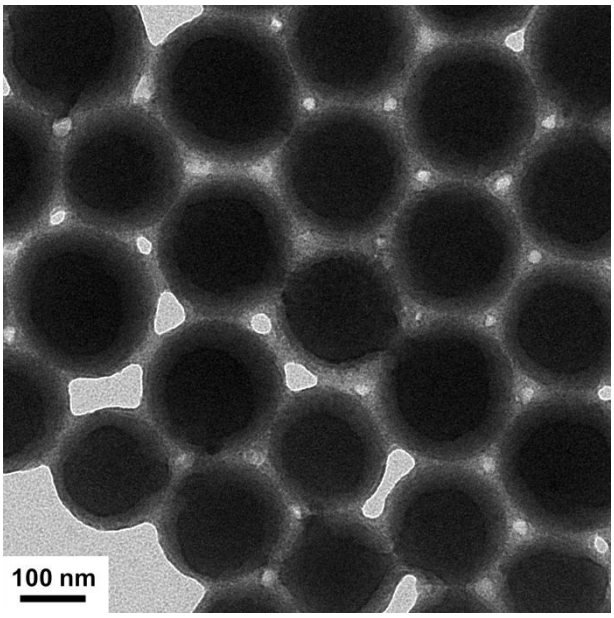

Figure A7. A top-view bright field TEM micrograph of MB-7 (P*t*BA M_n = 22.1 kDa, σ_{PtBA} = 0.10 chains/nm^2; PS M_n = 23.5 kDa, σ_{PS} = 0.022 chains/nm^2; $\sigma_{overall}$ = 0.122 chains/nm^2) after being cast from a $CHCl_3$ dispersion, annealed with $CHCl_3$ vapor for at least 3 h, and stained with RuO_4 vapor at room temperature for 20 min. $CHCl_3$ is a good solvent for both P*t*BA and PS.

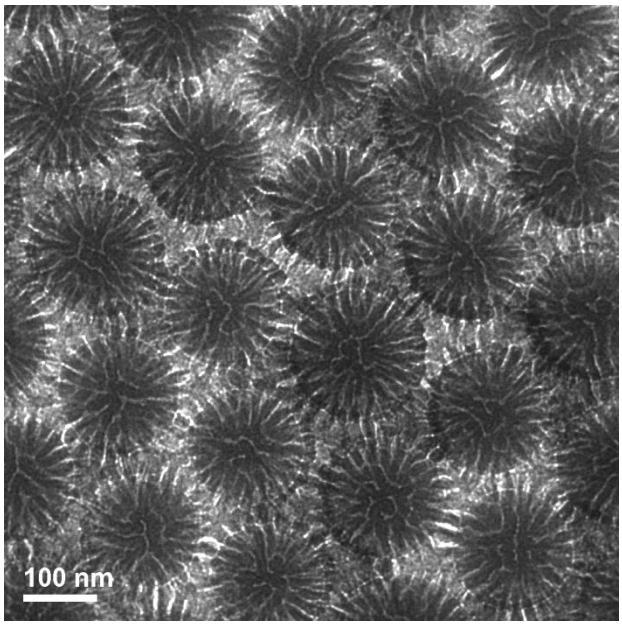

Figure A8. A top-view bright field TEM micrograph of MB-8 (P*t*BA M_n = 24.5 kDa, σ_{PtBA} = 0.36 chains/nm^2; PS M_n = 24.9 kDa, σ_{PS} = 0.27 chains/nm^2) after being cast from a $CHCl_3$ dispersion, annealed with $CHCl_3$ vapor for at least 3 h, and stained with RuO_4 vapor at room temperature for 20 min. $CHCl_3$ is a good solvent for both P*t*BA and PS. This TEM image was reprinted from a literature paper (*Macromolecules* **2010**, *43*, 8209-8217) with permission from American Chemical Society.

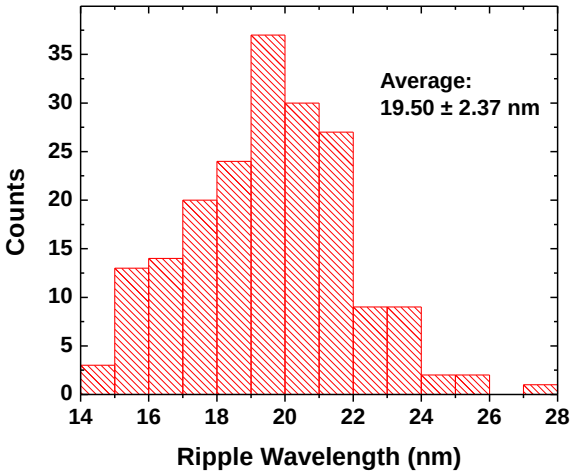

Figure A9. Distribution of ripple wavelengths of features (sum of widths of neighboring P*t*BA and PS stripes) obtained from TEM image analysis of Figure A8, MB-8. MB-8 is a mixed P*t*BA/PS brush sample grafted on 160 nm silica particles synthesized from monochlorosilane-terminated Y-initiator-functionalized silica particles (P*t*BA M_n = 24.5 kDa, PDI = 1.11, σ_{PtBA} = 0.36 chains/nm^2; PS M_n = 24.9 kDa, PDI = 1.17, σ_{PS} = 0.27 chains/nm^2; $\sigma_{overall}$ = 0.63 chains/nm^2).

A2. Synthesis and TEM Study of Two Additional Low Overall Grafting Density Mixed P*t*BA/PS Brush Samples.

To further confirm that there is no microphase separation when the overall grafting density of mixed brushes is sufficiently low, we synthesized two additional low grafting density mixed P*t*BA/PS brush-grafted particle samples from 181 nm silica particles using the same protocol described in Chapter 2. The TGA data are shown in Figure A10. The characterization data are summarized in Table A1. The overall grafting density was 0.20 chains/nm^2 for MB-A1 (σ_{PtBA}= 0.09 chains/nm^2 and σ_{PS} = 0.11 chains/nm^2) and 0.09 chains/nm^2 for MB-A2 (σ_{PtBA}= 0.06 chains/nm^2 and σ_{PS} = 0.03 chains/nm^2). Figures A11 and A12 show the typical top-view bright field TEM micrographs of MB-A1 and -A2, respectively, after being cast on carbon-coated TEM grids from chloroform dispersions, annealed with $CHCl_3$ vapor for 3 h, and then stained with RuO_4 vapor at room temperature for 20 min. Clearly, there was no microphase separation in both samples. In the interstitial areas, polymer brushes can be seen. This further confirmed that mixed P*t*BA/PS brushes with a sufficiently low overall grafting density do not undergo microphase separation.

Table A1. Characterization Data for Two Additional Mixed P*t*BA/PS Brush-Grafted Particle Samples with Low Overall Grafting Densities

Mixed P*t*BA/PS Brush-Grafted Silica Particles	$M_{n,SEC}$ and PDI of P*t*BA[a]	$M_{n,SEC}$ and PDI of PS [a]	σ_{PtBA}, σ_{PS}, and $\sigma_{overall}$ (chains/nm^2)[c]
MB-A1	22.3 kDa, 1.12	20.2 kDa, 1.15	0.09, 0.11, 0.20
MB-A2	21.8 kDa, 1.13	21.0 kDa, 1.15	0.06, 0.03, 0.09

[a] The values of number average molecular weight ($M_{n,SEC}$) and polydispersity index (PDI) were determined by size exclusion chromatography (SEC) using polystyrene standards for calibration. [c]σ_{PtBA}, σ_{PS}, and $\sigma_{overall}$ are P*t*BA grafting density, PS grafting density, and overall grafting density ($\sigma_{overall} = \sigma_{PtBA} + \sigma_{PS}$). The grafting densities were calculated by using TGA data and molecular weights of P*t*BA and PS.

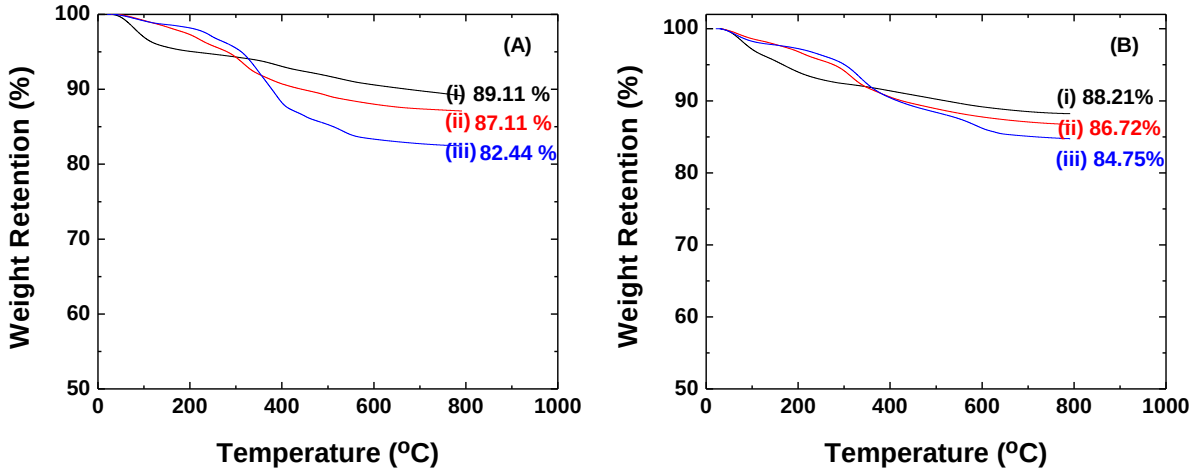

Figure A10. Thermogravimetric analysis (TGA) of (i) Y-initiator-functionalized silica particles, (ii) P*t*BA brush-grafted silica particles, and (iii) mixed P*t*BA/PS brush-grafted silica particles obtained in the preparation of mixed brush-grafted particle sample (A) MB-A1, (B) MB-A2.

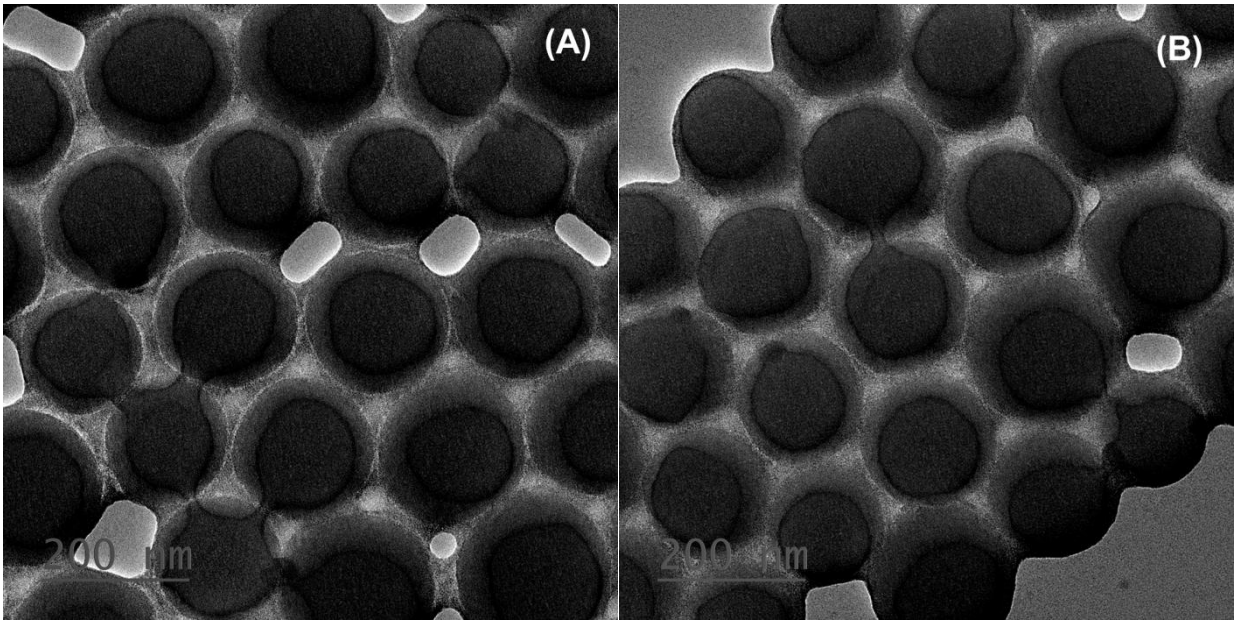

Figure A11. Top-view bright field TEM micrographs of MB-A1 (P*t*BAM_n = 22.3 kDa, σ_{PtBA} = 0.09 chains/nm^2; PS M_n = 20.2 kDa, σ_{PS} = 0.11 chains/nm^2; $\sigma_{overall}$ = 0.20 chains/nm^2) after being cast from a $CHCl_3$ dispersions and annealed with $CHCl_3$ vapor. The sample was stained with RuO_4 vapor at room temperature for 20 min.

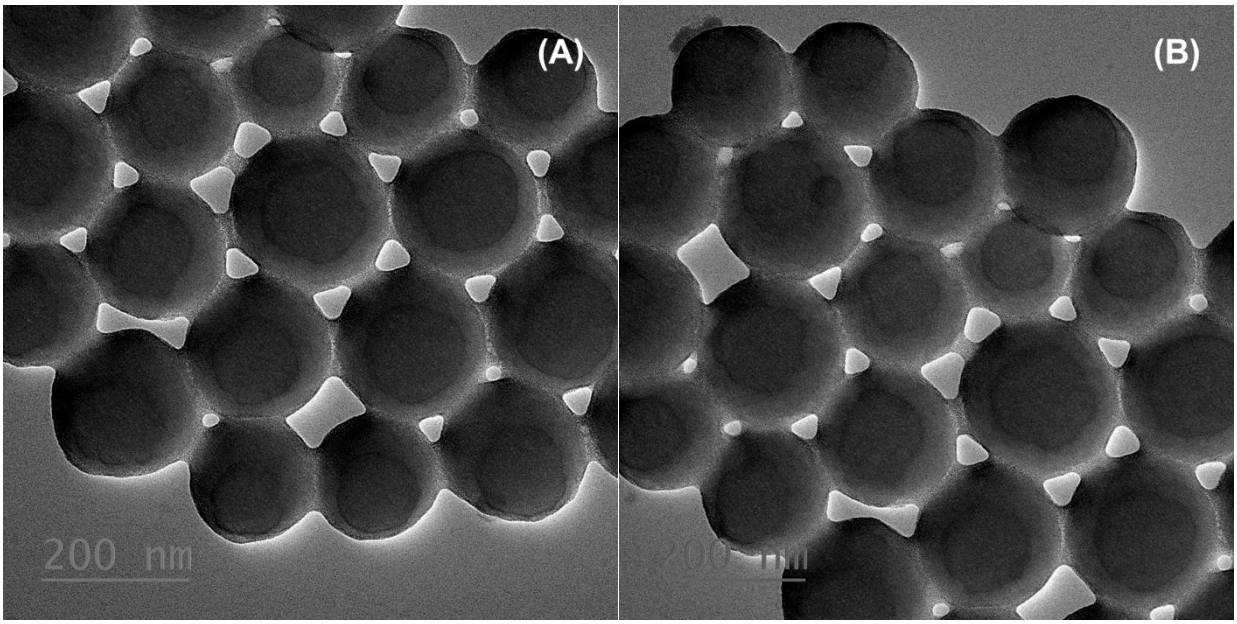

Figure A12. Top-view bright field TEM micrographs of MB-A2 (P*t*BAM_n = 21.8 kDa, σ_{PtBA} = 0.06 chains/nm^2; PS M_n = 21.0 kDa, σ_{PS} = 0.03 chains/nm^2; $\sigma_{overall}$ = 0.09 chains/nm^2) after being cast from a $CHCl_3$ dispersion and annealed with $CHCl_3$ vapor. The sample was stained with RuO_4 vapor at room temperature for 20 min.

Chapter 3. Effect of Molecular Weight on Lateral Microphase Separation of Mixed Homopolymer Brushes Grafted on Silica Particles

Abstract

This Chapter presents a systematic study on the effect of molecular weight (MW) on microphase separation of mixed poly(*tert*-butyl acrylate) (P*t*BA)/polystyrene (PS) brushes grafted on 172 nm silica particles. The brushes were synthesized by sequential surface-initiated atom transfer radical polymerization (ATRP) of *t*BA at 75 °C and nitroxide-mediated radical polymerization (NMRP) of styrene at 120 °C from silica particles functionalized with an asymmetric difunctional initiator bearing an ATRP initiator and an NMRP alkoxyamine. The MWs of the two polymers in each sample were controlled to be similar to each other. A series of mixed brush samples with different average MWs, from 13.8 to 33.1 kDa, but comparable overall grafting densities were made and their microphase separation was studied by transmission electron microscopy (TEM). The TEM samples were prepared by drop casting the dispersions of mixed brush-grafted particles in $CHCl_3$ and also in water (stabilized by a surfactant) and staining the brushes with RuO_4. While $CHCl_3$ is a good solvent for both P*t*BA and PS, making the brushes spread out on the carbon films of TEM grids, water is a nonselective poor solvent for the two polymers, causing the brushes to collapse uniformly on silica core. All samples exhibited lateral microphase separation, forming nearly bicontinuous rippled nanopatterns. The average ripple wavelength D increased with increasing the MW. For samples directly cast from chloroform, D scaled with $MW^{0.70}$ in the studied MW range. For uniformly collapsed mixed brushes cast from water, D was proportional to $MW^{0.56}$ in the MW range of 17.9 to 33.1 kDa. The latter is close to the theoretical prediction of $D \sim MW^{0.5}$ for perfect Y-shaped brushes in the melt and in nonselective poor solvents. We further compared the phase separation of mixed P*t*BA/PS brushes grafted on silica particles and P*t*BA-*b*-PS diblock copolymers and

found that the microphase separation of mixed brushes was weaker than that of diblock copolymers.

3.1 Introduction

Binary mixed homopolymer brushes, composed of two chemically distinct homopolymers randomly or alternately grafted on a solid substrate,[1] are an intriguing class of surface-responsive materials.[2-4] The two grafted polymers, which are not necessarily stimuli-responsive in the sense of the conventional definition, can undergo spontaneous reorganization in response to environmental changes and exhibit different structures and properties under different conditions.[2-4] The synthesis and responsive behavior of mixed brushes grafted on various substrates, including planar and curved surfaces such as silicon wafers and colloidal particles, has been well documented in the literature.[5-8] For example, Sidorenko et al. synthesized the first mixed brushes of polystyrene (PS) and poly(2-vinylpyridine) by a two-step surface-initiated conventional free radical polymerization process from azo initiator-functionalized silicon wafers and demonstrated the responsive properties by treating the mixed brushes with selective solvents.[5]

Besides environmentally responsive properties, the rich phase behavior of mixed homopolymer brushes has also received enormous interest, particularly from theoretical study.[1-4,9-13] The self-assembly of mixed brushes is governed by a number of factors, including molecular weights (MWs) of two grafted polymers, Flory-Huggins interaction parameters between two polymers and between each polymer and the environment, individual and overall grafting densities, distribution of grafting sites of two polymers on the substrate, and geometry and curvature of the substrate.[2] Marko and Witten were the first to investigate the two possible types of microphase separation of symmetric mixed homopolymer brushes on a flat surface under equilibrium melt conditions: lateral phase separation, resulting in a "rippled" nanostructure, and vertical phase segregation, producing a "layered" structure.[1] Their study

showed that the "rippled" nanostructure should be the one to appear and the feature size was predicted to be on the order of polymer chain root-mean-square end-to-end distance. Since this seminal work, the lateral phase separation of mixed brushes under melt conditions and in nonselective or nearly nonselective solvents has been confirmed by many researchers in theoretical and simulation studies, and a variety of intriguing nanostructures has been predicted.[9-12] It should be noted here that despite some success in the experimental verification of some predicted nanostructures,[6d,9d] the overall experimental study of the morphology of mixed brushes lags behind the theoretical study, largely because of the challenge in the preparation of well-defined mixed brushes and in the unequivocal identification of the self-assembled nanostructures.[2]

We have been particularly interested in the fundamental understanding of the effects of various factors on self-assembly of mixed brushes.[2,13-15] By combining two different "living"/controlled radical polymerization techniques, atom transfer radical polymerization (ATRP) and nitroxide-mediated radical polymerization (NMRP), our group developed a unique method to grow mixed brushes with controlled molecular weights and narrow polydispersities.[6a,13a] To ensure that the two grafted polymers are well-mixed, asymmetric difunctional initiators (Y-initiators) that bear an ATRP initiator and an NMRP alkoxyamine were designed and synthesized. The use of silica particles allows direct visualization of the nanostructures of mixed brushes by transmission electron microscopy (TEM).[13b-e,14] Using this synthetic method, Jiang et al. recently studied the effect of chain length disparity on morphology of mixed poly(*tert*-butyl acrylate) (P*t*BA)/polystyrene (PS) brushes grafted on silica particles.[13d] With the increase of PS MW from below to above that of P*t*BA, the morphology of mixed brushes evolved from isolated, nearly spherical PS nanodomains in the P*t*BA matrix, to

bicontinuous, random worm-like nanostructures, and to a two-layer structure in which the bottom layer was laterally phase separated and covered by the longer polymer chains. The effect of overall grafting density ($\sigma_{overall}$) were also investigated.[14a] By changing the mass ratio of a triethoxysilane-terminated Y-initiator to silica particles in the initiator immobilization step, we prepared a series of mixed P*t*BA/PS brushes with MWs of ~ 23 kDa for both polymers but different overall grafting densities. The ripple wavelength (i.e., the periodicity, *D*) of the nanopattern formed by lateral microphase separation of mixed brushes increased with decreasing $\sigma_{overall}$; the normalized *D* scaled with $\sigma_{overall}^{-0.47}$ in the $\sigma_{overall}$ range of 1.06 to 0.54 chains/nm^2, which was in qualitative agreement with the theoretical prediction of Zhulina and Balazs.[11]

In this Chapter, we focused on the effect of MW on the ripple wavelength of the nanopattern formed by mixed brushes. Although *D* has been predicted to scale with the square root of chain length for symmetric mixed brushes in the melt and in nonselective poor solvents,[10,11] the issue has not been experimentally investigated. By taking advantage of the "living" nature of ATRP and NMRP,[13-17] we synthesized a series of mixed P*t*BA/PS brushes from Y-initiator-functionalized, 172 nm silica particles with different MWs but similar individual and overall grafting densities (Scheme 3.1). In each mixed brush sample, the MWs of the two polymers were controlled to be as close to each other as possible with a goal of achieving bicontinuous nanostructures from nonselective solvents. TEM was employed to study the nanopatterns formed from lateral phase separation of mixed brushes. The TEM samples were prepared by drop-casting of particles from either $CHCl_3$ dispersions or surfactant-stabilized aqueous dispersions. The ripple wavelength was found to increase with the increase of average MW in both cases, and the scaling relationships between *D* and MW were obtained. We further compared the microphase separation behavior of mixed P*t*BA/PS brushes and P*t*BA-*b*-PS diblock copolymers.

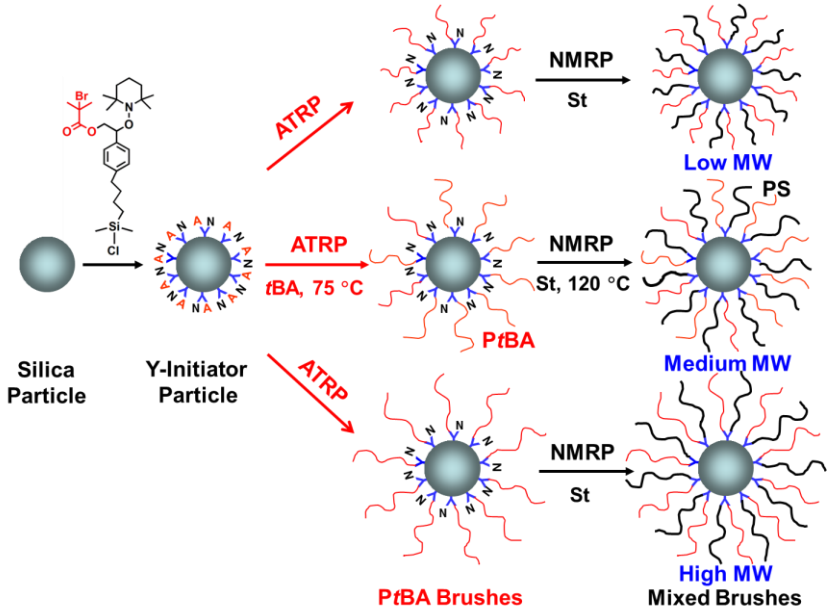

Scheme 3.1 Synthesis of mixed poly(*tert*-butyl acrylate) (P*t*BA)/polystyrene (PS) brushes from Y-initiator functionalized silica particles with varying average molecular weights (MWs) by combining atom transfer radical polymerization (ATRP) of *tert*-butyl acrylate at 75 °C and nitroxide-mediated radical polymerization (NMRP) of styrene at 120 °C.

3.2 Experimental Section

3.2.1 Materials

Tetraethyl orthosilicate (TEOS, 98%), ammonium hydroxide (25% in water), and 2,2,6,6-tetramethylpiperidinooxy (TEMPO) were purchased from Acros Organics and used as received. Chlorodimethylsilane (98%) was purchased from Aldrich and kept in a glove box before use. Platinum-divinyltetramethyldisiloxane complex in xylene (2.1~2.4% Pt concentration in xylene) was obtained from Gelest, Inc. 2-[4-(But-3-enyl)phenyl]-2-(2',2',6',6'-tetramethyl-1'-piperidinyloxy)ethyl 2-bromo-2-methylpropanoate (Y-silane precursor) was prepared according to a procedure described in the literature.[13a] Styrene (99%, Aldrich) and *tert*-butyl acrylate (*t*-BA, 99%, Aldrich) were dried with CaH_2, distilled under reduced pressure, and passed through a basic alumina column to remove the inhibitor. The purified monomers were stored in solvent storage flasks and kept in a refrigerator prior to use. CuBr (98%, Aldrich) was stirred in glacial acetic acid overnight, filtered, and washed with absolute ethanol and ethyl ether. The salt was then collected, dried under vacuum, and stored in a desiccator. *N*, *N*, *N'*, *N'*, *N''*-Pentamethyldiethylenetriamine (99 %, Aldrich) and ethyl 2-bromoisobutyrate were dried with calcium hydride, distilled under a reduced pressure, and stored in a desiccator. 1-Phenyl-1-(2',2',6',6'-tetramethyl-1'-piperidinyloxy)ethane (STEMPO), an initiator for NMRP, was prepared by following a procedure from the literature.[18] Benzyl dithiobenzoate, a chain transfer agent (CTA) for reversible addition fragmentation chain transfer (RAFT) polymerization, was prepared according to a procedure described in the literature,[19] and the molecular structure was confirmed by ^{1}H and ^{13}C NMR spectroscopy analysis. All other chemical reagents were purchased from either Aldrich or Fisher and used without further purification.

3.2.2 General Characterization

Size exclusion chromatography (SEC) was carried out at ambient temperature using PL-GPC 20 (an integrated SEC system from Polymer Laboratories, Inc.) with a refractive index detector, one PLgel 5 μm guard column (50 × 7.5 mm), and two PLgel 5 μm mixed-C columns (each 300 × 7.5 mm, linear range of molecular weight from 200 to 2,000,000 Da according to Polymer Laboratories, Inc.). THF was used as the carrier solvent at a flow rate of 1.0 mL/min. Polystyrene standards (Polymer Laboratories, Inc.) were employed for calibration. The data were processed using Cirrus GPC/SEC software (Polymer Laboratories, Inc.). ^{1}H NMR spectra were recorded on a Varian Mercury 300 MHz NMR spectrometer. Thermogravimetric analysis (TGA) was performed in air at a heating rate of 20 ℃/min from room temperature to 800 or 850 ℃ using either TA Q-series Q50 in air or a SII Nanotechnology TG/DTA 320 in pure O_2. The particle samples for TGA were dried at 45 ℃ in vacuum for > 5 h. DSC was performed on a TA Instruments Q2000 DSC at a heating rate of 20 ℃/min after the first cooling at 3 ℃/min. The P*t*BA-*b*-PS diblock copolymers were kept in vacuum oven overnight before DSC analysis. For each sample, ~ 5 mg was used.

3.2.3 Synthesis of Bare Silica Particles

Ammonium hydroxide (25 % in water, 19.904 g) and tetraethyl orthosilicate (TEOS, 10.501 g) were each mixed with 10 mL of ethanol. The two solutions were then added into a 500 mL one-necked flask that contained 280 mL of ethanol under the stirring condition. The concentrations of NH_3, TEOS, and water in the solution were 0.43 M, 0.15 M, 2.92 M, respectively. The mixture was stirred vigorously at room temperature for 8 h. The bare silica particles were isolated by centrifugation (Eppendorf 5804 Centrifuge, 8000 rpm), redispersed in ethanol, and centrifuged again. This washing process was repeated with ethanol an additional

two times, water four times, and ethanol two times again. The particles were dried with a stream of air flow. The average diameter of silica particles, measured from their transmission electron microscopy micrographs, was 172 ± 20 nm. The bare silica particles were used to prepare Y-initiator-functionalized silica particles.

3.2.4 Synthesis of Y-Initiator-Functionalized Silica Particles

The chlorodimethylsilane-terminated Y-initiator (Y-silane, Scheme 3.1) was immobilized onto the surface of bare silica particles with an average diameter of 172 ± 20 nm, which were made by the Stöber process, via the following procedure. 2-[4-(But-3-enyl)phenyl]-2-(2',2',6',6'-tetramethyl-1'-piperidinyloxy)ethyl 2-bromo-2-methylpropanoate (Y-silane precursor, 166.0 mg, 0.347 mmol) was added into a 25 mL two-necked flask, followed by the addition of chlorodimethylsilane (2.0 mL, 18.4 mmol) using a disposable plastic syringe under the N_2 atmosphere. The Pt complex in xylene (35 μL) was injected into the solution via a microsyringe. The mixture was stirred at room temperature under the nitrogen atmosphere; the hydrosilylation reaction was monitored by ^{1}H NMR spectroscopy analysis. Once the reaction was complete, excess chlorodimethylsilane was removed under high vacuum at room temperature, and the product, Y-silane, was used directly in the next step for the preparation of Y-initiator-functionalized silica particles.

Bare silica particles (600.5 mg) were dried at 110 °C in vacuum for 12 h and then dispersed in dry THF (7 mL) using a ultrasonic water bath. A solution of Y-silane freshly synthesized from 166.0 mg of Y-initiator in dry THF (1.5 mL) was injected into the dispersion via a syringe. After the reaction mixture was stirred at 70 °C under nitrogen atmosphere for 73 h, the particles were collected by centrifugation, redispersed in THF, and then centrifuged again. This washing process was repeated four times, followed by drying the initiator particles with a stream of air.

3.2.5 Synthesis of P*t*BA Brush-Grafted Silica Particles

The following is the procedure for the synthesis of P*t*BA brushes with $M_{n,SEC}$ of 22.0 kDa from the Y-initiator-functionalized silica particles. These P*t*BA hairy particles were used to prepare mixed P*t*BA/PS brush sample MB-MW-3 with P*t*BA $M_{n,SEC}$ of 22.0 kDa and PS $M_{n,SEC}$ of 22.3 kDa. Similar procedures were employed to synthesize other P*t*BA brushes.

The Y-initiator particles (50.2 mg) were added into a 25 mL two-necked flask and dried under high vacuum at 40 °C for 2 h. The initiator particles were then dispersed in DMF (1.008 g) by ultrasonication to form a stable dispersion. CuBr (11.3 mg, 0.079 mmol), *tert*-butyl acrylate (*t*BA, 6.021 g, 46.98 mmol), *N*,*N*,*N*′,*N*′,*N*″-pentamethyldiethylenetriamine (14.4 mg, 0.083 mmol), and ethyl 2-bromoisobutyrate (EBiB, 16.7 mg, 0.085 mmol) were added into a 50 mL two-necked flask and stirred under a N_2 atmosphere. The particle dispersion was transferred into the 50 mL flask using a syringe, and the mixture was degassed immediately by three freeze−pump−thaw cycles. The flask was then placed into an oil bath with a preset temperature of 75 ℃, and the polymerization was monitored by SEC and ^{1}H NMR spectroscopy analysis. After 24.5 h, the flask was removed from the oil bath and opened to air. THF (~10 mL) was added to dilute the mixture. The particles were isolated by centrifugation, and the supernatant was passed through a column of neutral, activated alumina to remove the copper catalyst. The P*t*BA brush-grafted silica particles were re-dispersed in THF. The dispersion was left to stand still at ambient conditions overnight, and the green precipitate was removed. The hairy particles were then separated by centrifugation again. This washing process was repeated with THF for a total of five times, followed by drying of the hairy particles with a stream of air flow. The $M_{n,SEC}$ and polydispersity index (PDI) of the free P*t*BA formed from free initiator EBiB in the

polymerization were 22.0 kDa and 1.08, respectively, determined from SEC using PS standards as calibration.

3.2.6 Preparation of Mixed P*t*BA/PS Brush-Grafted Silica Particles (MB-MW-3) from P*t*BA Brush-Grafted Silica Particles with P*t*BA $M_{n,SEC}$ of 22.0 kDa

The following is the procedure for the preparation of mixed P*t*BA/PS brush sample MB-MW-3 with P*t*BA $M_{n,SEC}$ of 22.0 kDa and PS $M_{n,SEC}$ of 22.3 kDa from P*t*BA brush-grafted silica particles with P*t*BA $M_{n,SEC}$ of 22.0 kDa. Similar procedures were used to synthesize other mixed brush samples.

The P*t*BA brush-grafted silica particles (P*t*BA $M_{n,SEC}$ = 22.0 kDa, 36.6 mg) were dispersed in anisole (2.528 g) in a 25 mL two-necked flask using an ultrasonic water bath. The hairy particle dispersion was then transferred into a 50 mL two-necked flask that contained free NMRP initiator 1-phenyl-1-(2',2',6',6'-tetramethyl-1'-piperidinyloxy)ethane (STEMPO, 16.8 mg, 0.064 mmol), followed by the addition of styrene (5.009 g, 48.09 mmol). After the mixture was degassed by three freeze-pump-thaw cycles, the flask was placed into an oil bath with a preset temperature of 120 °C. The polymerization was monitored by ^{1}H NMR spectroscopy and SEC. When the molecular weight of free polystyrene reached the desired value, the polymerization was stopped by removing the flask from the oil bath and diluting the mixture with THF. The mixed P*t*BA/PS brush-grafted particles were isolated by centrifugation, redispersed in THF, and centrifuged again. This washing process was repeated four times to remove the physically adsorbed polymer. The particles were then dried with a stream of N_2 flow. The $M_{n,SEC}$ and PDI of the free polystyrene, measured by SEC, were 22.3 kDa and 1.20, respectively.

3.2.7 Synthesis of Symmetric P*t*BA-*b*-PS Diblock Copolymers by Reversible Addition-Fragmentation Chain Transfer Polymerization

The following is the procedure for the synthesis of P*t*BA-*b*-PS with $M_{n,SEC}$ (SEC stands for size exclusion chromatography) of 21.6 kDa and PDI of 1.13. Monomer *t*BA (8.116 g, 63.32 mmol), benzyl dithiobenzoate (28.9 mg, 0.118 mmol), 2,2'-azobis(2-methylpropionitrile) (AIBN, 0.202 g of a solution of AIBN in anisole with a concentration of 0.97 wt %, 0.012 mmol), and anisole (3.023 g) were added into a 50 mL two-necked flask. The mixture was degassed by three freeze-pump-thaw cycles. After a small sample was taken for ^{1}H NMR spectroscopy analysis using a degassed syringe, the flask was immersed in a 70 °C oil bath. The polymerization was monitored by ^{1}H NMR spectroscopy and SEC. The flask was removed from the oil bath after 4.3 h and a sample was taken immediately for the determination of the monomer conversion by ^{1}H NMR spectroscopy. The polymerization mixture was diluted with THF (~5 mL) and then dried under high vacuum to remove the solvents and the unreacted monomer. The dried polymer was analyzed by ^{1}H NMR to ensure that the monomer and solvents were completely removed. SEC analysis results (PS standards): $M_{n,SEC}$ = 11.2 kDa; polydispersity index (PDI) =1.11. The DP of the obtained P*t*BA macro-CTA was 85, calculated from the monomer conversion and the monomer-to-CTA ratio.

P*t*BA macro-CTA ($M_{n,SEC}$ = 11.2 kDa, 0.809 g), AIBN (0.069 g of a solution of AIBN in anisole with a concentration of 0.97 %, 0.041 mmol), styrene (10.012 g, 96.13 mmol), and anisole (7.492 g) were added into a 50 mL two-necked flask. The mixture was stirred under a nitrogen atmosphere to dissolve the polymer. After the solution was degassed by three freeze-pump-thaw cycles, the flask was placed into an oil bath with a preset temperature of 70 °C. The polymerization was monitored by SEC. After the molecular weight of P*t*BA-*b*-PS reached the

desired value, the flask was removed from the oil bath and the mixture was dilute with THF. The final block copolymer was dried under high vacuum to remove the solvents and the monomer and analyzed by ^{1}H NMR spectroscopy and SEC. SEC analysis results (polystyrene standards): $M_{n,SEC}$ = 21.6 kDa and PDI = 1.13. The DP of PS in P*t*BA-*b*-PS was 112, which was determined from its ^{1}H NMR spectrum using the integral values of the peak from 2.0 to 2.4 ppm (-CH_2C*H*- of P*t*BA) and the aromatic peaks of PS from 6.2 to 7.2 ppm.

Using a similar procedure, a diblock copolymer P*t*BA-*b*-PS with a different molecular weight was prepared. The DP, $M_{n,SEC}$, and PDI of P*t*BA macro-CTA were 111, 15.2 kDa, and 1.11, espectively. The $M_{n,SEC}$ and PDI of P*t*BA-*b*-PS were 29.2 kDa and 1.15, respectively. The DP of PS in this diblock copolymer was 149. The SEC data and ^{1}H NMR spectra of the two block copolymers can be found in Figures B14-17 in Appendix B.

3.2.8 Transmission Electron Microscopy (TEM) Study of Mixed P*t*BA/PS Brush-Grafted Silica Particles

For mixed P*t*BA/PS brush-grafted silica particles, two methods were employed to prepare TEM samples. In the first one, chloroform, a nonselective good solvent for P*t*BA and PS, was used to prepare the particle dispersions. For each sample, ~ 1 mg of mixed P*t*BA/PS brush-grafted silica particles were dispersed in 1.4 g of chloroform in a small vial by ultrasonication in an ultrasonic water bath. The particle dispersion was drop cast onto a carbon-coated, copper TEM grid using a glass pipette and was allowed to dry at ambient conditions. The TEM samples were annealed with $CHCl_3$ vapor at room temperature as detailed below. The sample-loaded TEM grids were placed in a small glass dish with a diameter of 2". The dish was then transferred into a glass jar that contained ~ 2 mL of $CHCl_3$. The jar was covered with a watch glass. After being annealed by $CHCl_3$ vapor at room temperature for ≥ 5 h, the samples were removed from

the jar, allowed to dry at ambient conditions for 30 min, and then stained with RuO_4 at room temperature for 20 min.

In the second method, water, a nonselective poor solvent for both P*t*BA and PS, was used to prepare uniformly collapsed P*t*BA/PS brushes on the surface of silica particles. For each sample, ~ 1 mg of P*t*BA/PS brush-grafted silica particles was dispersed in ~ 1 g of chloroform. In another vial, 2 mg of cetyltrimethylammonium bromide (CTAB) was dissolved in 4 g of H_2O, followed by the gradual addition of the dispersion of mixed P*t*BA/PS brush-grafted silica particles in chloroform under the stirring condition. After the mixture was sonicated at room temperature for 1 h, the vial was opened to the air and the mixture was stirred overnight (for ~ 18 h) in a fume hood to allow chloroform to evaporate. The particles were then isolated by centrifugation (VWR® Micro 1207 Microcentrifuge, 10000 rpm, 15 min); the particles were redispersed in water and centrifuged again. The collected particles were then dispersed in water (1 mL) and drop cast onto carbon-coated TEM copper grids, followed by staining with RuO_4 at room temperature for 20 min.

3.3 Results and Discussion

3.3.1 Synthesis of Mixed P*t*BA/PS Brushes with Various Molecular Weights (MWs)

To systematically study the effect of MW on lateral microphase separation of mixed homopolymer brushes grafted on silica particles, we needed to synthesize a series of mixed brush samples with controlled MWs and similar individual and overall grafting densities. ATRP and NMRP are two "living"/controlled radical polymerization techniques, allowing the control of MWs and molecular weight distributions.[16,17] By using the Y-initiator-functionalized silica particles and taking advantage of the "living" nature of two radical polymerization techniques,

we prepared a set of 6 mixed P*t*BA/PS brush-grafted silica particle samples with various average MWs (averages of number average molecular weights, M_ns, of P*t*BA and PS) and narrow polydispersities by changing the monomer-to-initiator ratio and controlling the reaction time (i.e., monomer conversion).

The bare silica particles used in this Chapter 3 were made by the Stöber process[20] and had an average diameter of 172 ± 20 nm, determined from TEM particle size analysis. (2-(4-(4-(Chlorodimethylsilyl)butyl)phenyl)-2-((2,2,6,6-tetramethylpiperidin-1-yl)oxy)ethyl 2-bromo-2-methylpropanoate), a monochlorosilane-terminated Y-initiator capable of initiating both ATRP and NMRP (Y-silane), was used to functionalize the surface of bare silica particles.[13a] P*t*BA brushes were then grown from silica particles by surface-initiated ATRP of *t*BA. The polymerizations were carried out in anisole at 75 °C in the presence of a free initiator, ethyl 2-bromoisobutyrate (EBiB). The addition of EBiB facilitated the control of surface-initiated polymerizations and allowed the reactions to be monitored by ^{1}H NMR spectroscopy and size exclusion chromatography (SEC). The TEMPO group in the Y-initiator was previously confirmed to be stable under this ATRP condition.[6a] The polymerizations were stopped when the MWs of the free P*t*BA polymers reached the desired values. The P*t*BA brush-grafted silica particles were isolated by centrifugation, repeatedly washed with THF to remove the physically absorbed free polymer, characterized by thermogravimetric analysis (TGA), and then used to prepare mixed P*t*BA/PS brushes. The surface-initiated NMRPs of styrene from P*t*BA brush-grafted silica particles were performed in anisole at 120 °C. Again, a free initiator, 1-phenyl-1-(2',2',6',6'-tetramethyl-1'-piperidinyloxy)ethane (STEMPO),[14a,18] was added to the reaction mixtures. The polymerizations were stopped when the molecular weight of the free PS reached

the $M_{n,SEC}$ of the corresponding P*t*BA. The mixed P*t*BA/PS brush-grafted silica particles were isolated, purified by repeated washing with THF, and analyzed by TGA.

Through the two-step procedure, we prepared a total of six mixed brush particle samples with the average MW ranging from 13.8 (MB-MW-1) to 17.9 (MB-MW-2), to 22.2 (MB-MW-3), to 26.5 (MB-MW-4), to 31.9 (MB-MW-5), and finally 33.1 kDa (MB-MW-6) from the same batch of Y-initiator-functionalized silica particles (Table 3.1). The TGA characterization data of these mixed brush samples and the corresponding P*t*BA brush-grafted silica particles are shown in Figure 3.1 along with the thermogram for initiator particles. Clearly, there is a general trend that the weight retention of P*t*BA brush-grafted silica particles at ~ 800 °C decreased with the increase of P*t*BA $M_{n,SEC}$. Similarly, the weight retention of mixed P*t*BA/PS brush particles at ~ 800 °C is generally lower when the average MW is higher, though the values for MB-MW-5 and -6 were very similar. Both indicated that the surface-initiated polymerizations were controlled. Figure 3.1 also showed that the grafted P*t*BA began to decompose at ~ 230 °C while the onset decomposition temperature of PS was ~ 350 °C. The weight loss from room temperature to 100 °C is believed to come from the absorbed moisture.

Our group previously reported, via the cleavage of polymer brushes from silica particles using hydrofluoric acid and the hydrolysis of the ester bond in the Y-initiator with a strong base, that for both P*t*BA and PS the M_ns and PDIs of the grafted polymers and the free polymers were essentially the same.[13a] By using the average diameter and the standard deviation of silica particles (172 ± 20 nm), TGA data (Figure 3.1), and the molecular weights of free P*t*BA and PS formed from the free initiator in the polymerizations,[21] and assuming that the density of silica particles was the same as that of bulk SiO_2 (2.07 g/cm^3), the grafting densities of P*t*BA and PS in

Table 3.1. Characterization Data for Six Mixed P*t*BA/PS Brush-Grafted Particle Samples with Different Average Molecular Weights

Mixed Brush Particle Sample	$M_{n,SEC}$ (kDa) and PDI of P*t*BA [a]	$M_{n,SEC}$ (kDa) and PDI of PS [a]	Average MW (kDa)[b]	σ_{PtBA}, σ_{PS}, $\sigma_{overall}$, and standard deviations (chains/nm^2) [c,d]
MB-MW-1	13.3, 1.10	14.3, 1.22	13.8	0.47 ± 0.05, 0.31 ± 0.04, 0.78 ± 0.06
MB-MW-2	18.3, 1.08	17.5, 1.17	17.9	0.42 ± 0.05, 0.33 ± 0.04, 0.75 ± 0.06
MB-MW-3	22.0, 1.08	22.3, 1.20	22.2	0.37 ± 0.04, 0.41 ± 0.05, 0.78 ± 0.06
MB-MW-4	26.7, 1.06	26.3, 1.15	26.5	0.51 ± 0.06, 0.29 ± 0.03, 0.80 ± 0.07
MB-MW-5	32.1, 1.07	31.6, 1.14	31.9	0.51 ± 0.06, 0.41 ± 0.05, 0.92 ± 0.08
MB-MW-6	34.1, 1.06	32.1, 1.11	33.1	0.50 ± 0.06, 0.35 ± 0.04, 0.85 ± 0.07

[a] The values of number average molecular weight ($M_{n,SEC}$) and polydispersity index (PDI) were determined by size exclusion chromatography (SEC) using PS standards for calibration. [b] Average molecular weight (MW) = ($M_{n,SEC,PtBA}$ + $M_{n,SEC,PS}$)/2. [c] σ_{PtBA}, σ_{PS}, and $\sigma_{overall}$ are P*t*BA grafting density, PS grafting density, and overall grafting density ($\sigma_{overall}$ = σ_{PtBA} + σ_{PS}). The grafting densities were calculated by using the particle size, TGA data, and molecular weights of P*t*BA and PS.[21] [d] The calculation of standard deviations of grafting densities can be found in the Appendix B.

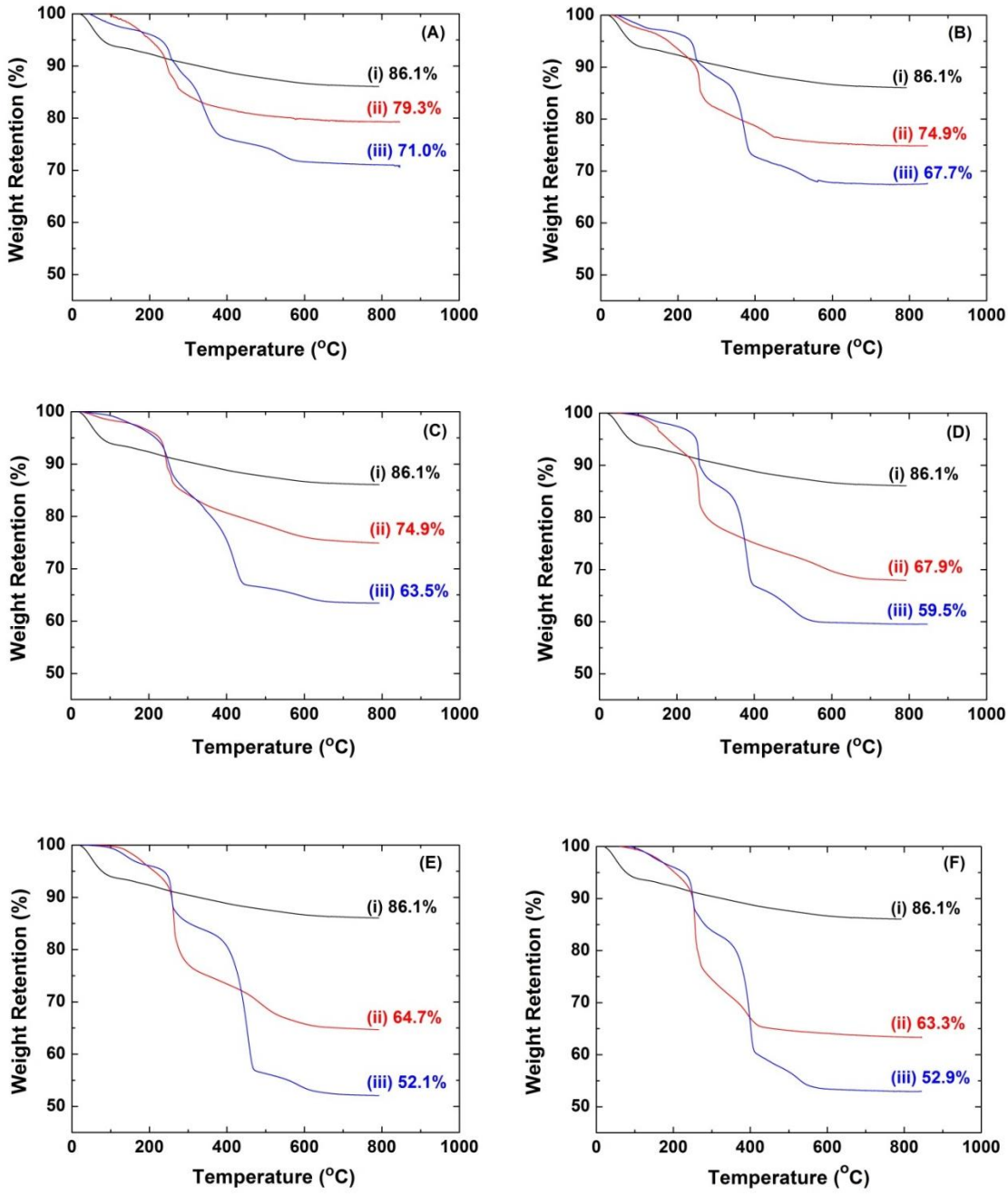

Figure 3.1. Thermogravimetric analysis (TGA) of (i) Y-initiator-functionalized silica particles, (ii) P*t*BA brush-grafted silica particles, and (iii) mixed P*t*BA/PS brush-grafted silica particles obtained in the preparation of mixed brush-grafted particle sample (A) MB-MW-1, (B) MB-MW-2, (C) MB-MW-3, (D) MB-MW-4, (E) MB-MW-5, and (F) MB-MW-6.

each mixed brush sample and their standard deviations were calculated and are summarized in Table 3.1. Figure 3.2 shows the plots of individual grafting densities of P*t*BA and PS (σ_{PtBA} and σ_{PS}, respectively) and overall grafting density ($\sigma_{overall}$) versus average MW of the two polymers.

From Table 3.1 and Figure 3.2, one can see that the overall grafting densities were similar, ~ 0.80 chains/nm^2, for all mixed brush samples except MB-MW-5, whose $\sigma_{overall}$ was 0.92 chains/nm^2. The individual grafting densities of P*t*BA and PS were comparable, though σ_{PtBA} appeared to be slightly larger than σ_{PS} in most of mixed brush samples. This is likely because of the steric hindrance presented by the existing P*t*BA chains when the PS chains were grown from the surface of silica particles. The slight increase in $\sigma_{overall}$ with the increase of molecular weight could be a result of the higher initiation efficiency at the longer polymerization time, particularly for NMRP. Our group previously observed before a similar trend in the grafting density with increasing time in the study of the effect of chain length disparity on microphase separation of mixed brushes.[13d,e]

Chapter 2 showed that the overall grafting density had an effect on the average rippled wavelength (*D*) of the nanopattern formed by microphase separation of mixed P*t*BA/PS brushes grafted on silica particles. We found that in the $\sigma_{overall}$ range of 0.54 – 1.06 chains/nm^2, the ripple wavelength scaled with -0.47 power of overall grafting density, i.e., $D \sim \sigma_{overall}^{-0.47}$. In this Chapter, we study the effect of MW on morphology of mixed P*t*BA/PS brushes, and we think that the small differences in the overall grafting densities of these mixed brush particle samples should not have much influence on average ripple wavelength. Wang and Müller showed that the lateral microphase separation can tolerate small variations in grafting densities and molecular weights of two end-tethered homopolymers.[9h] Nevertheless, we emphasize here that it is very

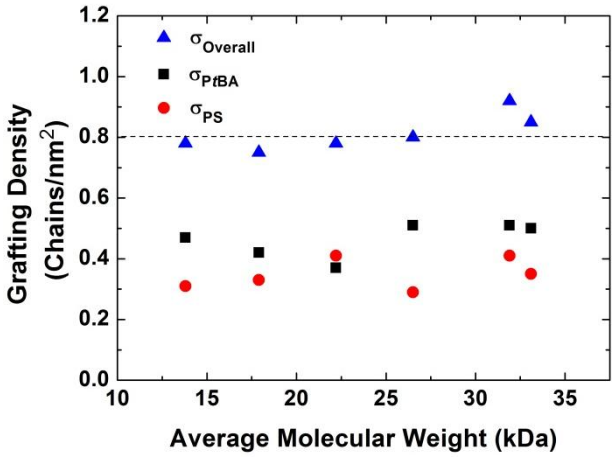

Figure 3.2 Plots of individual grafting density of P*t*BA (σ_{PtBA}, black square), individual grafting density of PS (σ_{PS}, red circle), and overall grafting density of mixed P*t*BA/PS brushes ($\sigma_{overall}$, blue triangle) versus average molecular weight of the two polymers.

difficult, if not impossible, to prepare a set of symmetric mixed brushes with a perfect polymer architecture and identical individual grafting densities.

3.3.2 TEM Study of Microphase Separation of Mixed P*t*BA/PS Brushes Grafted on Silica Particles with Various Average MWs Cast from Chloroform Dispersions

Our group previously showed that mixed P*t*BA/PS brushes with P*t*BA $M_{n,SEC}$ of 24.2 kDa and PS $M_{n,SEC}$ of 23.0 kDa phase separated into a bicontinuous worm-like striped nanopattern after the mixed brush-grafted silica particles were cast from $CHCl_3$, a good solvent for both P*t*BA and PS.[13c] The polymer brushes spread out on the carbon film and covered the interstitial space among the silica particles. Therefore, we first investigated the morphology of mixed brushes cast from $CHCl_3$ and examined how the feature size changed with the average MW. Note that we purposely synthesized mixed brushes with very similar P*t*BA and PS molecular weights.

The mixed brush particle samples were dispersed in $CHCl_3$ and drop cast onto carbon-coated TEM copper grids. After solvent annealing in a closed container, the samples were stained with RuO_4 at room temperature for 20 min and then examined under TEM. Note that RuO_4 stains PS, making PS nanodomains dark and P*t*BA nanodomains bright under TEM.[13b] Figure 3.3 shows representative top-view bright field TEM micrographs of six mixed brush particle samples arranged in the order of increasing average MW of mixed brushes (i.e., from MB-MW-1 to MB-MW-6). More TEM pictures can be found in the Appendix B. Clearly, all six mixed brush samples were microphase separated, forming rippled nanostructures composed of dark PS and bright P*t*BA nanostripes. Moreover, the feature size gradually increased with the increase of average MW of P*t*BA and PS, consistent with the theoretical prediction.[10,11] While clear microphase separation was observed both in the interstitial space and "on" the particle for higher

Figure 3.3 Top-view bright field TEM micrographs of (A) MB-MW-1 (P*t*BA M_n = 13.3 kDa, σ_{PtBA} = 0.47 chains/nm^2; PS M_n = 14.3 kDa, σ_{PS} = 0.31 chains/nm^2; $\sigma_{overall}$ = 0.78 chains/nm^2), (B) MB-MW-2 (P*t*BA M_n = 18.3 kDa, σ_{PtBA} = 0.42 chains/nm^2; PS M_n = 17.5 kDa, σ_{PS} = 0.33 chains/nm^2; $\sigma_{overall}$ = 0.75 chains/nm^2), (C) MB-MW-3 (P*t*BA M_n = 22.0 kDa, σ_{PtBA} = 0.37 chains/nm^2; PS M_n = 22.3 kDa, σ_{PS} = 0.41 chains/nm^2; $\sigma_{overall}$ = 0.78 chains/nm^2), (D) MB-MW-4 (P*t*BA M_n = 26.7 kDa, σ_{PtBA} = 0.51 chains/nm^2; PS M_n = 26.3 kDa, σ_{PS} = 0.29 chains/nm^2; $\sigma_{overall}$ = 0.80 chains/nm^2), (E) MB-MW-5 (P*t*BA M_n = 32.1 kDa, σ_{PtBA} = 0.51 chains/nm^2; PS M_n = 31.6 kDa, σ_{PS} = 0.41 chains/nm^2; $\sigma_{overall}$ = 0.92 chains/nm^2), (F) MB-MW-6 (P*t*BA M_n = 34.1 kDa, σ_{PtBA} = 0.50 chains/nm^2; PS M_n = 32.1 kDa, σ_{PS} = 0.35 chains/nm^2; $\sigma_{overall}$ = 0.85 chains/nm^2) after being cast from $CHCl_3$ dispersions and annealed with $CHCl_3$ vapor. The samples were stained with RuO_4 at room temperature for 20 min.

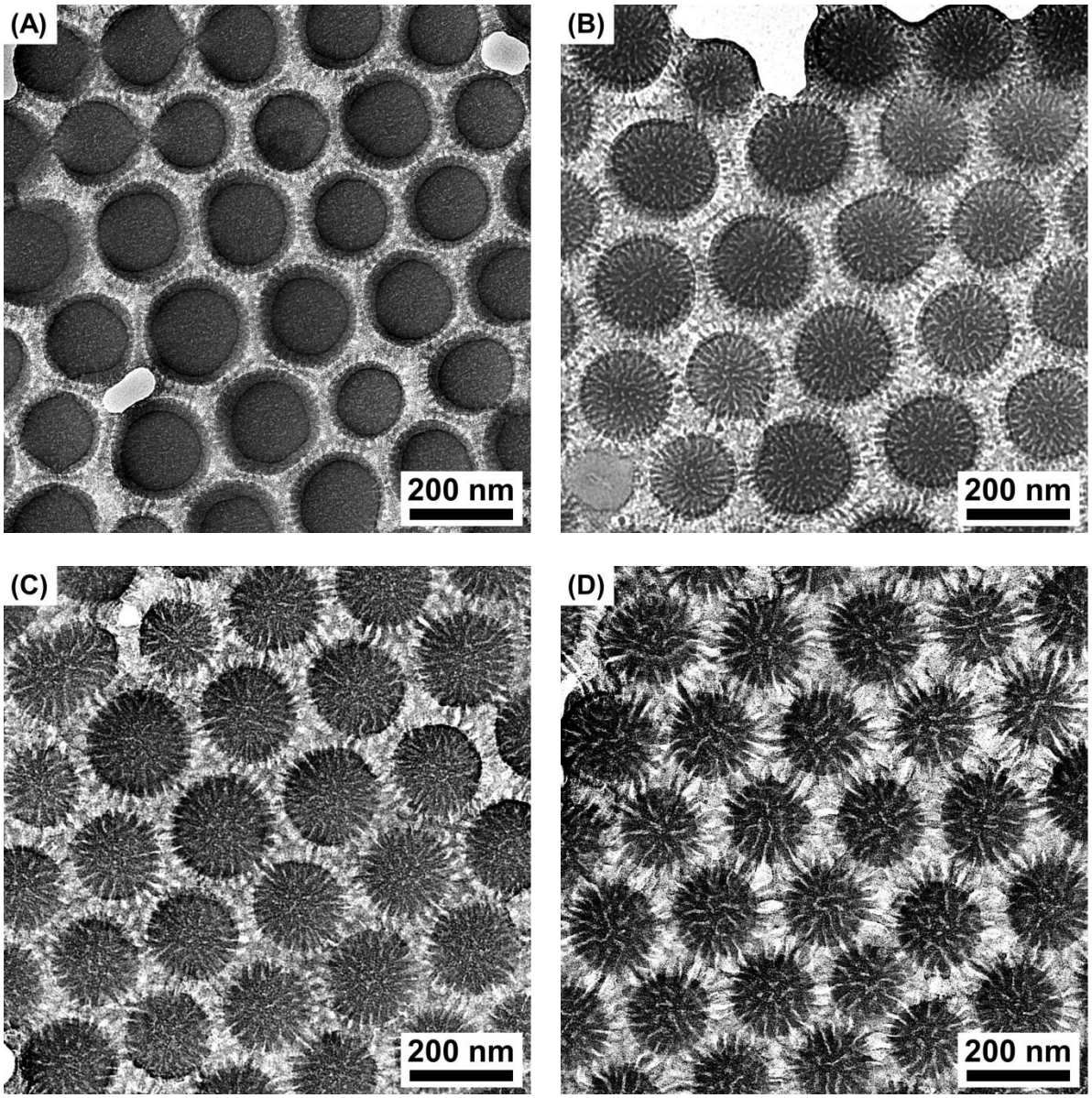

(Figure 3.3 continued)

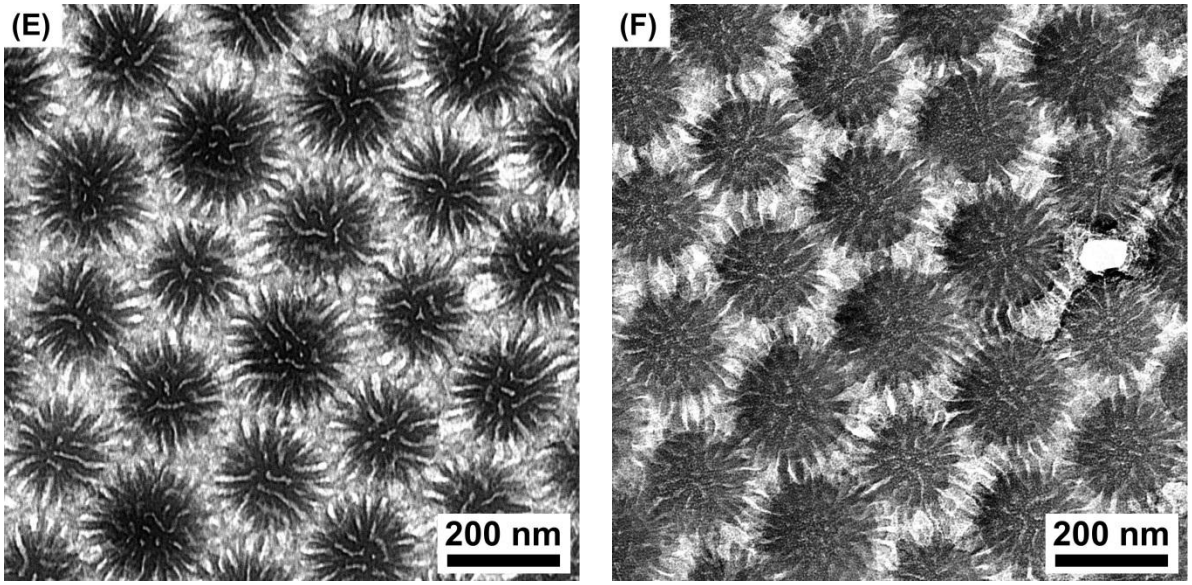

(Figure 3.3 continued)

MW samples from MB-MW-2 (average MW = 17.9 kDa) to MB-MW-6 (average MW = 33.1 kDa), it was only seen in the interstitial area for MB-MW-1 (average MW = 13.8 kDa). The dark and bright nanodomains on the silica particles were hardly discernible. This is likely because the MWs of the two polymers were low, perhaps just above the critical molecular weight for microphase separation of mixed P*t*BA/PS at this grafting density, resulting in weak phase separation.

In addition, the brush thickness "on" the particles of MB-MW-1 was thin, causing a lower contrast between P*t*BA and PS nanodomains "on" the particle. Tang et al. recently found from a TEM tomography study that the microphase separation of mixed P*t*BA/PS brushes on silica particles depended heavily on the location along the vertical direction of the particle film because the spreading of polymer brushes and the self-assembly of particles caused an uneven distribution of brush thickness.[22] The phase separation of the mixed brushes at the brush-vacuum interface was significantly weaker because of the lower brush thickness. For the same reason, clear microphase separation was seen in the bottom portion of individual mixed brush-grafted silica particles rather than in the top hemisphere. When the particles were cast from $CHCl_3$, the grafted polymer chains were pulled down toward the carbon film during the solvent evaporation process.

Using Nano Measurer 1.2 software, we performed image analysis of TEM micrographs B-F in Figure 3.3 by selecting the features in the area between the half radius ($R/2$) and the periphery (R) from the particle center (i.e., the edge view of the particles). In Figure 3.3A, the features in the interstitial area were chosen for TEM image analysis. The results are summarized in Figure 3.4 as plots of counts versus ripple wavelengths (sum of widths of neighboring P*t*BA and PS stripes). As expected, the average ripple wavelength (D) increased with the increase of average

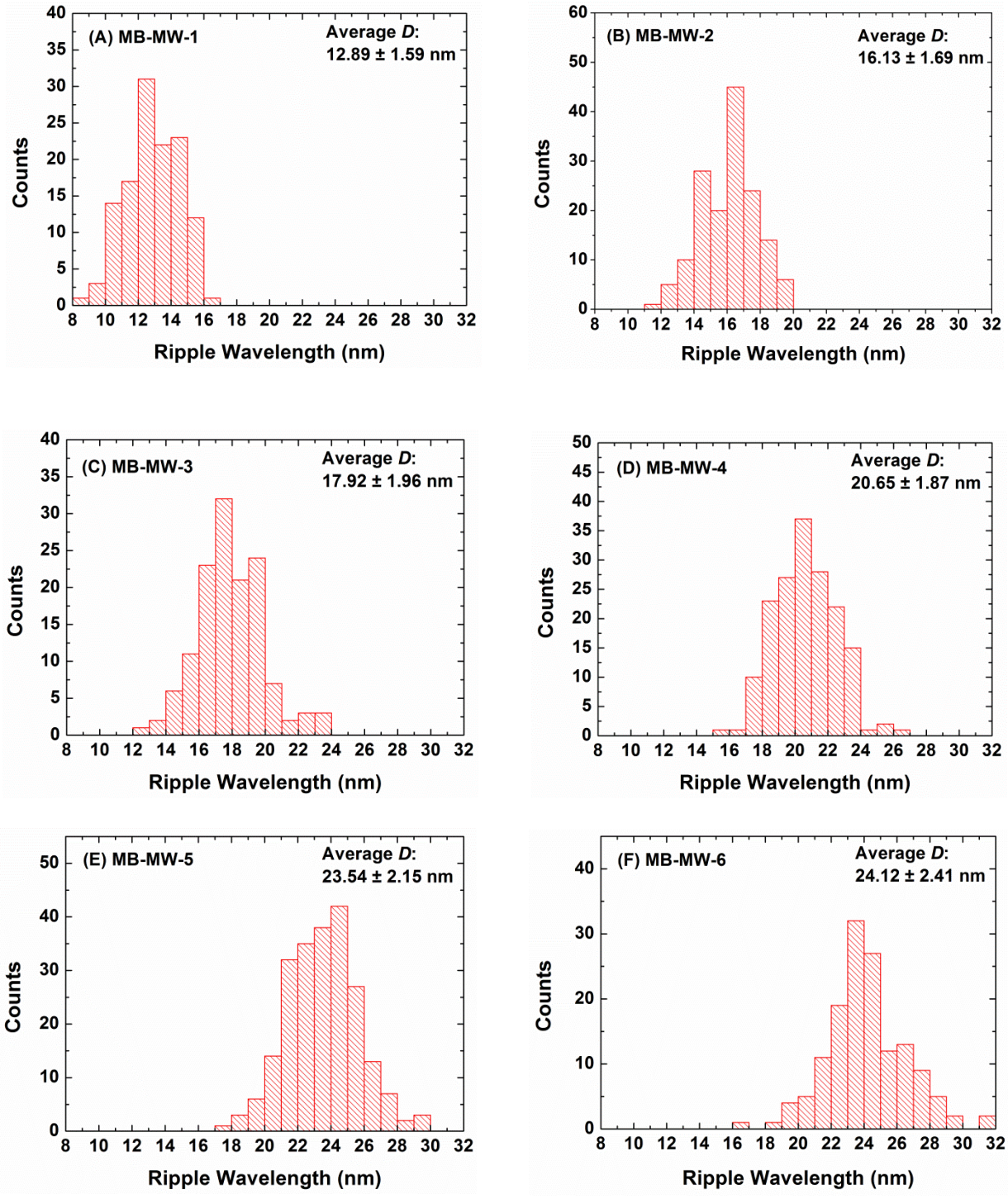

Figure 3.4 Distributions of ripple wavelengths of features (sum of both widths of neighboring P*t*BA and PS nanostripes) obtained from TEM image analysis of (A) Figure 3.3A, MB-MW-1, (B) Figure 3.3B, MB-MW-2, (C) Figure 3.3C, MB-MW-3, (D) Figure 3.3D, MB-MW-4, (E) Figure 3.3E, MB-MW-5, and (F) Figure 3.3F, MB-MW-6.

MW of mixed brushes, from 12.89 nm (MB-MW-1), to 16.13 nm (MB-MW-2), to 17.92 nm (MB-MW-3), to 20.65 nm (MB-MW-4), to 23.54 nm (MB-MW-5), and 24.12 nm (MB-MW-6).

Figure 3.5 shows the plot of average ripple wavelength *D* versus average MW of mixed P*t*BA/PS brushes on a double logarithmic scale. A linear dependence of log*D* on log(MW) with a slope of 0.70 and a linear fit *R* of 0.998 was observed. Although the standard error for the slope from the linear fitting was very small, only 0.03, the overall standard deviation was relatively large, 0.15, when the standard deviations of ripple wavelengths of six samples were taken into consideration.[23] If MB-MW-5, whose $\sigma_{overall}$ (0.92 chains/nm^2) is appreciably larger than those of other five samples, is not included in the linear fitting (see the inset in Figure 3.5), the slope and the standard error from the linear fitting were unchanged (0.70 and 0.03, respectively); the overall standard deviation for the slope was 0.11.[23] Our observation is slightly different from the theoretically predicted dependence of *D* on degree of polymerization (*N*) of perfect symmetric Y-shaped brushes, $D \sim N^{1/2}$ in melt and in nonselective poor solvents.[10,11] This discrepancy is likely caused by the effect of good solvent in the preparation of TEM samples. The mixed P*t*BA/PS brushes were not uniformly collapsed when the hairy particles were drop cast from chloroform dispersions onto the carbon-coated TEM grids;[22] the brushes spread out on the carbon film during the solvent evaporation process. The TEM micrographs shown in Figure 3.3 were actually the rippled nanopatterns formed in the bottom part close to the carbon film-polymer brush interface, where the microphase separation of mixed P*t*BA/PS brushes was the best, partly because of the grafted polymer chains concentrated in this region. We suspected that the non-uniform collapse of mixed brushes and the spreading effect, caused by the evaporation of good solvent $CHCl_3$, might change the MW dependence of ripple wavelength. On the other hand, the theoretical studies were based on mixed brushes grafted on flat substrates with

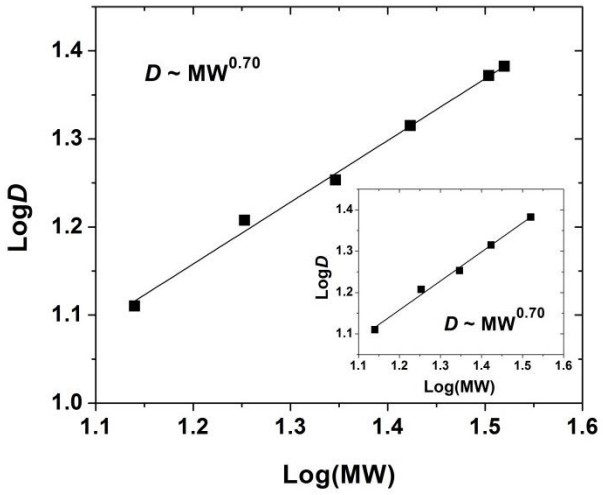

Figure 3.5 Plot of log*D* versus log(MW), where *D* is the average ripple wavelength, obtained from image analysis of TEM micrographs in Figure 3.3, and MW is the average molecular weight of P*t*BA and PS in the unit of kDa. The straight solid line is a linear fit with $R = 0.998$ and a slope of 0.70. The inset is the plot of log*D* versus log(MW) excluding MB-MW-5. The straight solid line is a linear fit with $R = 0.997$ and a slope of 0.70.

identical individual grafting densities for the two homopolymers, which are not the case for real mixed brushes on 172 nm silica particles. In addition, in the theoretical study of Zhulina and Balazs, the scaling relationship was obtained for perfect symmetric Y-brushes in the melt and in nonselective poor solvents,[11] where the two polymers were highly incompatible and grafting densities were high. To further look into this issue, it is necessary to prepare samples with uniformly collapsed mixed brushes on silica particles for TEM study.

3.3.3 TEM Study of Microphase Separation of Mixed P*t*BA/PS Brushes Grafted on Silica Particles with Various Average MWs Cast from Surfactant-Stabilized Aqueous Dispersions

We further studied the molecular weight dependence of ripple wavelength *D* by examining the uniformly collapsed mixed P*t*BA/PS brushes on silica particles. The hairy particle samples were dispersed in $CHCl_3$ and added into water in the presence of a surfactant, CTAB, under the vigorous stirring conditions, forming a microemulsion.[24] Chloroform was then gradually evaporated in a fume hood by stirring the mixtures. A control experiment showed that from ^1H NMR spectroscopy analysis, > 99% $CHCl_3$ was gone (see the Appendix B). CTAB, which is presumably neutral to both P*t*BA and PS, stabilized the small chloroform droplets containing mixed P*t*BA/PS brush-grafted silica particles in the aqueous emulsion. With the slow evaporation of chloroform, the mixed P*t*BA/PS brushes collapsed uniformly on the surface of silica core, and the microphase separated nanopatterns were gradually frozen due to the glass transition temperatures of PS (~ 100 °C) and P*t*BA (~ 34 °C) being higher than room temperature. The surfactant-stabilized aqueous dispersions of hairy particles were drop cast onto the carbon-coated TEM grids. When water, a nonselective poor solvent for both P*t*BA and PS, evaporated from the TEM grids, the mixed brushes were not spread out but stayed uniformly collapsed. The TEM samples were then stained with RuO_4 and examined under TEM.

Figure 3.6 Top-view bright field TEM micrographs of (A) MB-MW-1 (P*t*BA M_n = 13.3 kDa, σ_{PtBA} = 0.47 chains/nm^2; PS M_n = 14.3 kDa, σ_{PS} = 0.31 chains/nm^2; $\sigma_{overall}$ = 0.78 chains/nm^2), (B) MB-MW-2 (P*t*BA M_n = 18.3 kDa, σ_{PtBA} = 0.42 chains/nm^2; PS M_n = 17.5 kDa, σ_{PS} = 0.33 chains/nm^2; $\sigma_{overall}$ = 0.75 chains/nm^2), (C) MB-MW-3 (P*t*BA M_n = 22.0 kDa, σ_{PtBA} = 0.37 chains/nm^2; PS M_n = 22.3 kDa, σ_{PS} = 0.41 chains/nm^2; $\sigma_{overall}$ = 0.78 chains/nm^2), (D) MB-MW-4 (P*t*BA M_n = 26.7 kDa, σ_{PtBA} = 0.51 chains/nm^2; PS M_n = 26.3 kDa, σ_{PS} = 0.29 chains/nm^2; $\sigma_{overall}$ = 0.80 chains/nm^2), (E) MB-MW-5 (P*t*BA M_n = 32.1 kDa, σ_{PtBA} = 0.51 chains/nm^2; PS M_n = 31.6 kDa, σ_{PS} = 0.41 chains/nm^2; $\sigma_{overall}$ = 0.92 chains/nm^2), (F) MB-MW-6 (P*t*BA M_n = 34.1 kDa, σ_{PtBA} = 0.50 chains/nm^2; PS M_n = 32.1 kDa, σ_{PS} = 0.35 chains/nm^2; $\sigma_{overall}$ = 0.85 chains/nm^2) after being cast from surfactant-stabilized aqueous dispersions. The samples were stained with RuO_4 at room temperature for 20 min.

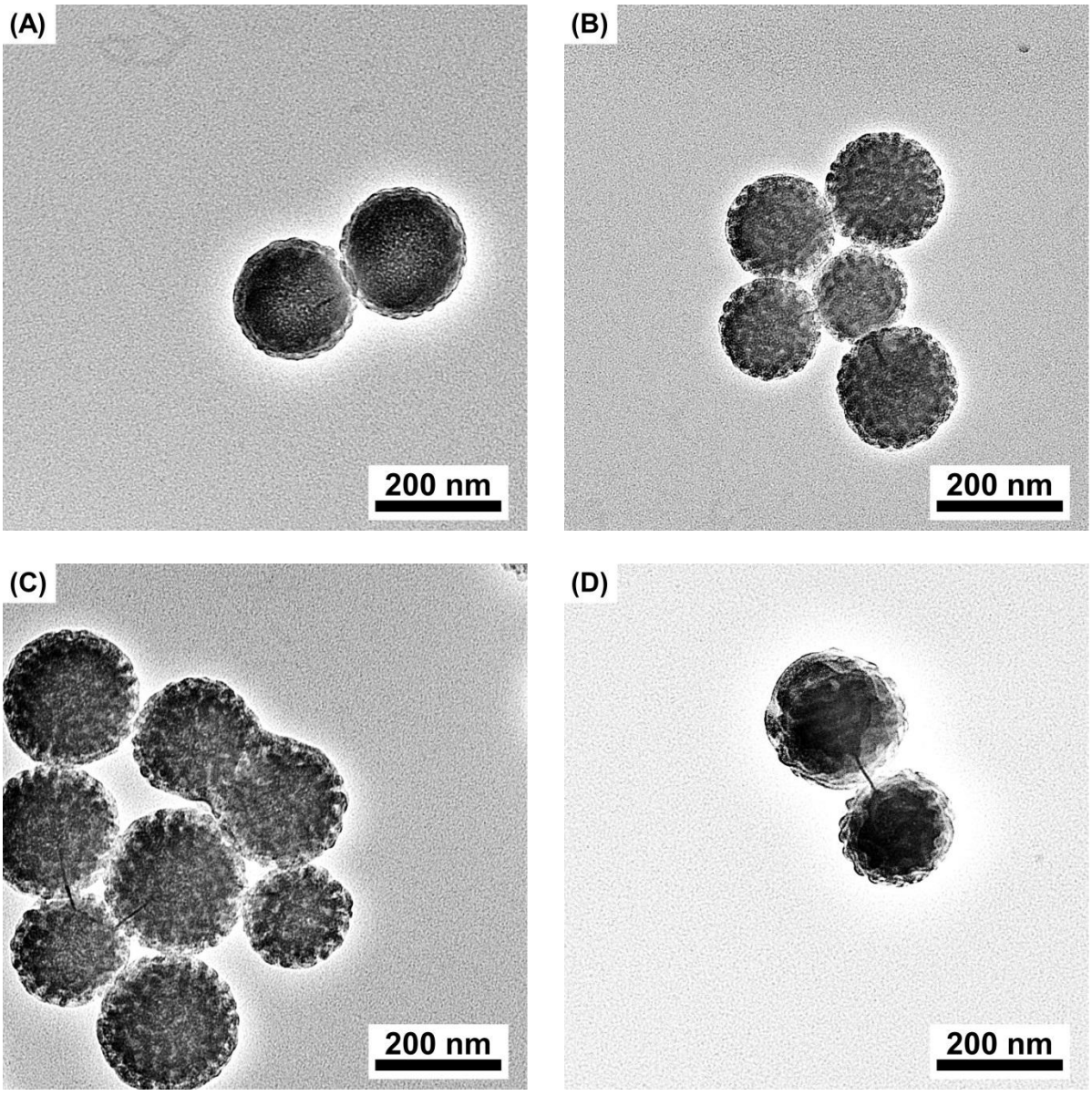

(Figure 3.6 continued)

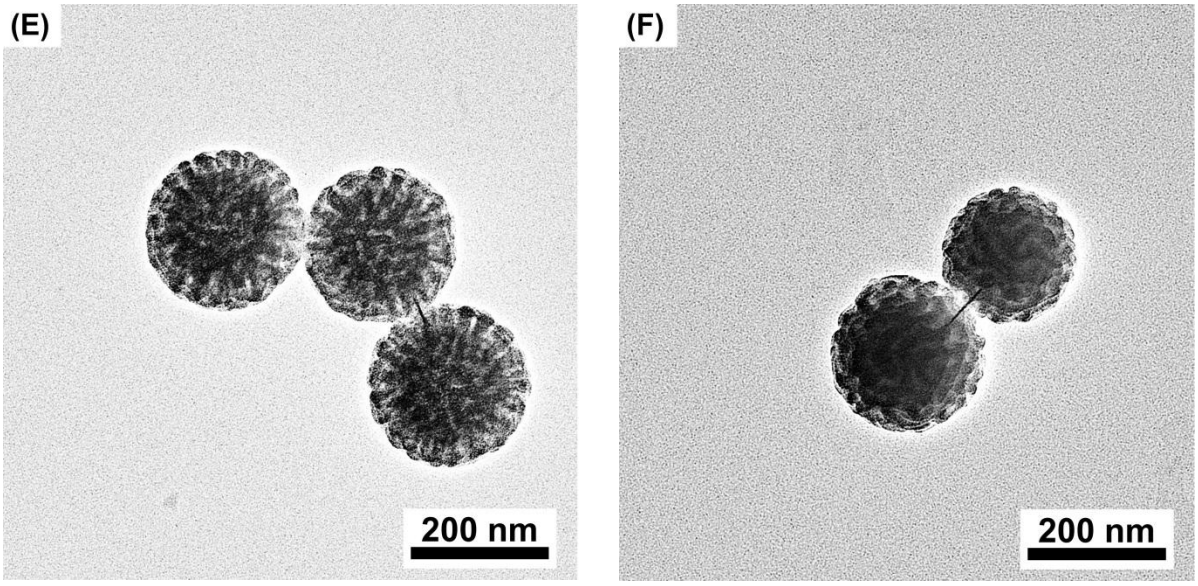

(Figure 3.6 continued)

Figure 3.6 shows representative top-view, bright field TEM micrographs of six mixed P*t*BA/PS brush particle samples arranged in the order of increasing average MW of mixed brushes. More images can be found in the Appendix B. By browsing through the TEM images in Figure 3.6, again, one can easily tell that samples MB-MW-2 to MB-MW-6 exhibited clear lateral microphase separation, producing worm-like rippled nanostructures, and the feature size increased with increasing average MW. In contrast, the microphase separation of MB-MW-1 was weak, consistent with the observation from Figure 3.3A.

We also performed TEM image analysis for Figure 3.6B-F and the TEM images Figure B8-12 in Appendix B, and the results are presented in Figure 3.7. The average ripple wavelength increased with the increase of average MW, from 16.39 nm (MB-MW-2), to 18.62 nm (MB-MW-3), to 20.73 nm (MB-MW-4), to 22.56 nm (MB-MW-5), to 23.24 nm (MB-MW-6). It should be noted here that the average ripple wavelength for the same mixed P*t*BA/PS brush-grafted particle sample cast from the aqueous dispersion is slightly different from that cast from $CHCl_3$. The values of average ripple wavelength D of mixed brushes from $CHCl_3$ were 16.13 nm for MB-MW-2, 17.92 nm for MB-MW-3, 20.65 nm for MB-MW-4, 23.54 nm for MB-MW-5, and 24.12 nm for MB-MW-6. Figure 3.8 shows the plot of D versus average MW of mixed brushes on a double logarithmic scale. A linear dependence of log$D$ on log(MW) with a slope of 0.56 was observed (linear fit R = 0.999, standard error = 0.02). By including the errors in the measurements of ripple wavelengths, the calculated overall standard deviation was 0.21.[23] If MB-MW-5 is excluded in the linear fitting (see the inset in Figure 3.8), the slope and the standard error were 0.57 and 0.02, respectively; the overall standard deviation was 0.19.[23] The calculated overall standard deviations are relatively large likely because of the propagation and amplification of standard errors from the measurements of ripple wavelengths in the linear

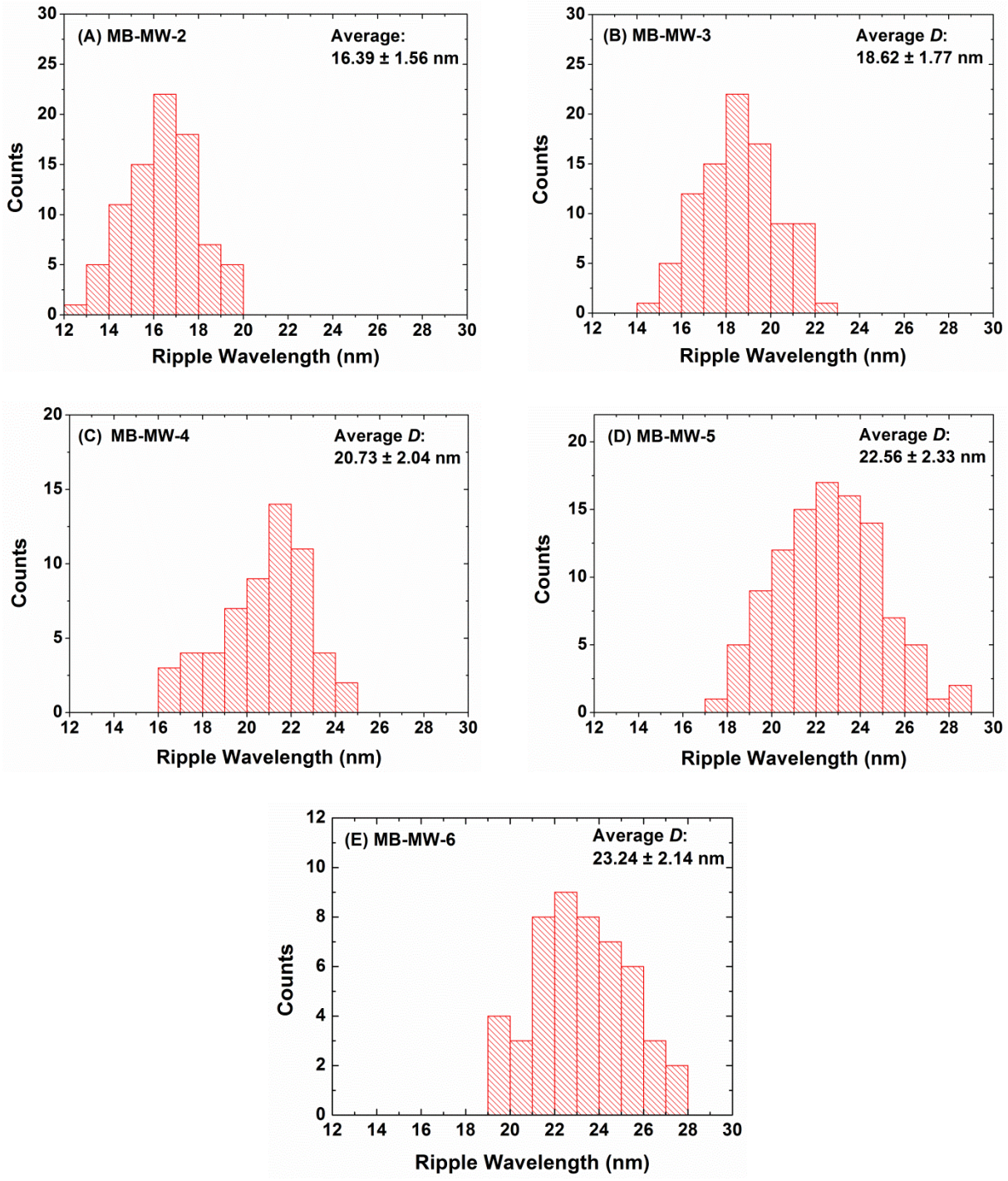

Figure 3.7 Distributions of ripple wavelengths of features (sum of both widths of neighboring P*t*BA and PS stripes) obtained from analysis of TEM micrographs of (A) MB-MW-2, (B) MB-MW-3, (C) MB-MW-4, (D) MB-MW-5, and (E) MB-MW-6 in Figure 3.6 and Figures B8-12 (in the Appendix B).

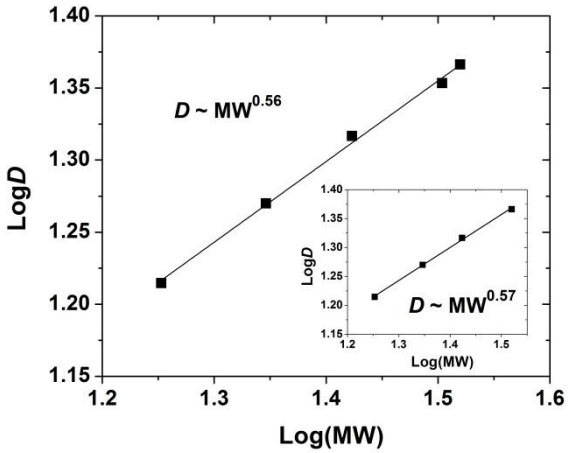

Figure 3.8 Plot of log*D* versus log(MW), where *D* is the average ripple wavelength and MW is the average molecular weight of mixed P*t*BA/PS brushes in unit of kDa. The straight solid line is a linear fit with $R = 0.999$ and a slope of 0.56. The inset is a linear fit of four points with R of 0.999 and a slope of 0.57 (MB-MW-5 is excluded).

fitting. The result from the analysis of hairy particles from aqueous dispersions is close to the theoretical prediction ($D \sim MW^{0.5}$), although there is still a small difference. The discrepancy probably came from the fact that our mixed brushes are not perfect symmetric Y-brushes with exactly the same chain lengths and grafting densities for the two polymers.

3.3.4 Comparison of Microphase Separation of Mixed P*t*BA/PS Brushes Grafted on Silica Particles and P*t*BA-*b*-PS Diblock Copolymers

Marko and Witten predicted that symmetric mixed homopolymer brushes tethered on a flat substrate underwent lateral microphase separation forming a "rippled" phase rather than vertical phase segregation producing a "layered" structure under equilibrium melt condition. The microphase separation is expected to occur at a critical point with $(\chi N)_c = 9.08$, where χ is Flory-Huggins interaction parameter and $N = N_A + N_B$ (N_A and N_B are the degrees of polymerizations (DPs) of grafted polymers A and B).[1] From the mean-field theory of symmetric diblock copolymers, microphase separation takes place at a critical point of $(\chi N)_c = 10.5$.[25] Thus according to these theories for mixed homopolymer brushes and diblock copolymers, mixed brushes should undergo microphase separation at lower molecular weights than the corresponding diblock copolymers.

It was previously found that a mixed P*t*BA/PS brush sample grafted on 180 nm silica particles with P*t*BA $M_{n,SEC}$ of 10.4 kDa (PDI = 1.15), σ_{PtBA} of 0.32 chains/nm^2, PS $M_{n,SEC}$ of 11.9 kDa (PDI = 1.19), and σ_{PS} of 0.35 chains/nm^2 , which is designated as MB-MW-M, did not exhibit microphase separation.[13b] A representative TEM micrograph of this mixed brush sample is shown in Figure 3.9. Combining the observations for MB-MW-M (Figure 3.9) and MB-MW-1 (Figure 3.3A), we can conclude that the critical average MW for microphase separation of mixed P*t*BA/PS brushes at an overall grafting density of ~ 0.7 – 0.8 chains/nm^2 should be between 11.2

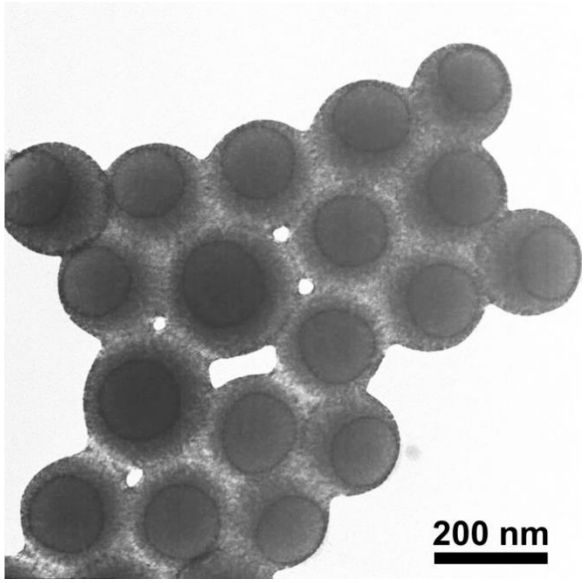

Figure 3.9 Top-view bright field TEM micrograph of MB-MW-M (P*t*BA M_n = 10.4 kDa, σ_{PtBA} = 0.32 chains/nm^2; PS M_n = 11.9 kDa, σ_{PS} = 0.35 chains/nm^2; $\sigma_{overall}$ = 0.67 chains/nm^2) cast from $CHCl_3$, a good solvent for P*t*BA and PS, and annealed thermally at 120 ℃ for 3 h. The sample was stained with RuO_4 at room temperature for 20 min.

kDa (MB-MW-M), and 13.3 kDa (MB-MW-1). To compare the phase separation behavior of mixed brushes and diblock copolymers, we synthesized two symmetric P*t*BA-*b*-PS diblock copolymers by reversible addition-fragmentation chain transfer (RAFT) polymerization. The characterization data for these two polymer samples are summarized in Table 3.2. Note that the M_n of DB-1 was essentially the same as the sum of the M_n values of two polymers in MB-MW-M. The volume fractions of P*t*BA in DB-1 and DB-2 were 49.5 % and 48.9 %, which were very close to the 50% for symmetric diblock copolymers.

Differential scanning calorimetry (DSC) studies showed that for both DB-1 and DB-2, two distinct glass transitions were observed at ~ 45 and ~ 90 °C (Figure 3.10), which were attributed to the glass transitions of P*t*BA and PS blocks, respectively, suggesting that both diblock copolymers were microphase separated. SAXS and TEM, two popular characterization tools commonly used to study microphase separation in block copolymers, were also employed to investigate the morphologies of DB-1 and DB-2.[26] They both confirmed that DB-1 and DB-2 formed lamellar structures in melt. Unfortunately, for mixed P*t*BA/PS brushes grafted on 170-180 nm silica particles, SAXS could not be employed to study the microphase separation due to the interference of strong scattering from silica cores. However, the TEM study clearly showed that MB-MW-M did not phase separate after annealing in vacuum at 120 ℃ for 3 h. Considering these results and the fact that the molecular weights of MB-MW-M and DB-1 are essentially the same, we can conclude that it is more difficult for mixed P*t*BA/PS brushes to undergo microphase separation at an overall grafting density of ~ 0.7 – 0.8 chains/nm^2 than P*t*BA-*b*-PS diblock copolymers. This is inconsistent with the theoretical prediction by Marko and Witten.[1] However, in the theoretical work by Marko and Witten, the grafting density of mixed homopolymer brushes was not taken into account. We speculate that the grafting density might

Table 3.2 Characterization Data for Two P*t*BA-*b*-PS Diblock Copolymers Synthesized by RAFT

Sample No. [a]	$M_{n,SEC}$ and PDI of P*t*BA [b]	DP and $M_{n,NMR}$ of P*t*BA[c]	$M_{n,SEC}$ and PDI of P*t*BA-*b*-PS [b]	DP of PS [d]	P*t*BA Volume Fraction [e]
DB-1	11.2 kDa, 1.11	85, 10.9 kDa	21.6 kDa, 1.13	112	49.5 %
DB-2	15.1 kDa, 1.11	111, 14.2 kDa	29.2 kDa, 1.15	149	48.9 %

[a] P*t*BA-*b*-PS diblock copolymers were synthesized by RAFT from P*t*BA macro-CTAs. [b] The values of number average molecular weight ($M_{n,SEC}$) and polydispersity index (PDI) were determined by size exclusion chromatography (SEC) relative to polystyrene standards. [c] Degree of polymerization (DP) of P*t*BA was calculated from the monomer-to-CTA ratio and the monomer conversion determined by ^{1}H NMR spectroscopy. $M_{n,NMR}$ = DP × molecular weight of *t*BA. [d] DP of PS in P*t*BA-*b*-PS was determined from the ^{1}H NMR spectrum using the integral values of the peak from 2.0 to 2.4 ppm (-CH_2C*H*-) and the aromatic peak of PS from 6.2 to 7.2 ppm. The synthesis and characterization data for DB-1 and -2 can be found in the Appendix B [e] The density values of P*t*BA (1.008 g/cm^3) and PS (1.052 g/cm^3) were used in the calculation of volume fractions.

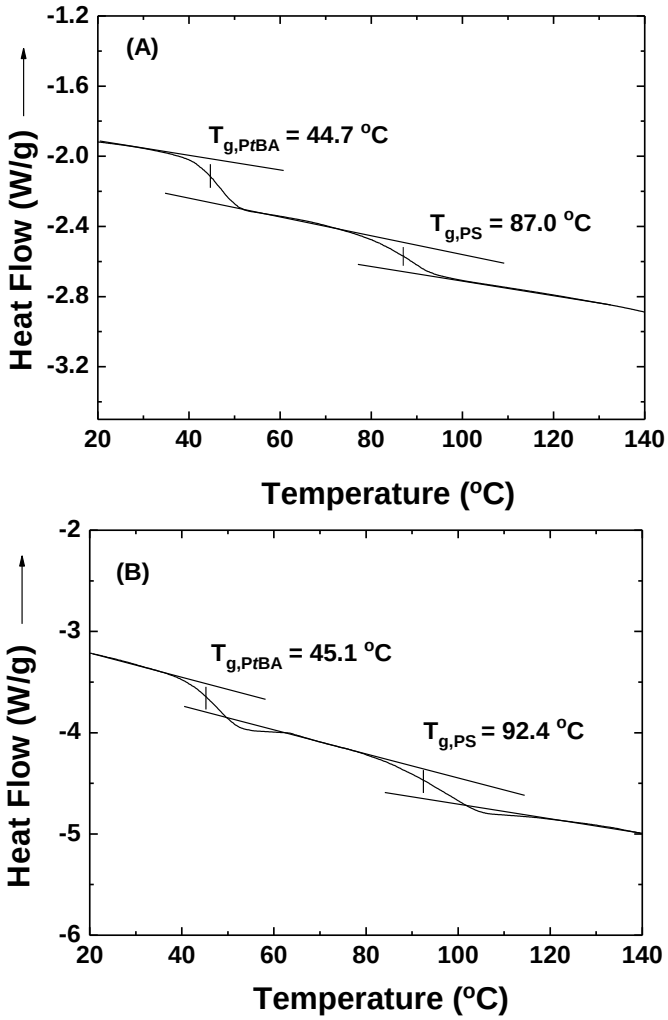

Figure 3.10 Differential scanning calorimetry (DSC) analysis of block copolymer P*t*BA-*b*-PS (A) DB-1, $M_{n,SEC}$ = 21.6 kDa, PDI = 1.13 and (B) DB-2, $M_{n,SEC}$ = 29.2 kDa, PDI = 1.15. The heating and cooling rates in the DSC analysis were 20 and 3 °C/min, respectively.

play a role in the ordering of the mixed P*t*BA/PS brushes. Moreover, unlike diblock copolymers, the lateral microphase separation of mixed brushes involves the formation of a crossover zone in the bottom part of the mixed brush layer, which would increase the free energy of the system and thus decrease the tendency of mixed brushes to phase separate.

Interestingly, for almost all mixed brush samples in Figure 3.3, P*t*BA microdomains in the TEM micrographs appeared to be thinner than PS microdomains. On the basis of the finding that microphase separation of mixed homopolymer brushes was weaker than that of diblock copolymers, this observation could be attributed to the relatively weak microphase separation of mixed P*t*BA/PS brushes. In other words, there could be a relatively thick interface layer between pure P*t*BA and PS microdomains. Both the PS microdomains and the interface layers were stained by RuO_4, making the P*t*BA layers appear thinner than expected. A similar phenomenon was also observed in the previous TEM studies of mixed P*t*BA/PS brushes grafted on silica particles.[13e]

3.4 Conclusions

A systematic study of the effect of MW on microphase separation of mixed P*t*BA/PS brushes grafted on 172 nm silica particles was conducted.[27] A set of six mixed P*t*BA/PS brush-grafted silica particle samples with various average MW, ranging from 13.8 to 33.1 kDa, but similar individual and overall grafting densities were made by sequential ATRP of *t*BA at 75 °C and NMRP of styrene at 120 °C. Each mixed brush sample had similar MWs for the two polymers. TEM studies showed that the feature size of the nanopattern formed from lateral microphase separation increased with the increase of average MW. For the TEM samples prepared by drop casting from $CHCl_3$ dispersions, the grafted polymer chains spread out, and the ripple

wavelength D was found to be proportional with $MW^{0.70}$ in the studied MW range from 13.8 to 33.1 kDa. The scaling relationship was slightly different, $D \sim MW^{0.56}$, when the mixed brush-grafted particle samples were cast from surfactant-stabilized aqueous dispersions, where mixed P*t*BA/PS brushes were collapsed uniformly. Our results were in qualitative agreement with the theoretical predictions. This is the first time that the effect of MW on lateral microphase separation of mixed homopolymer brushes was systematically and quantitatively investigated. We further compared the phase separation behavior of mixed brushes and P*t*BA-*b*-PS diblock copolymers and found that it is more difficult for mixed brushes to microphase separate than diblock copolymers. These findings can be used to guide the design of responsive, nanostructured polymer-inorganic hybrid materials for potential applications based on mixed homopolymer brushes.

References

1. Marko, J. F.; Witten, T. A. *Phys. Rev. Lett.* **1991,** *66*, 1541-1544.
2. Zhao, B.; Zhu, L. *Macromolecules* **2009**, *42*, 9369-9383.
3. Moffitt, M. G. *J. Phys. Chem. Lett.* **2013**, *4*, 3654-3666.
4. Chen, L.; Klok, H.-A. *Soft Matter* **2013**, *9*, 10678-10688.
5. Sidorenko, A.; Minko, S.; Schenk-Meuser, K.; Duschner, H.; Stamm, M. *Langmuir* **1999,** *15*, 8349-8355.
6. (a) Zhao, B.; He, T. *Macromolecules* **2003**, *36*, 8599-8602. (b) Zhao, B.; Haasch, R. T.; MacLaren, S. *J. Am. Chem. Soc.* **2004**, *126*, 6124-6134. (c) Zhao, B.; Haasch, R. T.; MacLaren, S. *Polymer* **2004**, *45*, 7979-7988. (d) Usov, D.; Gruzdev, V.; Nitschke, M.; Stamm, M.; Hoy, O.; Luzinov, I.; Tokarev, I.; Minko, S. *Macromolecules* **2007**, *40*, 8774-8783. (e) Santer, S.; Kopyshev, A.; Yang, H. K.; Rühe, J. *Macromolecules* **2006,** *39*, 3056-3064. (f) Tsujii, Y.; Ohno, K.; Yamamoto, S.; Goto, A.; Fukuda, T. *Adv. Polym. Sci.* **2006**, *197*, 1-45. (g) Santer, S.; Kopyshev, A.; Donges, J.; Rühe, J.; Jiang, X. G.; Zhao, B.; Müller, M. *Langmuir* **2007,** *23*, 279-285.
7. (a) Filimon, M.; Kopf, I.; Ballout, F.; Schmidt, D. A.; Brändermann, E.; Rühe, J.; Santer, S.; Havenith, M. *Soft Matter*, **2010**, *6*, 3764-3768. (b) Estillore, N. C.; Advincula, R. C. *Langmuir* **2011**, *27*, 5997-6008. (c) Ochsmann, J. W.; Lenz, S.; Lellig, P.; Emmerling, S. G. J.; Golriz, A. A.; Reichert, P.; You, J.; Perlich, J.; Roth, S. V.; Beger, R.; Gutmann, J. S. *Macromolecules* **2012**, *45*, 3129-3136. (d) Price, A. D.; Hur, S.-M.; Fredrickson, G. H.; Frischknecht, A. L.; Huber, D. L. *Macromolecules* **2012**, *45*, 510-524. (e) Ye, P. L.; Dong, H. C.; Zhong, M. J.; Matyjaszewski, K. *Macromolecules* **2011**, *44*, 2253-2260. (f) Wang,

Z. L.; Xu, J. T.; Du, B. Y.; Fan, Z. Q., *J. Colloid & Interface Sci.* **2011**, *360*, 350-354. (g) Kotsuchibashi, Y.; Ebara, M.; Aoyagi, T.; Narain, R., *Polym. Chem.* **2012**, *3*, 2545-2550.

8. (a) Wang, J.; Kara, S.; Long, T. E.; Ward, T. C. *J. Polym. Sci., Polym. Chem.* **2000**, *38*, 3742-3750. (b) Cheng, J.; He, J.; Li, C.; Yang, Y. *Chem. Mater.* **2008**, *20*, 4224-4230. (c) Chiu, J. J.; Kim, B. J.; Kramer, E. J.; Pine, D. J. *J. Am. Chem. Soc.* **2005**, *127*, 5036-5037. (d) Shan, J.; Nuopponen, M.; Jiang, H.; Viitala, T.; Kauppinen, E.; Kontturi, K.; Tenhu, H. *Macromolecules* **2005**, *38*, 2918-2926. (e) Guo, Y.; Moffitt, M. G. *Macromolecules* **2007**, *40*, 5868-5878. (f) Rungta, A.; Natarajan, B.; Neely, T.; Dukes, D.; Schadler, L. S.; Benicewicz, B. C. *Macromolecules* **2012**, *45*, 9303-9311. (g) Huang, X.; Hauptmann, N.; Appelhans, D.; Formanek, P.; Frank, S.; Kaskel, S.; Temme, A.; Voit, B. *Small* **2012**, *8*, 3579-3583.

9. (a) Marko, J. F.; Witten, T. A. *Macromolecules* **1992,** *25*, 296-307. (b) Brown, G.; Chakrabarti, A.; Marko, J. F. *Europhys. Lett.* **1994,** *25*, 239-244. (c) Müller, M. *Phys. Rev. E* **2002,** *65*, 030802. (d) Minko, S.; Müller, M.; Usov, D.; Scholl, A.; Froeck, C.; Stamm, M. *Phys. Rev. Lett.* **2002,** *88*, 035502. (e) Wenning, L.; Müller, M.; Binder, K. *Europhys. Lett.* **2005**, *71*, 639-645. (f) Merlitz, H.; He, G. L.; Sommer, J. U.; Wu, C. X. *Macromolecules* **2009**, *42*, 445-451. (g) Egorov, S.A. *Soft Matter* **2012**, *8*, 3971-3979. (h) Wang, J.; Müller, M. *J. Phys. Chem. B.* **2009**, *113*, 11384-11402. (i) Roan, J.-R. *Phys. Rev. Lett.* **2006**, *96*, 248301. (j) Hur, S.-M.; Frischknecht, A. L.; Huber, D. L.; Fredrickson, G. H. *Soft Matter* **2013**, *9*, 5341-5354.

10. Dong, H. *J. Phys. II Fr.* **1993,** *3*, 999-1020.

11. Zhulina, E.; Balazs, A. C. *Macromolecules* **1996,** *29*, 2667-2673.

12. (a) Wang, Y. Q.; Yang, G. A.; Tang, P.; Qiu, F.; Yang, Y. L.; Zhu, L. *J. Chem. Phys.* **2011**, *134*, 134903. (b) Ma, X.; Yang, Y. Z.; Zhu, L.; Zhao, B.; Tang, P.; Qiu, F. *J. Chem. Phys.* **2013**, *139*, 214902.

13. (a) Li, D. J.; Sheng, X.; Zhao, B. *J. Am. Chem. Soc.* **2005**, *127*, 6248−6256. (b) Zhao, B.; Zhu, L. *J. Am. Chem. Soc.* **2006,** *128*, 4574-4575. (c) Zhu, L; Zhao, B. *J. Phys. Chem. B* **2008**, *112*, 11529-11536. (d) Jiang, X. M.; Zhong, G. J.; Horton, J. M.; Jin, N. X.; Zhu, L.; Zhao, B. *Macromolecules* **2010**, *43*, 5387-5395. (e) Jiang X. M.; Zhao, B.; Zhong, G. J.; Jin, N. X.; Horton, J. M.; Zhu, L.; Hafner, R. S.; Lodge, T. P. *Macromolecules* **2010**, *43*, 8209-8217.

14. (a) Bao, C. H.; Tang, S. D.; Horton, J. M.; Jiang, X. M.; Tang, P.; Qiu, F.; Zhu, L.; Zhao, B. *Macromolecules* **2012**, *45*, 8027-8036. (b) Horton, J. M.; Tang, S. D.; Bao, C. H.; Tang, P.; Qiu, F.; Zhu, L.; Zhao, B. *ACS Macro Letters* **2012**, *1*, 1061-1065.

15. Li, W.; Bao, C. H.; Wright, R. A. E.; Zhao, B. *RSC Advances* **2014**, *4*, 18772-18781.

16. (a) Matyjaszewski, K.; Xia, J. *Chem. Rev.* **2001**, *101*, 2921-2990. (b) Hui, C. M.; Pietrasik, J.; Schmitt, M.; Mahoney, C.; Choi, J.; Bockstaller, M. R.; Matyjaszewski, K. *Chem. Mater.* **2014**, *26*, 745-762.

17. Hawker, C. J.; Bosman, A. W.; Harth, E. *Chem. Rev.* **2001,** *101*, 3661-3688.

18. Matyjaszewski, K.; Woodworth, B. E.; Zhang, X.; Gaynor, S. G.; Metzner, Z. *Macromolecules* **1998**, *31*, 5955-5957.

19. Chong, Y. K.; Krstina, J.; Le, T. P. T.; Moad, G.; Postma, A.; Rizzardo, E.; Thang, S. H. *Macromolecules* **2003**, *36*, 2256- 2272.

20. (a) Stöber, W.; Fink, A.; Bohn, E. *J. Colloid & Interface Sci.* **1968**, *26*, 62-69. (b) Horton, J. M.; Bao, C. H.; Bai, Z. F.; Lodge, T. P.; Zhao, B. *Langmuir* **2011**, *27*, 13324-13334.

21. The molecular weights of P*t*BA measured by SEC against PS standards were used in the calculation of P*t*BA grafting densities. We previously observed that the P*t*BA molecular weights from SEC were very close to those calculated from the monomer-to-initiator ratios and monomer conversions. See references 13a, 13d, and 13e. The difference between weight retentions of Y-initiator-functionalized silica particles and polymer brush-grafted silica particles at 100 °C is presumably caused by the water content, though all samples were dried under high vacuum at 45 °C for at least 5 h. This difference was taken into consideration in the calculation of grafting densities of polymer brushes by vertically shifting the curves to the same position – the highest weight retention at 100 °C among three curves as described in reference 20b.

22. Tang, S. D.; Lo, T.-Y.; Horton, J. M.; Bao, C. H.; Tang, P.; Qiu, F.; Ho, R.-M.; Zhao, B.; Zhu, L. *Macromolecules* **2013**, *46*, 6575-6584.

23. The calculation of overall standard deviations for the slopes can be found in the Appendix B.

24. Jang, S. G.; Audus, D. J.; Klinger, D.; Krogstad, D. V.; Kim, B. J.; Cameron, A.; Kim, S. W.; Delaney, K. T.; Hur, S. M.; Killops, K. L.; Fredrickson, G. H.; Kramer, E. J.; Hawker, C. J. *J. Am. Chem. Soc.* **2013**, *135*, 6649-6657.

25. Hamley, I. W. *The Physics of Block Copolymers*; Oxford University Press: Oxford, UK, 1998.

26. Bao, C.; Tang, S,; Wright, R. A. E.; Tang, P.; Qiu, F.; Zhu, L.; Zhao, B. *Macromolecules* **2014**, *47*, 6824-6835.

27. The work described in this Chapter has been published in *Macromolecules* (*Macromolecules* **2014**, *47*, 6824-6835).

Appendix B

for

Chapter 3. Effect of Molecular Weight on Lateral Microphase Separation of Mixed Homopolymer Brushes Grafted on Silica Particles

B1. Standard Deviations of Grafting Densities of Polymer Brushes Grafted on Silica Particles

Generally, the standard deviation or error is calculated according to Equation (1),

$$s = \sqrt{\frac{\sum(x - \bar{x})^2}{n - 1}} \qquad (1)$$

where s is the standard deviation, x is the value of each measurement, $\bar{x}$ is the mean value, and n is the number of measurements.

The standard deviations of the values of grafting densities mainly came from the standard deviation of the bare silica particle size in the calculation of grafting density. The size of silica particle was 172 ± 20 nm (the average diameter was 172 nm and the standard deviation was 20 nm), which was determined from the TEM micrographs. Analysis showed that the standard deviation of the silica particle size propagated linearly in the calculation of individual grafting densities. The standard deviations of overall grafting densities ($\sigma_{overall} = \sigma_{PtBA} + \sigma_{PS}$) are calculated according to $s_{overall} = (s_{PtBA}^2 + s_{PS}^2)^{1/2}$. The results are included in Table 3.1.

B2. Standard Deviations of Exponents in the Scaling Relationships between *D* and MW

As shown in this Chapter, the exponents in the scaling relationships between D and MW were the slopes from the linear fitting of the plots of log$D$ versus log(MW). The standard deviations of the measured ripple wavelengths D shown in Figures 3.4 and 3.7 propagated into the linear fitting of data points in Figures 3.5 and 3.8, respectively. The standard deviations of exponents in the linear fitting were calculated using the method described below. Equation 2 is the general error propagation expression for calculating the total error in the linear fitting when each of the data used in the fitting has uncertainties.

$$s_f = \sqrt{\left(\frac{\partial f}{\partial x}\right)^2 s_x^2 + \left(\frac{\partial f}{\partial y}\right)^2 s_y^2 + \left(\frac{\partial f}{\partial z}\right)^2 s_z^2 + \ldots} \quad (2)$$

where s_f is the final standard deviation, f is the function of exponent (slope in the double logarithmic plot) with each data point in the linear fitting (x, y, z……), s_x, s_y, and s_z are standard deviations of data points determined by repeated measurements. The standard deviations of ripple wavelengths are shown in Figures 3.4 and 3.7, and were used in the calculation of the total error in the linear fitting between log*D* and log (MW).

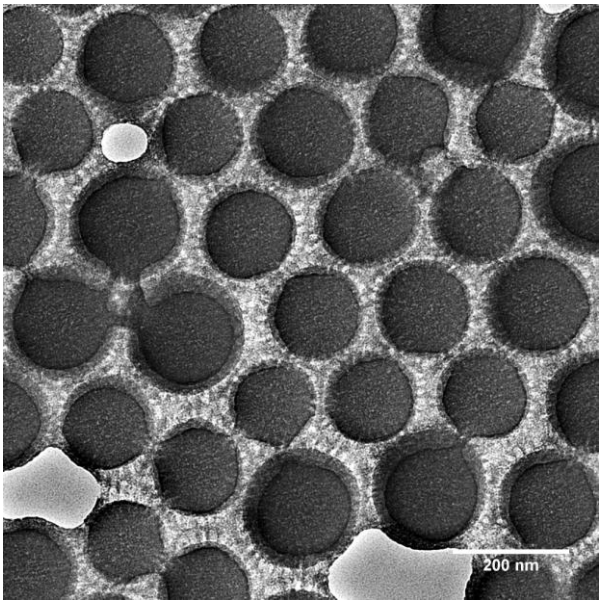

Figure B1. Top-view, bright field TEM micrograph of MB-MW-1 (P*t*BA M_n = 13.3 kDa, σ_{PtBA} = 0.47 chains/nm^2; PS M_n = 14.3 kDa, σ_{PS} = 0.31 chains/nm^2; $\sigma_{overall}$ = 0.78 chains/nm^2) after being cast from a $CHCl_3$ dispersion and annealed with $CHCl_3$ vapor. The sample was stained with RuO_4 vapor at room temperature for 20 min.

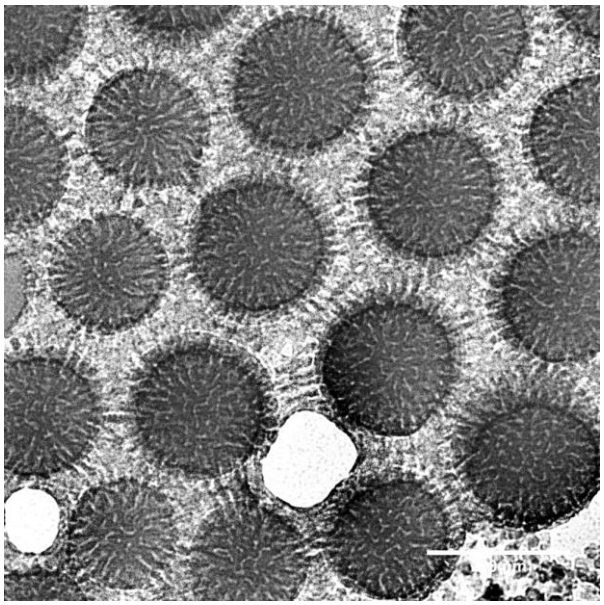

Figure B2. Top-view, bright field TEM micrograph of MB-MW-2 (P*t*BA M_n = 18.3 kDa, σ_{PtBA} = 0.42 chains/nm^2; PS M_n = 17.5 kDa, σ_{PS} = 0.33 chains/nm^2; $\sigma_{overall}$ = 0.75 chains/nm^2) after being cast from a $CHCl_3$ dispersion and annealed with $CHCl_3$ vapor. The sample was stained with RuO_4 vapor at room temperature for 20 min.

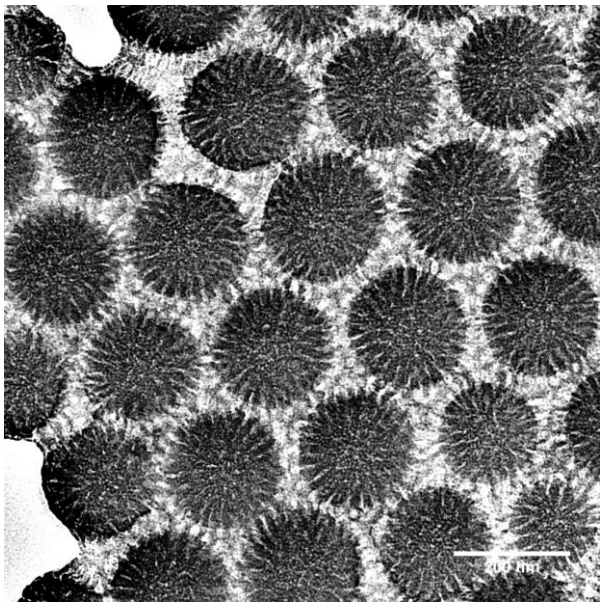

Figure B3. Top-view, bright field TEM micrograph of MB-MW-3 (P*t*BA M_n = 22.0 kDa, σ_{PtBA} = 0.37 chains/nm^2; PS M_n = 22.3 kDa, σ_{PS} = 0.41 chains/nm^2; $\sigma_{overall}$ = 0.78 chains/nm^2) after being cast from a $CHCl_3$ dispersion and annealed with $CHCl_3$ vapor. The sample was stained with RuO_4 vapor at room temperature for 20 min.

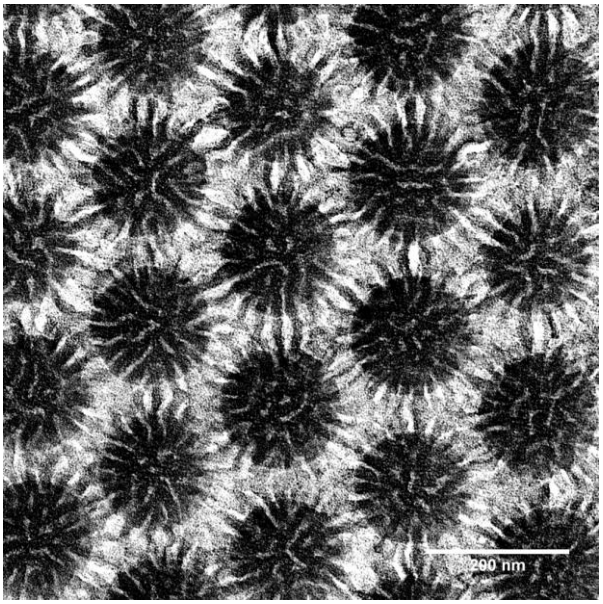

Figure B4. Top-view bright field TEM micrograph of MB-MW-4 (P*t*BA M_n = 26.7 kDa, σ_{PtBA} = 0.51 chains/nm^2; PS M_n = 26.3 kDa, σ_{PS} = 0.29 chains/nm^2; $\sigma_{overall}$ = 0.80 chains/nm^2) after being cast from a $CHCl_3$ dispersion and annealed with $CHCl_3$ vapor. The sample was stained with RuO_4 vapor at room temperature for 20 min.

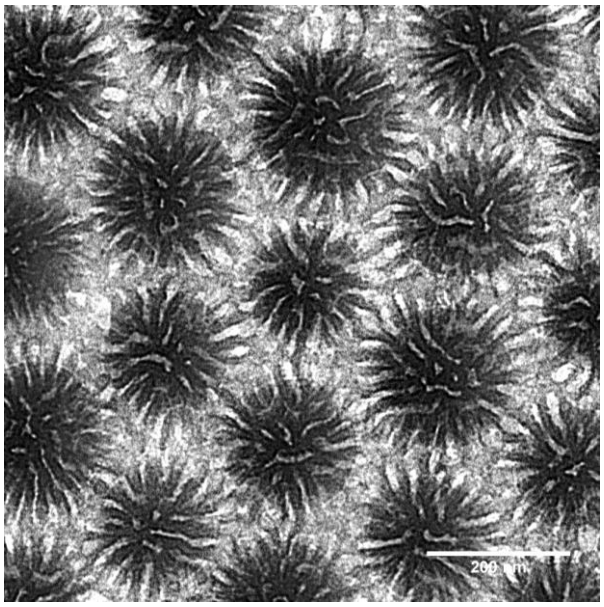

Figure B5. Top-view, bright field TEM micrograph of MB-MW-5 (P*t*BA M_n = 32.1 kDa, σ_{PtBA} = 0.51 chains/nm^2; PS M_n = 31.6 kDa, σ_{PS} = 0.41 chains/nm^2; $\sigma_{overall}$ = 0.92 chains/nm^2) after being cast from a $CHCl_3$ dispersion and annealed with $CHCl_3$ vapor. The sample was stained with RuO_4 vapor at room temperature for 20 min.

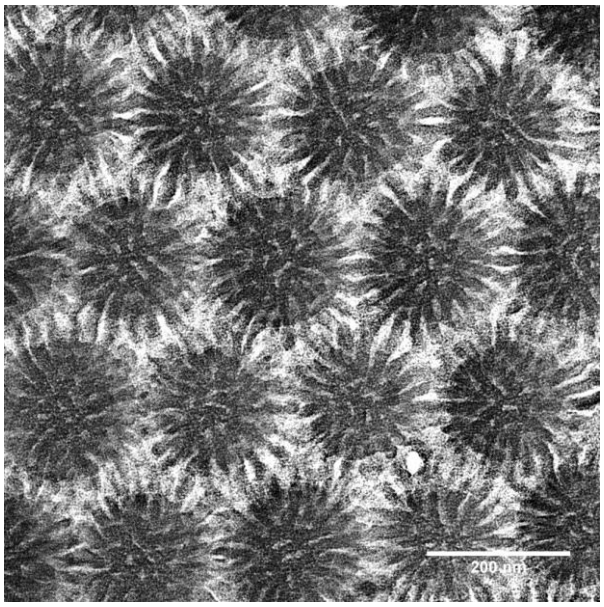

Figure B6. Top-view, bright field TEM micrograph of MB-MW-6 (P*t*BA M_n = 34.1 kDa, σ_{PtBA} = 0.50 chains/nm^2; PS M_n = 32.1 kDa, σ_{PS} = 0.35 chains/nm^2; $\sigma_{overall}$ = 0.85 chains/nm^2) after being cast from a $CHCl_3$ dispersion and annealed with $CHCl_3$ vapor. The sample was stained with RuO_4 vapor at room temperature for 20 min.

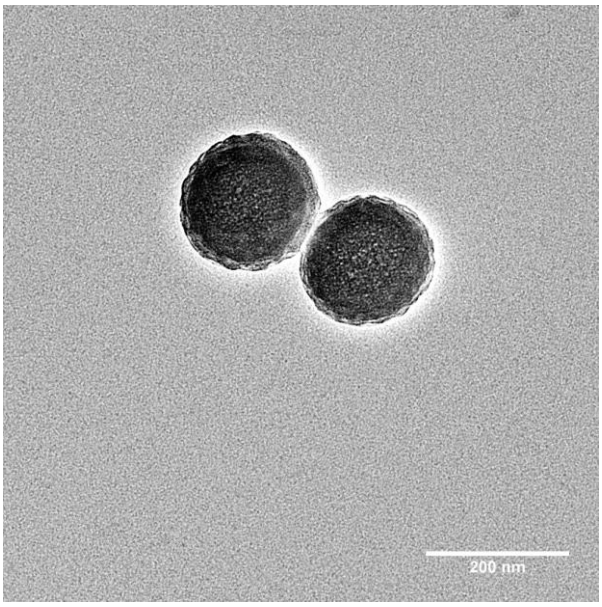

Figure B7. Top-view, bright field TEM micrograph of MB-MW-1 (P*t*BA M_n = 13.3 kDa, σ_{PtBA} = 0.47 chains/nm^2; PS M_n = 14.3 kDa, σ_{PS} = 0.31 chains/nm^2; $\sigma_{overall}$ = 0.78 chains/nm^2) after being cast from a surfactant-stabilized aqueous dispersion. The sample was stained with RuO_4 vapor at room temperature for 20 min.

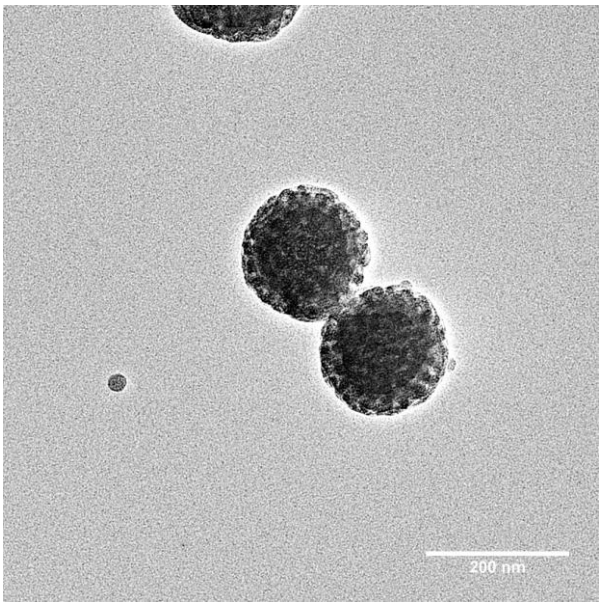

Figure B8. Top-view, bright field TEM micrograph of MB-MW-2 (P*t*BA M_n = 18.3 kDa, σ_{PtBA} = 0.42 chains/nm^2; PS M_n = 17.5 kDa, σ_{PS} = 0.33 chains/nm^2; $\sigma_{overall}$ = 0.75 chains/nm^2) after being cast from a surfactant-stabilized aqueous dispersion. The sample was stained with RuO_4 vapor at room temperature for 20 min.

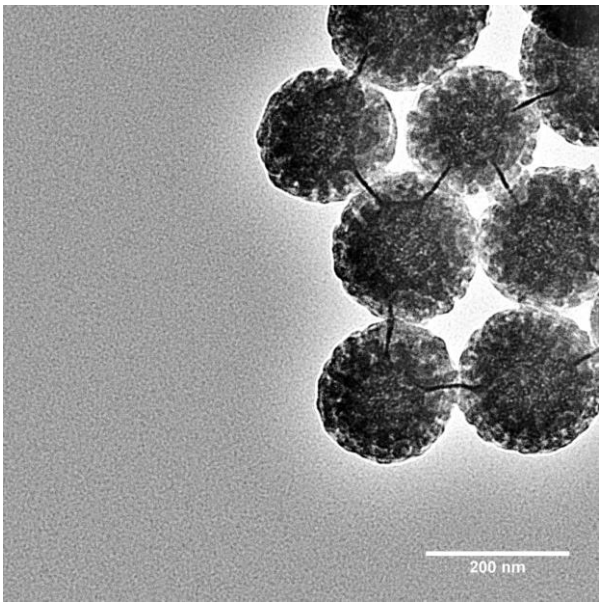

Figure B9. Top-view, bright field TEM micrograph of MB-MW-3 (P*t*BA M_n = 22.0 kDa, σ_{PtBA} = 0.37 chains/nm^2; PS M_n = 22.3 kDa, σ_{PS} = 0.41 chains/nm^2; $\sigma_{overall}$ = 0.78 chains/nm^2) after being cast from a surfactant-stabilized aqueous dispersion. The sample was stained with RuO_4 vapor at room temperature for 20 min.

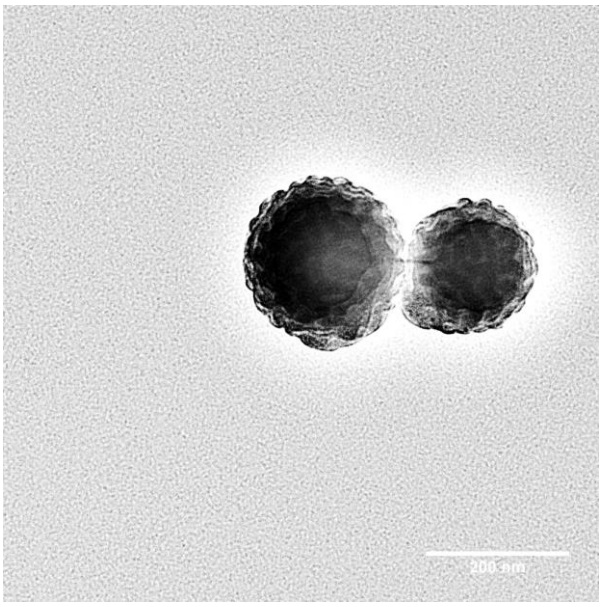

Figure B10. Top-view, bright field TEM micrograph of MB-MW-4 (P*t*BA M_n = 26.7 kDa, σ_{PtBA} = 0.51 chains/nm^2; PS M_n = 26.3 kDa, σ_{PS} = 0.29 chains/nm^2; $\sigma_{overall}$ = 0.80 chains/nm^2) after being cast from a surfactant-stabilized aqueous dispersion. The sample was stained with RuO_4 vapor at room temperature for 20 min.

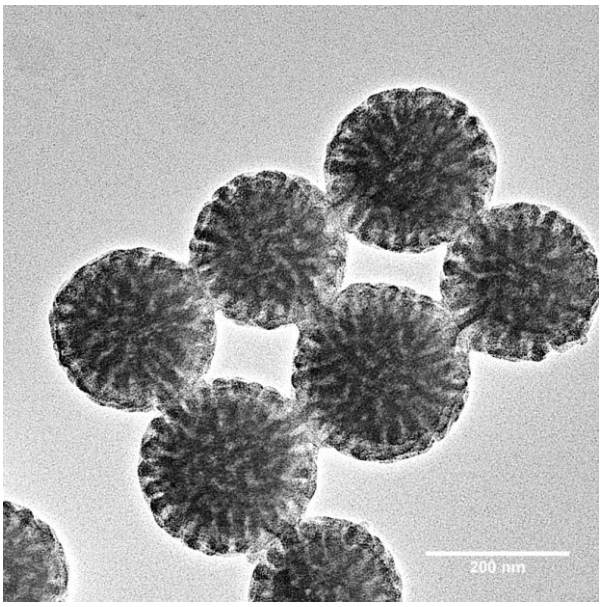

Figure B11. Top-view, bright field TEM micrograph of MB-MW-5 (P*t*BA M_n = 32.1 kDa, σ_{PtBA} = 0.51 chains/nm^2; PS M_n = 31.6 kDa, σ_{PS} = 0.41 chains/nm^2; $\sigma_{overall}$ = 0.92 chains/nm^2) after being cast from a surfactant-stabilized aqueous dispersion. The sample was stained with RuO_4 vapor at room temperature for 20 min.

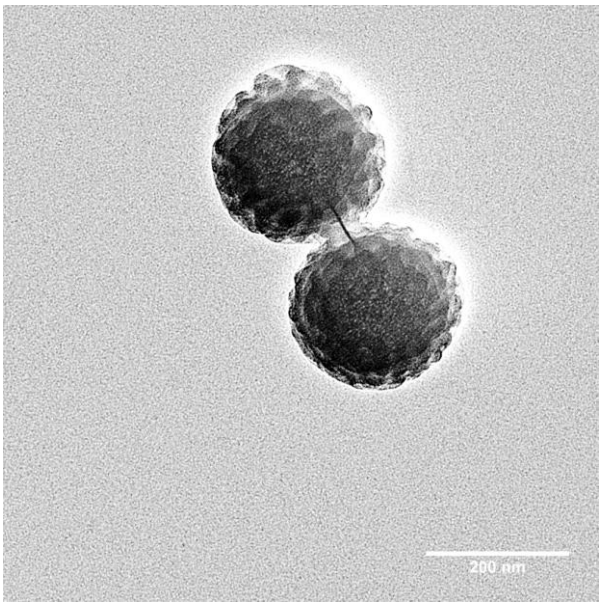

Figure B12. Top-view, bright field TEM micrograph of MB-MW-6 (P*t*BA M_n = 34.1 kDa, σ_{PtBA} = 0.50 chains/nm^2; PS M_n = 32.1 kDa, σ_{PS} = 0.35 chains/nm^2; $\sigma_{overall}$ = 0.85 chains/nm^2) after being cast from a surfactant-stabilized aqueous dispersion. The sample was stained with RuO_4 vapor at room temperature for 20 min.

B3. Control Experiment of Evaporation of $CHCl_3$ from Its Aqueous Emulsion Stabilized by Cetyltrimethylammonium Bromide

Cetyltrimethylammonium bromide (2 mg) was dissolved in 4.001 g of water in a small glass vial, followed by addition of chloroform (1.004 g). The vial was capped and the mixture was stirred and sonicated in an ultrasonic water bath for 1 h to form an emulsion. A sample was taken as 0 min for ^{1}H NMR spectroscopy analysis. The glass vial that contained the emulsion was open to air and put in a fume hood to allow chloroform to evaporate. After the mixture was stirred at room temperature overnight (~ 17 h), an NMR sample was taken. Figure B13 shows the ^{1}H NMR spectra of the two samples with the DMSO residual peak intensities set to be the same for comparison. A quantitative analysis indicates that > 99% chloroform was gone.

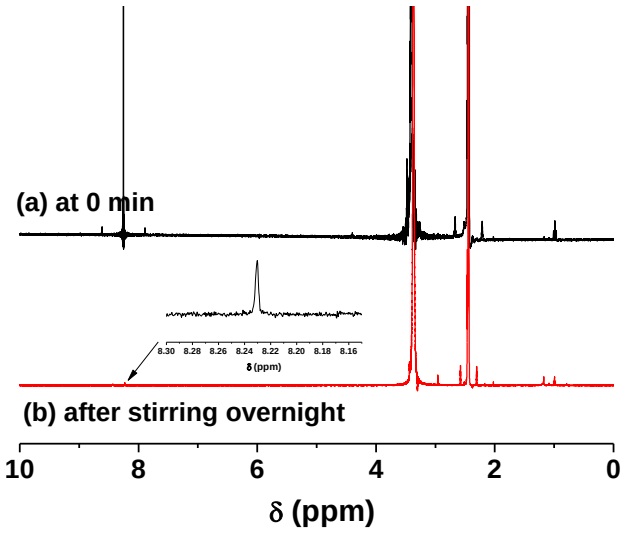

Figure B13. ^{1}H NMR spectra of a CTAB-stabilized, no particle-containing aqueous emulsion of $CHCl_3$, prepared using the same procedure as for the CTAB-stabilized emulsions of chloroform dispersions of mixed P*t*BA/PS brush-grafted silica particles in water, (a) at 0 min and (b) after stirring in a fume hood overnight. DMSO-d_6 was used as solvent in ^{1}H NMR spectroscopy analysis, and the intensities of the DMSO residual peaks in the two spectra are set to be the same for comparison. The analysis showed that that > 99% $CHCl_3$ was gone after stirring in a fume hood overnight.

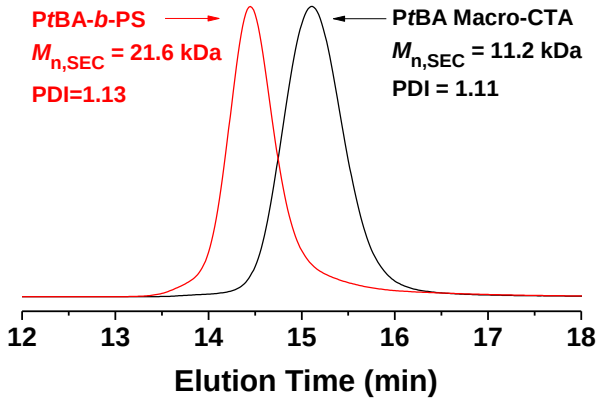

Figure B14. Size exclusion chromatography (SEC) analysis of macro-CTA poly(*tert*-butyl acrylate) (P*t*BA) and diblock copolymer poly(*tert*-butyl acrylate)-*b*-polystyrene (P*t*BA-*b*-PS, DB-1). P*t*BA macro-CTA was synthesized by RAFT polymerization; [*t*BA]:[CTA]:[AIBN] = 536:1.0:0.10, anisole, 70 °C. P*t*BA-*b*-PS was synthesized using P*t*BA as macro-CTA in anisole at 70 °C. SEC analysis was conducted using THF as eluent solvent with a flow rate at 1 mL/min.

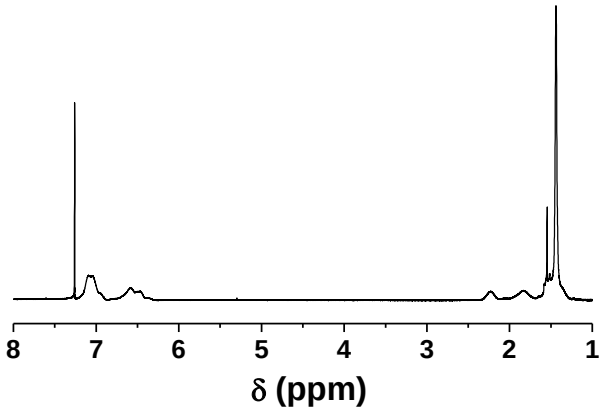

Figure B15. ^{1}H NMR spectrum of poly(*tert*-butyl acrylate)-*b*-polystyrene (P*t*BA-*b*-PS) (DB-1, $M_{n,SEC}$ = 21.6 kDa, PDI = 1.13). $CDCl_3$ was used as solvent.

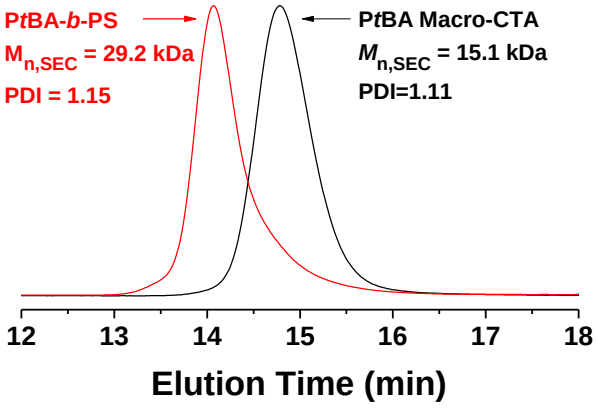

Figure B16. Size exclusion chromatography (SEC) analysis of macro-CTA poly(*tert*-butyl acrylate) (P*t*BA) and diblock copolymer poly(*tert*-butyl acrylate)-*b*-polystyrene (P*t*BA-*b*-PS, DB-2). SEC analysis was conducted using THF as eluent solvent with a flow rate at 1 mL/min.

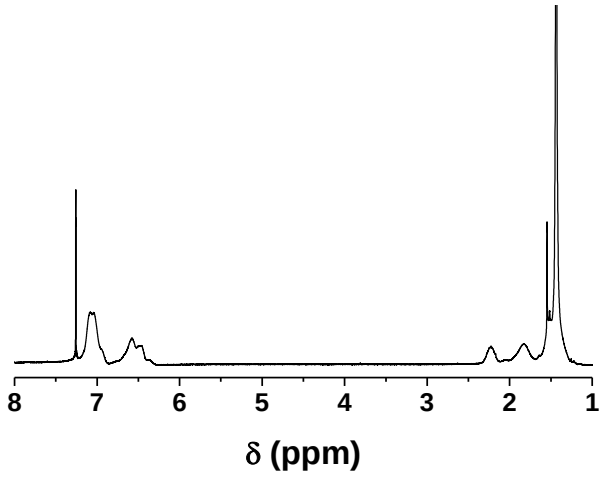

Figure B17. ^{1}H NMR spectrum of poly(*tert*-butyl acrylate)-*b*-polystyrene (P*t*BA-*b*-PS) (DB-2, $M_{n,SEC}$ = 29.2 kDa, PDI = 1.15). $CDCl_3$ was used as solvent.

Chapter 4. Synthesis of Mixed Poly(ε-caprolactone)/Polystyrene Brushes on Silica Particles by Combining Surface-Initiated Ring-Opening Polymerization and Nitroxide-Mediated Radical Polymerization

Abstract

This Chapter presents the synthesis of mixed homopolymer brushes grafted on silica particles composed of poly(ε-caprolactone) (PCL) and polystyrene (PS) by sequential surface-initiated ring-opening polymerization (ROP) of ε-caprolactone (εCL) at 75 °C and nitroxide-mediated radical polymerization (NMRP) of styrene at 120 °C. The silica particles were functionalized with an asymmetric difunctional initiator (Y-initiator) bearing a hydroxyl group, an initiator for ROP, and an alkoxyamine moiety, an initiator for NMRP. It was found that for ROP, PCL with $M_{n,SEC}$ values of ~ 25 kDa and narrow polydispersity indexes (≤ 1.20) relative to PS standards can be reproducibly synthesized at 75 °C using tin(II) 2-ethylhexanoate as catalyst after the Y-initiator-functionalized silica particles and the catalyst were thoroughly dried. Both surface-initiated ROP and NMRP polymerizations were carried out in the presence of a free initiator. The overall grafting density of mixed PCL/PS brushes can be tuned by varying the mass ratio of the triethoxysilane-terminated Y-initiator to bare silica particles in the initiator immobilization step. However, the grafting density of PS was always higher than that of PCL.

4.1 Introduction

Mixed homopolymer brushes, composed of two chemically distinct polymers randomly or alternately grafted by one end on a solid substrate, are an intriguing class of surface-responsive materials.[1-5] These brushes can undergo spontaneous self-reorganization in response to environmental changes, exhibiting different nanostructures and properties under different conditions. The intriguing self-assembly behavior of binary mixed brushes has attracted considerable interest in both theoretical and experimental studies in the past years.[1-5] Marko and Witten were the first to study symmetric mixed homopolymer brushes on planar substrates; they predicted that mixed brushes phase separate laterally in melt and the feature size of the formed "ripple" nanopattern is on the order of the polymer chain root-mean-square end-to-end distance.[1] Their seminal work stimulated tremendous research activities on mixed brushes.[1-14] The effects of various factors on the self-assembly behavior of mixed brushes were elucidated by theoretical and computer simulation studies, and a rich variety of nanostructures was predicted.[1-8]

Generally, mixed brushes can be prepared by three methods: (i) "grafting from", where two different polymers are grown from the surface by surface-initiated polymerization,[9-11] (ii) "grafting to", where functionalized polymers are grafted onto a solid substrate via the reaction with surface functional groups,[12,13] and (iii) combination of "grafting to" and "grafting from", where one polymer is grafted onto the substrate and another polymer is grown from the surface.[14] Sidorenko et al. reported the synthesis of first binary mixed brushes of polystyrene (PS)/poly(2-vinylpyridine) (PVP) by a "grafting from" method.[9a] An azo free radical initiator was immobilized on silicon wafers, followed by a two-step conventional free radical polymerization process to grow two polymers; the second polymer was grown from the residual surface azo initiator that did not decompose in the synthesis of the first polymer.[9a] The obtained mixed

brushes exhibited switching properties in response to environmental changes. Our group previously reported the synthesis of well-defined mixed brushes by sequential atom transfer radical polymerization (ATRP) and nitroxide-mediated radical polymerization (NMRP) from asymmetric difunctional initiator (Y-initiator)-functionalized silica substrates.[10] The use of Y-initiators ensures that the two types of initiators are well mixed at the molecular level on the silica surface and thus it is possible to make well-mixed binary polymer brushes. The molecular weights and molecular weight distributions of two tethered polymers can be well controlled, allowing the study of microphase separation of mixed brushes by transmission electron microscopy and differential scanning calorimetry.[10f-l]

The "grafting to" method is straightforward and allows the use of polymers with controlled molecular weights, well-defined functional groups, and predetermined architectures for the preparation of binary mixed brushes.[12,13] For example, Minko et al. reported the synthesis of mixed PS/PVP brushes by sequentially grafting carboxyl-terminated PS and PVP onto silica wafers that were functionalized with 3-glycidoxypropyltrimethoxysilane.[12a,b] Julthongpiput et al. prepared Y-shaped brushes by grafting diblock copolymers to silicon wafers via the reaction between the carboxylic acid group at the junction point of the two blocks and the silica surface.[13a] ABC triblock copolymers with a reactive, short central B block were also employed to make mixed brushes by reacting the B block with the surface of a solid substrate, either flat or curved.[13b-e] Although "grafting to" is simple, the thickness of the obtained brushes tends to be low because of the steric hindrance presented by the grafted polymer to the incoming polymer chains.

Binary mixed brushes have also been synthesized on gold nanoparticles by combining "grafting to" and "grafting from" techniques.[14] A thiol-terminated poly(ethylene glycol) (PEG)

with a molecular weight of 5 kDa and a disulfide-terminated ATRP initiator were co-assembled onto gold nanoparticles via the formation of Au-S bonds, followed by surface-initiated ATRP to grow the second polymer from gold nanoparticles, yielding well-defined binary mixed brushes.[14]

The experimental studies of mixed brushes thus far mainly focus on the brush systems composed of two vinyl polymers; there are only a few examples of mixed brushes containing nonvinyl polymers or chemically or biologically degradable polymers in the literature.[9h,14] Recent experimental studies have shown that mixed brushes can phase separate into a variety of morphologies ranging from isolated, nearly spherical nanodomains in the matrix of another polymer, to short cylindrical nanodomains, to bicontinuous wormlike nanopatterns, and two-layered structures.[10h,i] If one polymer is etchable under mild conditions, many interesting porous nanostructures can be fabricated from such multicomponent hairy particles, and the obtained nanomaterials may find applications, e.g., in separation or catalysis. Therefore, it is of significance to synthesize mixed brushes on silica particles composed of one degradable polymer and one vinyl polymer.

This Chapter presents the synthesis of mixed poly(ε-caprolactone) (PCL)/PS brushes from silica particles that were functionalized with an asymmetric difunctional initiator (Y-initiator) bearing a hydroxyl group, an initiator for ring-opening polymerization (ROP),[15] and an NMRP initiator by combining metal-catalyzed ROP of ε-caprolactone (εCL) and NMRP of styrene (Scheme 4.1). The triethoxysilane-terminated Y-initiator was immobilized onto the surface of bare silica particle via an ammonia-catalyzed hydrolysis and condensation process.[10i-k,16] The surface-initiated ROP of εCL was carried out at 75 °C in the presence of a free initiator with tin(II) 2-ethylhexanoate ($Sn(Oct)_2$) as catalyst, followed by the NMRP of styrene at 120 °C. We also showed that the overall grafting density of mixed PCL/PS brushes can be tuned by changing

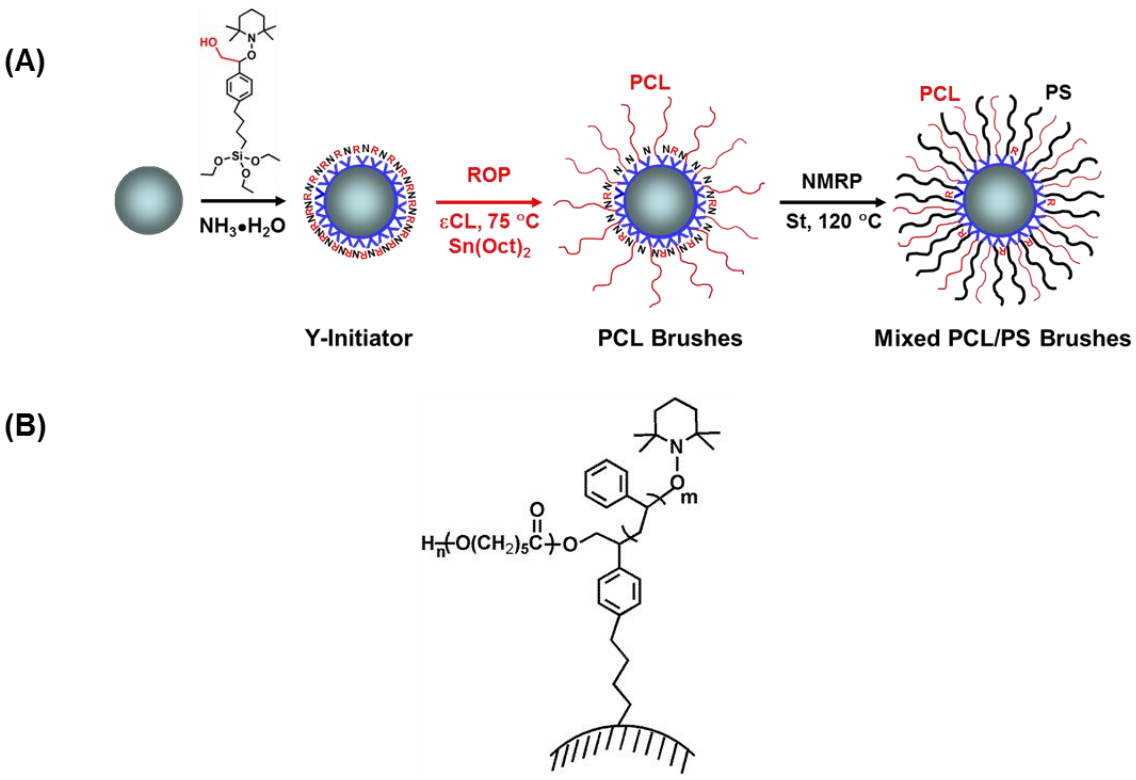

Scheme 4.1 (A) Synthesis of mixed poly(ε-caprolactone) (PCL)/polystyrene (PS) brushes on silica particles functionalized with a Y-initiator bearing a hydroxyl group and a TEMPO moiety by combining $Sn(Oct)_2$-catalyzed ring-opening polymerization (ROP) of ε-caprolactone (εCL) and nitroxide-mediated radical polymerization (NMRP) of styrene (B) Schematic illustration of mixed PCL/PS brushes on silica particles

the mass ratio of the triethoxysilane-terminated Y-initiator to bare silica particles in the initiator immobilization step. The method described here can be extended to the synthesis of mixed brushes containing other degradable polymers, which could open up new opportunities for applications of mixed brush-grafted particles. Note that the preparation of block copolymers by combining ROP and NMRP from difunctional initiators in solution has been previously demonstrated.[17]

4.2 Experimental Section

4.2.1 Materials

Tetraethyl orthosilicate (or tetraethoxysilane, TEOS, 98%), ammonium hydroxide (25% in water), triethoxysilane ($HSi(OC_2H_5)_3$, 95%), and 2,2,6,6-tetramethylpiperidinooxy (TEMPO, 98%) were purchased from Acros Organics and used as received. The platinum−divinyltetramethyldisiloxane complex in xylene (2.1−2.4% Pt concentration in xylene) was obtained from Gelest, Inc. 2-[4-(But-3-enyl)phenyl]-2-(2′,2′,6′,6′-tetramethyl-1′-piperidinyloxy)ethanol (Y-Silane-B precursor) was prepared according to a literature procedure.[10d] Styrene (99%, Aldrich) and ε-caprolactone (εCL, 99%, Acros Organics) were dried with CaH_2 and distilled under reduced pressure. The purified monomers were stored in a refrigerator prior to use. Tin(II) 2-ethylhexanoate ($Sn(Oct)_2$, ~ 95%) was obtained from Sigma-Aldrich. ω-Undecylenyl alcohol (98%) was purchased from Aldrich and used as the free initiator for ROP in the synthesis of PCL brushes on silica particles. 1-Phenyl-1-(2′,2′,6′,6′-tetramethyl-1′-piperidinyloxy)ethane (STEMPO), an initiator for NMRP, was prepared by following a procedure from the literature.[10k,18] Toluene and tetrahydrofuran (THF) were dried by refluxing over sodium and benzophenone under nitrogen atmosphere until the color changed to purple, and

then distilled and used immediately. Ethanol (200 proof) was obtained from Decon Laboratories, Inc. All other chemical reagents were purchased from either Aldrich or Fisher and used without further purification.

4.2.2 General Characterization

Size exclusion chromatography (SEC) was carried out at ambient temperature using PL-GPC 20 (an integrated SEC system from Polymer Laboratories, Inc.) with a differential refractive index detector, one PLgel 5 μm guard column (50 × 7.5 mm), and two PLgel 5 μm mixed-C columns (each 300 × 7.5 mm, linear range of molecular weight from 200 to 2000000 according to Polymer Laboratories, Inc.). THF was used as the carrier solvent at a flow rate of 1.0 mL/min. Polystyrene standards (Polymer Laboratories, Inc.) were employed for calibration. The data were processed using Cirrus GPC/SEC software (Polymer Laboratories, Inc.). PCL free polymers, formed from the free initiator in the synthesis of PCL brushes, were also analyzed at 40 °C by PL-GPC 120 equipped with a Precision Detector PD2040 (a two angle static light scattering detector, 15° and 90°), Viscotek 220 differential viscometer, and a Polymer Laboratories differential refractometer. The system consists of four Polymer Laboratories PLgel columns (300 × 7.5, 10 μm particles with pore sizes of 500, 10^3, 10^5, and 10^6 Å, respectively). The calibration range is 600 to 7500000 Da using either PS or PMMA standards. A dn/dc value of 0.075 mL/g for PCL, which was from a literature paper,[19] was employed in the measurements of PCL absolute molecular weights by PL-GPC 120 with a two-angle light scattering detector. ^{1}H NMR spectra were recorded on a Varian Mercury 300 MHz NMR spectrometer with tetramethylsilane (TMS) as the internal standard in ^{1}H NMR spectra. Thermogravimetric analysis (TGA) was performed at a heating rate of 20 ℃/min from room temperature to 800 ℃ using either TA Q-series Q50 in air or a SII Nanotechnology TG/DTA 320 in pure oxygen. The hairy particle

samples were dried at 55 ℃ in vacuum for at least 6 h prior to TGA analysis. Mass spectrometric analysis was performed using a QSTAR Elite quadrupole time-of-flight (QTOF) mass spectrometer equipped with an ESI ion source and an integrated syringe pump (AB Sciex, Foster City, CA, USA).

Transmission electron microscopy (TEM) was employed to study PCL brush-grafted and mixed PCL/PS brush-grafted silica particles. Chloroform, a good solvent for PCL and PS, was used to prepare hairy particle dispersions. For each sample, 1 − 2 mg of particles was dispersed in 1 mL of chloroform in a small vial by ultrasonication. The particle dispersion was drop cast onto a carbon-coated, copper TEM grid using a glass pipette and was allowed to dry at ambient condition. The samples were solvent annealed with $CHCl_3$ vapor in a closed container at room temperature for > 3 h. Transmission electron microscopy (TEM) images were acquired using a Zeiss Libra 200 MC transmission electron microscope equipped with a Gatan UltraScan US1000XP CCD camera.

4.2.3 Synthesis of 2-[4-(1-Triethoxysilylbutyl)phenyl]-2-(2',2',6',6'-tetramethyl-1'-piperidinyloxy)ethanol (Y-Silane-B)

2-[4-(But-3-enyl)phenyl]-2-(2',2',6',6'-tetramethyl-1'-piperidinyloxy)ethanol (Y-Silane-B precursor, 0.465 g, 1.404 mmol) was added into a 25 mL two-necked flask and dried under vacuum at room temperature for 1 h. Triethoxysilane ($HSi(OC_2H_5)_3$, 2.50 mL, 13.5 mmol) was injected into the flask via a syringe under N_2 atmosphere, followed by addition of the platinum-divinyltetramethyldisiloxane complex in xylene (80 μL). The mixture was stirred at 45 °C under nitrogen and the hydrosilylation reaction was monitored by ^1H NMR spectroscopy analysis. Once the reaction was complete, excess triethoxysilane was removed under high vacuum at 45 °C, and the product was further purified by silica gel column chromatography using methylene

chloride as eluent (yield: 64.3%). ^{1}H NMR δ (ppm, $CDCl_3$, tetramethylsilane (TMS) as internal standard): 0.59 (t, 2H, SiC*H*$_2$CH$_2$-), 1.08, 1.18, 1.27, 1.43 (each s, 12H, -C(C*H*$_3$)$_2$), 1.14 (t, 9H, -OCH$_2$C*H*$_3$), 1.30-1.66 (m, 10H, -C(CH$_3$)$_2$C*H*$_2$C*H*$_2$C*H*$_2$C(CH$_3$)$_2$- and -SiCH$_2$C*H*$_2$C*H*$_2$CH$_2$-), 2.53 (t, 2H, -ArC*H*$_2$CH$_2$-), 3.62 (dd, 1H, HOC*H*H-), 3.73 (q, 6H, -SiOC*H*$_2$CH$_3$), 4.15 (dd, 1H, HOCH*H*-), 5.20 (dd, 1H, HOCH$_2$C*H*O-), 5.83 (br, 1H, -O*H*), 7.13 (dd, 4H, Ar*H*). ^{13}C NMR δ (ppm, TMS as internal standard): 9.23, 16.13, 17.29, 21.44, 28.69, 33.71, 34.23, 39.18, 39.39, 57.30, 68.73, 82.42, 125.65, 127.34, 135.04, 141.41. Mass spectrum: $[M + H]^+$ at *m/z* 496.343.

4.2.4 Synthesis of Bare Silica Particles

Ammonium hydroxide (25% in water, 14.181 g) and tetraethoxysilane (TEOS, 7.101 g) were each mixed with ethanol (5 mL) to form homogeneous solutions. The two solutions were added into a 500 mL flask that contained 190 mL of ethanol under stirring. The concentrations of NH_3, TEOS, and water in the solution were 0.45, 0.15, and 3.10 M, respectively. After the mixture was stirred vigorously at room temperature for 12 h, the silica particles were isolated by centrifugation (Eppendorf 5804 centrifuge, 6000 rpm), redispersed in ethanol, and centrifugated again. This washing process was repeated with ethanol one more time, water three times, and ethanol again. Particles were then dried with a stream of air flow (1.936 g).

4.2.5 Synthesis of Y-Initiator-Functionalized Silica Particles

The triethoxysilane-terminated Y-initiator (Y-Silane-B) was immobilized onto the surface of silica particles via an ammonia-catalyzed hydrolysis/condensation process.[10i-k,16] Four batches of Y-initiator-functionalized silica particles (YI-B-Particles) were prepared using different mass ratios of Y-Silane-B to bare silica particles. The following is the procedure for the preparation of YI-B-P-II (Table 4.1) using a Y-Silane-B-to-silica particle mass ratio of 87.5%. Other initiator

particles were made using the same procedure except different mass ratios of Y-Silane-B to bare silica particles.

Bare silica particles (149.2 mg) were dispersed in ethanol (10 mL) in a flask by ultrasonication to form a homogeneous, stable dispersion. A solution of ammonium hydroxide (25% in water, 1.10 g) in ethanol (5.0 mL) was added dropwise into the particle dispersion. The mixture was stirred at 40 °C for 2 h, followed by the addition of a solution of Y-silane in ethanol with a concentration of 3.21 wt % (4.065 g). After the immobilization reaction proceeded at 40 °C for 19 h, the Y-initiator-functionalized silica particles were isolated by centrifugation and re-dispersed in THF. This washing process was repeated for a total of five times. The obtained initiator particles, YI-B-P-II, were then dried with a stream of air flow (127.9 mg) and used for the preparation of mixed PCL/PS brush-grafted silica particles.

4.2.6 Synthesis of PCL Brushes from Y-Initiator-Functionalized Silica Particles by Surface-Initiated Ring Opening Polymerization of ε-Caprolactone (εCL)

The synthesis of PCL brushes from YI-B-P-II by surface-initiated ROP of εCL is described in the following. Similar procedures were used to grow PCL brushes from other initiator particles.

Y-initiator functionalized silica particles (YI-B-P-II, 116.9 mg) and dry toluene (2.0 mL) were added into a 25 mL two-necked flask. The mixture was ultrasonicated in an ultrasonic water bath to form a dispersion. The toluene was then distilled under vacuum to remove the trace amount of water in the flask. The azeotropic distillation with dry toluene was repeated one more time, and the initiator particles were further dried at 55 ℃ in vacuum for 8 h. The catalyst for ROP, tin(II) 2-ethylhexanoate ($Sn(Oct)_2$, 343.3 mg, 0.847 mmol), was weighed into a 50 mL two-necked flask and dried first at room temperature via azeotropic distillation with dry toluene

and then at 100 °C in vacuum for 8 h. The flasks were removed from the oil bath and allowed to cool to room temperature. Freshly dried THF (4.0 mL) was injected via a dry syringe into the flask that contained the initiator particles under the N_2 atmosphere. The mixture was ultrasonicated to form a homogeneous stable dispersion, which was then transferred into the catalyst flask using a syringe. The mixture was stirred at 40 °C under N_2 for 30 min. After the flask was cooled to room temperature, ω-undecylenyl alcohol (54.7 mg, 0.321 mmol) and ε-caprolactone (16.575 g, 145.2 mmol) were injected using syringes while stirring. The polymerization mixture was degassed by three freeze−pump−thaw cycles, and then the flask was placed in an oil bath with a preset temperature of 75 ℃ to start the polymerization. SEC was employed to monitor the reaction. After 13 h, the flask was removed from the oil bath and opened to air. THF (20 mL) was added into the flask to dilute the mixture and a small amount of acetic acid was added to quench the polymerization. The particles were separated by centrifugation and redispersed in THF. This washing process was repeated with THF for a total of five times, followed by drying the particles with a stream of air flow. The $M_{n,SEC}$ and polydispersity index (PDI) of the free PCL formed from the free initiator in the polymerization were 24.3 kDa and 1.20, respectively, measured by SEC analysis using PS standards for calibration.

4.2.7 Synthesis of Mixed PCL/PS Brushes from PCL Brush-Grafted Silica Particles by Surface-Initiated Nitroxide-Mediated Radical Polymerization

The PCL brush-grafted silica particles (made from YI-B-P-II, PCL $M_{n,SEC}$ = 24.3 kDa, 0.0695 g) were dispersed in anisole (8.019 g) in a 25 mL two-necked flask using an ultrasonic water bath. The particle dispersion was then transferred into a 50 mL two-necked flask that contained 1-phenyl-1-(2′,2′,6′,6′-tetramethyl-1′-piperidinyloxy)ethane (STEMPO, 46.6 mg, 0.178 mmol)

and 2,2,6,6-tetramethylpiperidinooxy (TEMPO, 1.0 mg, 0.0064 mmol), followed by the addition of styrene (10.165 g, 97.6 mmol). After the mixture was degassed by three freeze-pump-thaw cycles, the polymerization was started by placing the flask in a 120 °C oil bath and monitored by SEC. The polymerization was stopped after 19.5 h. The mixed PCL/PS brush-grafted particles were isolated by centrifugation, redispersed in THF, and centrifugated again. This washing process was repeated four times to remove the physically adsorbed free polymer. The hairy particle samples were then dried with a stream of air flow.

4.3 Results and Discussion

4.3.1 Synthesis of Y-Initiator-Functionalized Silica Particles

The triethoxysilane-terminated Y-initiator (Y-Silane-B) bearing a hydroxyl group, an initiator for ROP of cyclic esters,[15] and an NMRP initiator was synthesized by platinum-catalyzed hydrosilylation reaction of 2-[4-(but-3-enyl)phenyl]-2-(2′,2′,6′,6′-tetramethyl-1′-piperidinyloxy)ethanol (Y-silane precursor) with $HSi(OC_2H_5)_3$ (Scheme 4.2). The combination of two different initiators into one molecule ensures that they are well mixed in the initiator layer on the surface of silica particles, allowing the preparation of well-mixed PCL/PS brushes. The obtained Y-Silane-B, 2-[4-(1-triethoxysilylbutyl)phenyl]-2-(2',2',6',6'-tetramethyl-1'-piperidinyloxy)ethanol, was purified by silica gel column chromatography using methylene chloride as eluent, and the molecular structure was confirmed by ^{1}H and ^{13}C NMR spectroscopy and mass spectrometry analysis. Figure 4.1 shows the ^{1}H NMR spectrum of Y-silane with the characteristic peaks assigned and labelled.

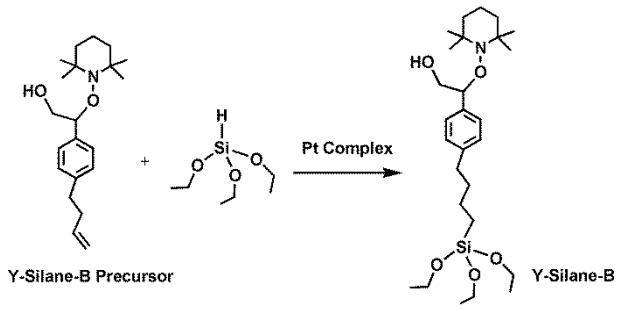

Scheme 4.2 Synthesis of Y-Silane-B by platinum-catalyzed hydrosilylation of Y-Silane-B precursor with triethoxysilane ($HSi(OC_2H_5)_3$).

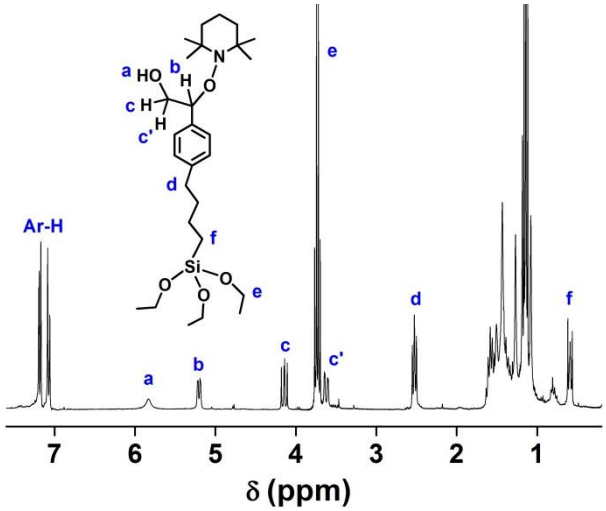

Figure 4.1 ^{1}H NMR spectra of 2-[4-(1-triethoxysilylbutyl)phenyl]-2-(2',2',6',6'-tetramethyl-1'-piperidinyloxy)ethanol (Y-Silane-B). $CDCl_3$ was used as solvent.

The bare silica particles used in the present work were made by the Stöber process.[20] The average diameter of the bare silica particles was 157 nm, measured from transmission electron microscopy (TEM) micrographs (a typical TEM image is shown in Figure 4.2a). The Y-initiator was immobilized onto the surface of silica particles via an ammonia-catalyzed hydrolysis and condensation process in ethanol, similar to those reported in the literature for other triethoxysilane-terminated initiators.[10i-k,16] As shown in Chapter 2, the initiator density and hence the grafting density of polymer brushes can be systematically tuned by varying the mass ratio of the triethoxysilane-terminated initiator to bare silica particles in the initiator immobilization process.[10k] Using this method, a series of Y-initiator-functionalized silica particles (YI-B-Particles) with the mass ratio of Y-Silane-B to silica particles ranging from 153.4% (the obtained initiator-functionalized particles denoted as YI-B-P-I), to 87.5% (YI-B-P-II), to 64.3% (YI-B-P-III), to 18.7% (YI-B-P-IV). After the immobilization reactions proceeded at 40 °C for 19 h, the initiator particles were isolated by centrifugation and repeatedly washed with THF. The YI-B-Particles were then characterized by thermogravimetric analysis (TGA). Figure 4.3a and b shows the TGA curves of bare silica particles and YI-B-P-II with the weight retentions at 800 °C of 90.7%, and 88.5%, respectively, which are similar to the observations for similarly sized bare silica particles and corresponding silica particles functionalized with a Y-initiator containing ATRP and NMRP initiators.[10k] A typical TEM micrograph of YI-B-P-II is shown in Figure 4.2b.

4.3.2 Synthesis of PCL Brushes from Y-Initiator-Functionalized Silica Particles

Ring-opening polymerization of εCL catalyzed by $Sn(Oct)_2$ is usually carried out at relatively high temperatures, typically around 120 °C.[15] This condition cannot be applied to the synthesis of PCL brushes from Y-initiator-functionalized silica particles because of the thermally induced decomposition of the NMRP initiator. Therefore, we focused on the growth of PCL brushes by

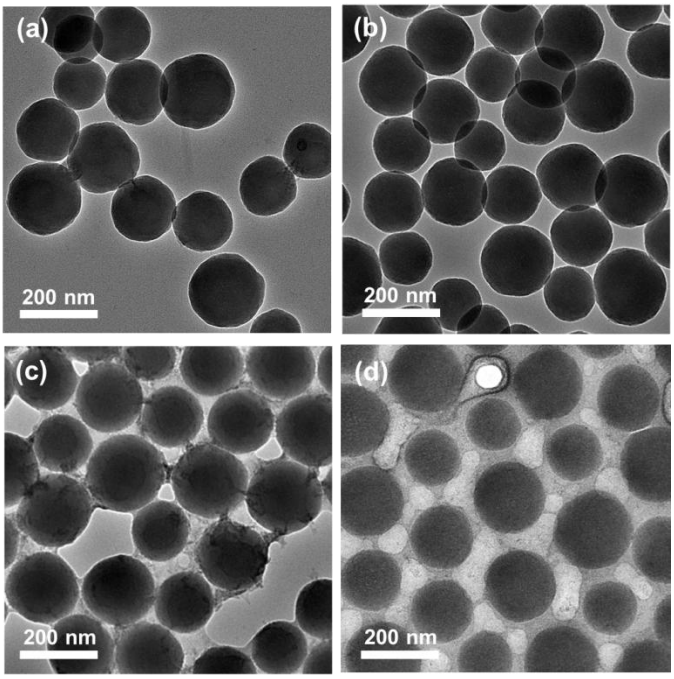

Figure 4.2 Transmission electron microscopy micrographs of (a) bare silica particles, (b) Y-initiator-functionalized silica particles prepared by using the mass ratio of Y-silane to bare silica particles of 87.5% in the initiator immobilization step (YI-B-P-II), (c) PCL brush-grafted silica particles made from YI-B-P-II with PCL $M_{n,SEC}$ of 24.3 kDa, and (d) mixed PCL/PS brush-grafted silica particles prepared from YI-B-P-II with PCL $M_{n,SEC}$ of 24.3 kDa and PS $M_{n,SEC}$ of 24.6 kDa.

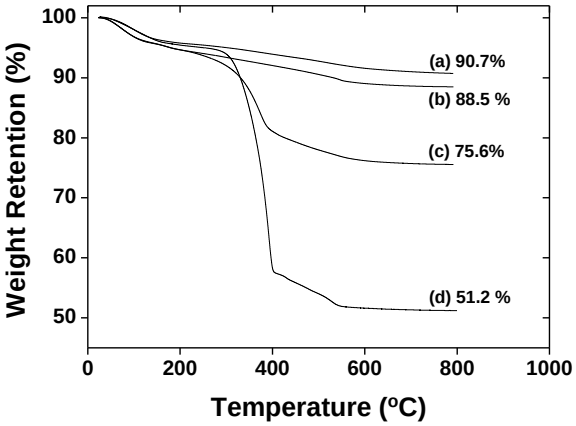

Figure 4.3 Thermogravimetric analysis (TGA) of (a) bare silica particles, (b) Y-initiator-functionalized silica particles (YI-B-P-II), (c) PCL brush-grafted silica particles with PCL $M_{n,SEC}$ of 24.3 kDa synthesized from YI-B-P-II, (d) mixed PCL/PS brush-grafted particles with PCL $M_{n,SEC}$ of 24.3 kDa and PS $M_{n,SEC}$ of 24.6 kDa. TGA was performed in air (curves a-c) or in pure oxygen (curve d) at a heating rate of 20 ^{o}C/min from room temperature to 800 °C.

ROP of εCL at 75 °C, at which the TEMPO moiety has been proven to be stable.[10a-d] Our initial attempt in the synthesis of PCL brushes from Y-initiator particles in dry THF at 75 °C using $Sn(Oct)_2$ as catalyst and ω-undecylenyl alcohol as the free initiator produced relatively low molecular weights even after prolonged polymerization time and broad molecular weight distributions. The reproducibility was also poor. Recognizing that the moisture in the reaction system could affect the ROP, we azeotropically distilled freshly dried toluene twice from YI-B-particles to remove water and further dried the particles under high vacuum at 55 °C for 8 h. The catalyst for ROP of εCL, tin(II) 2-ethylhexanoate, was also dried by azeotropic distillation with toluene and then under high vacuum at 100 °C for 8 h. Moreover, we increased the amount of the catalyst with respect to the free initiator from a molar ratio of ~ 1 : 1 to ~ 2.5 : 1.[21] We found that this condition reproducibly yielded PCL polymers with $M_{n,SEC}$ of ~ 25 kDa (relative to polystyrene standards) and polydispersity indexes of ≤ 1.20.

Using this condition, we carried out a surface-initiated ROP of εCL to grow PCL brushes from YI-B-P-II in THF at 75 °C in the presence of a free initiator, ω-undecylenyl alcohol. The molar ratios of εCL : ω-undecylenyl alcohol : $Sn(Oct)_2$ = 452 : 1.0 : 2.6. After the polymerization proceeded for 13 h, the viscosity of the reaction mixture was high and the stir bar stopped moving. The flask was removed from the oil bath and the mixture was diluted with THF, and the particles were isolated by centrifugation, re-dispersed in THF, and centrifugated again. This washing process was repeated for a total of five times to remove the physically adsorbed PCL. The $M_{n,SEC}$ and PDI of the free PCL formed from ω-undecylenyl alcohol was 24.3 kDa and 1.20 (Figure 4.4a), relative to polystyrene standards. The narrow PDI indicated that the polymerization was controlled. The actual molecular weight $M_{n,abs}$ of the free PCL determined by SEC using a multi-angle light scattering detector was 16.0 kDa, using a dn/dc value of 0.0750 for

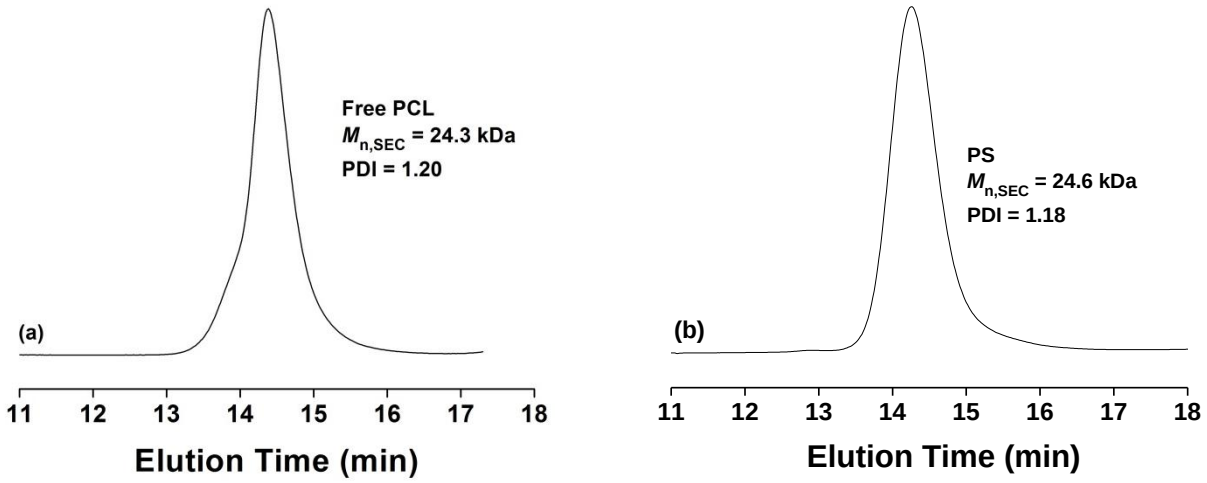

Figure 4.4 Size exclusion chromatography analysis of (a) the free PCL, formed from the free initiator in the synthesis of PCL brush-grafted silica particles from YI-B-P-II, and (b) the free polystyrene formed from the free initiator STEMPO in the synthesis of mixed PCL/PS brush-grafted silica particles from PCL brush-grafted silica particles by NMRP of styrene at 19.5 h.

PCL in THF.[19] Thermogravimetric analysis showed that the weight retention of the obtained PCL brush-grafted silica particles at 800 °C was 75.6 %, much lower than that of YI-B-P-II. From the TEM micrograph (Figure 4.2c), the PCL brushes can be clearly seen. By using the size of silica particles (157 nm), TGA data, and the $M_{n,abs}$ of PCL, and assuming that the density of silica particles was identical to that of bulk SiO_2 (2.07 g/cm^3)[10k] and the molecular weights of the grafted PCL and the free PCL are the same, the grafting density of PCL (σ_{PCL}) was calculated to be 0.40 chains/nm^2.[22]

4.3.3 Synthesis of Mixed PCL/PS Brushes from PCL Brush-Grafted Silica Particles by Surface-Initiated NMRP

The PCL brush-grafted silica particles made from YI-B-P-II with PCL $M_{n,SEC}$ of 24.3 kDa were then used for the synthesis of mixed PCL/PS brushes by surface-initiated NMRP of styrene. The polymerization was carried out in anisole at 120 °C with addition of a free initiator, 1-phenyl-1-(2′,2′,6′,6′-tetramethyl-1′-piperidinyloxy)ethane (STEMPO), and a small amount of free radical TEMPO (3.6 mol% with respect to STEMPO), and was monitored by SEC. The polymerization was stopped at 19.5 h. The hairy particles were separated by centrifuge and repeatedly washed; the free PS polymers were analyzed by SEC.

Figure 4.4b shows the GPC trace of the free PS polymer. The $M_{n,SEC}$ of PS was 24.6 kDa (the particles designated as MB-II). The PDI was 1.18, indicating that the polymerization was controlled. The mixed PCL/PS brush-grafted silica particles were characterized by TGA. As can be seen from Figure 4.3d, the weight retention of mixed PCL/PS brush-grafted silica particles (MB-II) at 800 ^{o}C decreased to 51.2%. Figure 4.2d shows a typical TEM micrograph of MB-II. Clearly, the interstitial space among silica particles was filled with the grafted polymers;

compared with the corresponding PCL brush-grafted particles (Figure 4.2c), the interparticle distance became larger, consistent with the increased polymer content in the hairy particles.

By using the bare silica particle size, TGA data, and the molecular weights of free PS, and assuming that the density of silica particles was identical to that of bulk SiO_2 (2.07 g/cm^3) and the M_n values of the grafted PS and the free PS are the same, the grafting density of PS in the mixed brush sample was calculated to be 0.83 chains/nm^2.[22] Note that the grafting density of PS in the mixed brush sample is significantly higher than that of PCL (0.40 chains/nm^2). This is likely because the initiating radicals in NMRP are generated by thermal decomposition of the TEMPO moiety, which is a unimolecular process,[23] while the initiation in ROP involves the formation of Sn-alkoxide on the surface and the insertion of monomer molecules.[15] Consequently, the surface-initiated ROP is more sensitive than NMRP to the steric hindrance presented by the confined geometry on the surface of silica particles and the inherent heterogeneity of the particle surface and the initiator layer.

4.3.4 Tuning Overall Grafting Density of Mixed PCL/PS Brushes - Effect of Different Mass Ratios of Y-Silane to Bare Silica Particles Used in the Initiator Immobilization Step

The work presented in Chapter 2 showed that the overall grafting density of mixed homopolymer brushes synthesized by sequential ATRP and NMRP can be tuned by changing the mass ratio of the initiator to bare silica particles in the initiator immobilization process.[10k] In this work, we prepared a series of Y-initiator-functionalized silica particles from the same batch of bare silica particles using different mass ratios of Y-silane to bare particles: 153.4% (YI-B-P-I), 87.5% (YI-B-P-II), 64.3% (YI-B-P-III), and 18.7% (YI-B-P-IV). Using the same procedure for the synthesis of mixed PCL/PS brushes from YI-B-P-II, we carried out surface-initiated ROP of ε-CL and NMRP of styrene sequentially from other initiator-functionalized silica particles. The

values of $M_{n,SEC}$ of PCL and PS (relative to polystyrene standards) were targeted at ~ 25 kDa. The obtained PCL brush- and mixed PCL/PS brush-grafted silica particles were characterized by TGA (Figures 4.5 – 4.7), and the absolute molecular weights of free PCL were measured by SEC with a multiangle light scattering detector. The data are summarized in Table 4.1. Using the same assumptions that we made in the calculation of grafting densities of polymer brushes prepared from YI-B-P-II, we estimated the grafting densities of PCL (σ_{PCL}) and PS (σ_{PS}) in each mixed brush particle sample (Table 4.1) as well as the overall grafting density ($\sigma_{overall} = \sigma_{PCL} + \sigma_{PS}$). For comparison, the data for MB-II are also included in Table 4.1.

As can be seen from Table 4.1, there is a general trend that the overall grafting density decreased with the decrease of the mass ratio of Y-silane to bare silica particles in the initiator immobilization step, from above 1.0 chains/nm^2 in MB-I, and -II to 0.64 chains/nm^2 for MB-IV**,** though the $\sigma_{overall}$ of MB-I (1.06 chains/nm^2) was slightly lower than that of MB-II (1.23 chains/nm^2). The individual grafting densities of PCL and PS also exhibited a similar trend. Similar to MB-II, the PCL grafting density was noticeably smaller than that of the corresponding PS for other three samples; σ_{PCL} was only about half of σ_{PS} or even smaller. Overall, Table 4.1 showed that the overall grafting density can be tuned by changing the mass ratio of Y-Silane-B to bare silica particles.

Hydrofluoric acid was used to etch the silica core of MB-II. SEC analysis showed that the molecular weights of the grafted polymers were close to those of the free polymers formed from the free initiators.[24]

4.4 Conclusions

Mixed PCL/PS brushes were grown from silica particles functionalized with a Y-initiator bearing a hydroxyl group and a TEMPO moiety by sequential ROP of εCL at 75 °C using

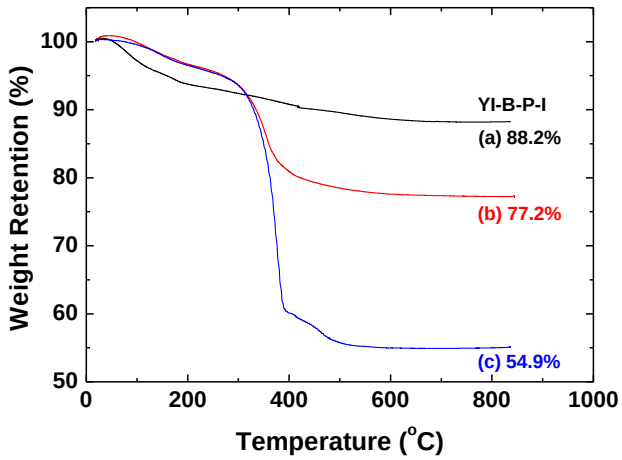

Figure 4.5. Thermogravimetric analysis (TGA) of (a) Y-initiator-functionalized silica particles (YI-B-P-I), (b) PCL brush-grafted silica particles with PCL $M_{n,SEC}$ of 25.8 kDa synthesized from YI-B-P-I, and (c) mixed PCL/PS brush-grafted silica particles with PCL $M_{n,SEC}$ of 25.8 kDa and PS $M_{n,SEC}$ of 24.5 kDa. TGA was performed in air at a heating rate of 20 °C/min from room temperature to 800 °C.

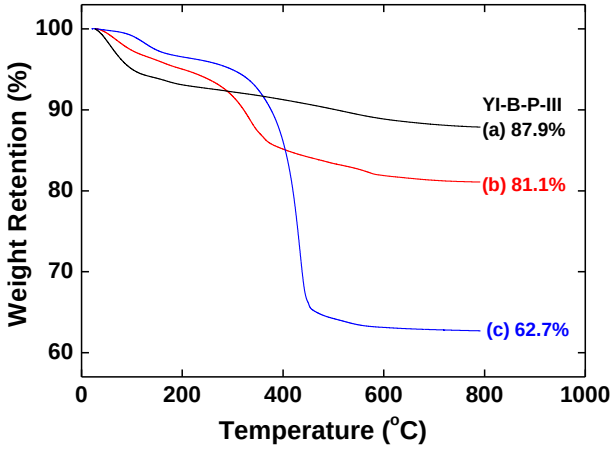

Figure 4.6. Thermogravimetric analysis (TGA) of (a) Y-initiator-functionalized silica particles (YI-B-P-III), (b) PCL brush-grafted silica particles with PCL $M_{n,SEC}$ of 24.0 kDa synthesized from YI-B-P-III, and (c) mixed PCL/PS brush-grafted silica particles with PCL $M_{n,SEC}$ of 24.0 kDa and PS $M_{n,SEC}$ of 24.0 kDa. TGA was performed in air at a heating rate of 20 °C/min from room temperature to 800 °C.

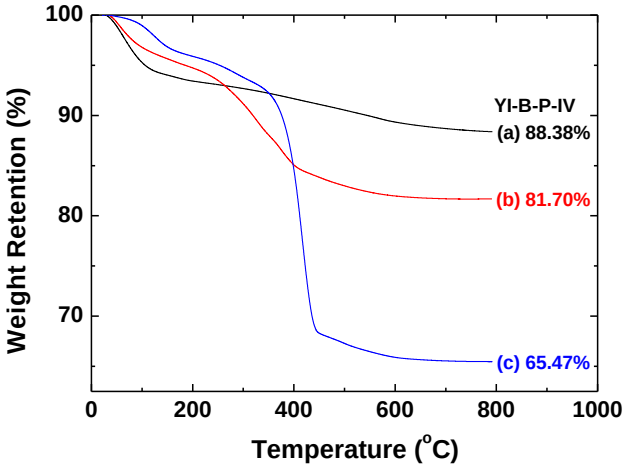

Figure 4.7. Thermogravimetric analysis (TGA) of (a) Y-initiator-functionalized silica particles (YI-B-P-IV), (b) PCL brush-grafted silica particles with PCL $M_{n,SEC}$ of 27.1 kDa synthesized from YI-B-P-IV, and (c) mixed PCL/PS brush-grafted silica particles with PCL $M_{n,SEC}$ of 27.1 kDa and PS $M_{n,SEC}$ of 24.2 kDa. TGA was performed in air at a heating rate of 20 °C/min from room temperature to 800 °C.

Table 4.1 Characterization Data for Mixed PCL/PS Brush-Grafted Silica Particles Synthesized by Sequential Surface-Initiated ROP and NMRP from Y-Initiator-Functionalized Particles Prepared by Using Different Mass Ratios of Y-Silane to Bare Particles in the Initiator-Immobilization Step

Sample No	Initiator Particles	Mass Ratio of Y-Silane-B to Bare Particles [a]	PCL $M_{n,SEC}$ and PDI [b]	PCL $M_{n,abs}$ [c]	PS $M_{n,SEC}$ and PDI [b]	σ_{PCL}, σ_{PS} (chains/nm^2)[d]	$\sigma_{overall}$ (chains/nm^2)
MB-I	YI-B-P-I	153.4%	25.8 kDa, 1.14	17.0 kDa	24.5 kDa, 1.16	0.37, 0.69	1.06
MB-II	YI-B-P-II	87.5%	24.3 kDa, 1.20	16.0 kDa	24.6 kDa, 1.18	0.40, 0.83	1.23
MB-III	YI-B-P-III	64.3%	24.0 kDa, 1.20	16.0 kDa	24.0 kDa, 1.15	0.25, 0.53	0.78
MB-IV	YI-B-P-IV	18.7%	27.1 kDa, 1.19	18.7 kDa	24.2 kDa, 1.16	0.19, 0.45	0.64

[a] The mass ratio of the triethoxysilane-terminated Y-initiator (Y-Silane-B) to the bare silica particles in the initiator immobilization step. [b] Molecular weight ($M_{n,SEC}$) and polydispersity index (PDI) were determined by using SEC relative to polystyrene standards. [c] PCL absolute molecular weight ($M_{n,abs}$) determined by SEC with a multi-angle light scattering detector. [d] The grafting densities were calculated using the size of bare silica particles (157 nm), TGA data, and the molecular weights of free polymers ($M_{n,abs}$ for PCL and $M_{n,SEC}$ for PS), and assuming that the density of silica particles was identical to that of bulk SiO_2 (2.07 g/cm^3) and the molecular weights of the grafted PCL and the free PCL are the same.

$Sn(Oct)_2$ as catalyst and NMRP of styrene at 120 °C.[25] Both surface-initiated polymerizations were carried out in the presence of a free initiator. By carefully drying Y-initiator-functionalized silica particles and catalyst $Sn(Oct)_2$, PCL with $M_{n,SEC}$ values of ~ 25 kDa and narrow polydispersities (PDI ≤ 1.20) can be reproducibly synthesized by ROP. The grafting density of PCL was found to be lower than that of PS, likely because of the different initiation mechanisms of ROP and NMRP. The overall grafting density of mixed PCL/PS brushes can be tuned by changing the mass ratio of the triethoxysilane-terminated Y-initiator to bare silica particles in the initiator immobilization step. This method can be extended to the synthesis of mixed brushes containing other chemically or biologically degradable polymers.

References

1. Marko, J. F.; Witten, T. A. *Phys. Rev. Lett.* **1991,** *66*, 1541-1544.
2. Luzinov, I.; Minko, S.; Tsukruk, V. V. *Prog. Polym. Sci.* **2004**, *29*, 635-698.
3. Zhao, B.; Zhu, L. *Macromolecules* **2009**, *42*, 9369-9383.
4. Moffitt, M. G. *J. Phys. Chem. Lett.* **2013**, *4*, 3654-3666.
5. Chen, L.; Klok, H.-A. *Soft Matter* **2013**, *9*, 10678-10688.
6. Dong, H. *J. Phys. II Fr.* **1993,** *3*, 999-1020.
7. (a) Zhulina, E.; Balazs, A. C. *Macromolecules* **1996,** *29*, 2667-2673. (b) Müller, M. *Phys. Rev. E* **2002,** *65*, 030802. (c) Minko, S.; Müller, M.; Usov, D.; Scholl, A.; Froeck, C.; Stamm, M. *Phys. Rev. Lett.* **2002,** *88*, 035502. (d) Wenning, L.; Müller, M.; Binder, K. *Europhys. Lett.* **2005**, *71*, 639-645. (e) Merlitz, H.; He, G. L.; Sommer, J. U.; Wu, C. X. *Macromolecules* **2009**, *42*, 445-451. (f) Egorov, S. A. *Soft Matter* **2012**, *8*, 3971-3979. (g) Hur, S.-M.; Frischknecht, A. L.; Huber, D. L.; Fredrickson, G. H. *Soft Matter* **2013**, ***9***, 5341-5354. (h) Wang, J.; Müller, M. *J. Phys. Chem. B.* **2009**, *113*, 11384-11402.
8. (a) Roan, J.-R. *Phys. Rev. Lett.* **2006**, *96*, 248301. (b) Wang, Y. Q.; Yang, G. A.; Tang, P. Qiu, F.; Yang, Y. L.; Zhu, L. *J. Chem. Phys.* **2011**, *134*, 134903. (c) Ma, X.; Yang, Y. Z.; Zhu, L.; Zhao, B.; Tang, P.; Qiu, F. *J. Chem. Phys.* **2013**, *139*, 214902.
9. (a) Sidorenko, A.; Minko, S.; Schenk-Meuser, K.; Duschner, H.; Stamm, M. *Langmuir* **1999,** *15*, 8349-8355. (b) Minko, S.; Usov, D.; Goreshnik, E.; Stamm, M. *Macromol. Rapid Commun.* **2001,** *22*, 206-211. (c) Motornov, M.; Minko, S.; Eichhorn, K. J.; Nitschke, M.; Simon, F.; Stamm, M. *Langmuir* **2003,** *19*, 8077-8085. (d) Lemieux, M.; Usov, D.; Minko, S.; Stamm, M.; Shulha, H.; Tsukruk, V. V. *Macromolecules* **2003,** *36*, 7244-7255. (e) Usov, D.; Gruzdev, V.; Nitschke, M.; Stamm, M.; Hoy, O.; Luzinov, I.; Tokarev, I.;

Minko, S. *Macromolecules* **2007**, *40*, 8774-8783. (f) Santer, S.; Kopyshev, A.; Yang, H. K.; Rühe, J. *Macromolecules* **2006,** *39*, 3056-3064. (g) Tsujii, Y.; Ohno, K.; Yamamoto, S.; Goto, A.; Fukuda, T. *Adv. Polym. Sci.* **2006**, *197*, 1-45. (h) Wang, Y.; Brittain, W. J. *Macromol. Rapid Commun.* **2007**, *28*, 811-815.

10. (a) Zhao, B.; He, T. *Macromolecules* **2003**, *36*, 8599-8602. (b) Zhao, B.; Haasch, R. T.; MacLaren, S. *J. Am. Chem. Soc.* **2004**, *126*, 6124-6134. (c) Zhao, B.; Haasch, R. T.; MacLaren, S. *Polymer* **2004**, *45*, 7979-7988. (d) Li, D. J.; Sheng, X.; Zhao, B. *J. Am. Chem. Soc.* **2005**, *127*, 6248−6256. (e) Santer, S.; Kopyshev, A.; Donges, J.; Rühe, J.; Jiang, X. G.; Zhao, B.; Müller, M. *Langmuir* **2007**, *23*, 279-285. (f) Zhao, B.; Zhu, L. *J. Am. Chem. Soc.* **2006**, *128*, 4574-4575. (g) Zhu, L.; Zhao, B. *J. Phys. Chem. B* **2008**, *112*, 11529-11536. (h) Jiang, X. M.; Zhong, G. J.; Horton, J. M.; Jin, N. X.; Zhu, L.; Zhao, B. *Macromolecules* **2010**, *43*, 5387-5395. (i) Jiang, X. M.; Zhao, B.; Zhong, G. J.; Jin, N. X.; Horton, J. M.; Zhu, L.; Hafner, R. S.; Lodge, T. P. *Macromolecules* **2010**, *43*, 8209-8217. (j) Horton, J. M.; Tang, S. D.; Bao, C. H.; Tang, P.; Qiu, F.; Zhu, L.; Zhao, B. *ACS Macro Letters* **2012**, *1*, 1061-1065. (k) Bao, C. H.; Tang, S. D.; Horton, J. M.; Jiang, X. M.; Tang, P.; Qiu, F.; Zhu, L.; Zhao, B. *Macromolecules* **2012**, *45*, 8027-8036. (l) Tang, S. D.; Lo, T.-Y.; Horton, J. M.; Bao, C. H.; Tang, P.; Qiu, F.; Ho, R.-M.; Zhao, B.; Zhu, L. *Macromolecules* **2013**, *46*, 6575-6584.

11. (a) Ye, P. L.; Dong, H. C.; Zhong, M. J.; Matyjaszewski, K. *Macromolecules* **2011**, *44*, 2253-2260. (b) Price, A. D.; Hur, S.-M.; Fredrickson, G. H.; Frischknecht, A. L.; Huber, D. L. *Macromolecules* **2012**, *45*, 510-524. (c) Estillore, N. C.; Advincula, R. C. *Langmuir* **2011**, *27*, 5997-6008. (d) Filimon, M.; Kopf, I.; Ballout, F.; Schmidt, D. A.; Brändermann, E.; Rühe, J.; Santer, S.; Havenith, M. *Soft Matter* **2010**, 6, 3764-3768. (e) Ochsmann, J. W.;

Lenz, S.; Lellig, P.; Emmerling, S. G. J.; Golriz, A. A.; Reichert, P.; You, J.; Perlich, J.; Roth, S. V.; Beger, R.; Gutmann, J. S. *Macromolecules* **2012**, *45*, 3129-3136. (f) Huang, X.; Hauptmann, N.; Appelhans, D.; Formanek, P.; Frank, S.; Kaskel, S.; Temme, A.; Voit, B. *Small* **2012**, *8*, 3579-3583. (g) Rungta, A.; Natarajan, B.; Neely, T.; Dukes, D.; Schadler, L.S.; Benicewicz, B. C. *Macromolecules* **2012**, *45*, 9303-9311.

12. (a) Minko, S.; Patil, S.; Datsyuk, V.; Simon, F.; Eichhorn, K. J.; Motornov, M.; Usov, D.; Tokarev, I.; Stamm, M. *Langmuir* **2002,** *18*, 289-296. (b) Minko, S.; Luzinov, I.; Luchnikov, V.; Müller, M.; Patil, S.; Stamm, M. *Macromolecules* **2003,** *36*, 7268-7279. (c) Minko, S.; Müller, M.; Motornov, M.; Nitschke, M.; Grundke, K.; Stamm, M. *J. Am. Chem. Soc.* **2003,** *125*, 3896-3900.

13. (a) Julthongpiput, D.; Lin, Y. H.; Teng, J.; Zubarev, E. R.; Tsukruk, V. V. *Langmuir* **2003,** *19*, 7832-7836. (b) Wang, J.; Kara, S.; Long, T. E.; Ward, T. C. *J. Polym. Sci., Polym. Chem.* **2000**, *38*, 3742-3750. (c) Zubarev, E. R.; Xu, J.; Sayyad, A.; Gibson, J. D. *J. Am. Chem. Soc.* **2006**, *128*, 4958-4959.

14. Cheng, L.; Liu, A. P.; Peng, S.; Duan, H. W. *ACS Nano* **2010**, *4*, 6098-6104.

15. (a) Storey, R. F.; Sherman J. W. *Macromolecules* **2002**, *35*, 1504-1512. (b) Labet, M.; Thielemans, W. *Chem. Soc. Rev.* **2009**, *38*, 3484-3504.

16. (a) Ohno, K.; Morinaga, T.; Koh, K.; Tsujii, Y.; Fukuda, T. *Macromolecules* **2005**, *38*, 2137-2142. (b) Ohno, K.; Morinaga, T.; Takeno, S.; Tsujii, Y.; Fukuda, T. *Macromolecules* **2006**, *39*, 1245-1249.

17. (a) Miura, Y.; Sakai, Y.; Yamaoka, K. *Macromolecular Chemistry and Physics* **2005**, *206*, 504-512. (b) Hawker, C. J.; Hedrick, J. L.; Malmström, E. E.; Trollsås, M.; Mecerreyes, D.; Moineau, G.; Dubois, P.; Jérôme, R. *Macromolecules* **1998**, *31*, 213-219. (c) Pratt, R. C.;

Lohmeijer, B. G. G.; Long, D. A.; Lundberg, P. N. P.; Dove, A. P.; Li, H.; Wade, C. G.; Waymouth, R. M.; Hedrick, J. L. *Macromolecules* **2006**, *39*, 7863-7871. (d) Nederberg, F.; Lohmeijer, B. G. G.; Leibfarth, F.; Pratt, R. C.; Choi, J.; Dove, A. P.; Waymouth, R. M.; Hedrick, J. L. *Biomacromolecules* **2006**, *8*, 153-160.

18. Matyjaszewski, K.; Woodworth, B. E.; Zhang, X.; Gaynor, S. G.; Metzner, Z. *Macromolecules* **1998**, *31*, 5955-5957.
19. Zhou, J. X.; Wang, W. X.; Villarroya, S.; Thurecht, K. J.; Howdle, S. M. *Chem. Commun.* **2008**, 5806-5808.
20. Stöber, W.; Fink, A.; Bohn, E. *J. Colloid & Interface Sci.* **1968**, *26*, 62-68.
21. Möller, M.; Nederberg, F.; Lim, L. S.; Kånge, R.; Hawker, C. J.; Hedrick, J. L.; Gu, Y. D. Shah, R.; Abbott, N. L. *J. Polym. Sci. Part A: Polym. Chem.* **2001**, *39*, 3529-3538.
22. The difference between weight retentions of Y-initiator-functionalized silica particles and polymer brush-grafted silica particles at 100 °C is presumably caused by the water or other volatiles. This difference was taken into consideration in the calculation of grafting densities of polymer brushes by vertically shifting the curves to the same position – the higher weight retention at 100 °C as described in the following paper: Horton, J. M.; Bao, C. H.; Bai, Z. F.; Lodge, T. P.; Zhao, B. *Langmuir* **2011**, *27*, 13324-13334.
23. Hawker, C. J.; Bosman, A. W.; Harth, E. *Chem. Rev.* **2001**, *101*, 3661-3688.
24. Husseman, M.; Malmström, E. E.; McNamara, M.; Mate, M.; Mecerreyes, D.; Benoit, D. G.; Hedrick, J. L.; Mansky, P.; Huang, E.; Russell, T. P.; Hawker, C. J. *Macromolecules*, **1999**, *32*, 1424-1431.
25. The work presented in this Chapter is included in a paper published in *RSC Advances* (*RSC Advances* **2014**, *4*, 18772-18781).

Chapter 5. Synthesis and Application of Acidic Polymer Brush-Grafted Silica Particles as Catalysts for Dehydration of Fructose in Water to 5-Hydroxymethylfurfural

Abstract

This Chapter presents the synthesis of two polymer brush-supported acid catalysts, poly(3-(3-sulfopropyl)-1-(4-vinylbenzyl)-1H-imidazol-3-ium trifluoromethanesulfonate) brush- and poly(4-vinylbenzenesulfonic acid) brush-grafted silica particles, and the use of these hairy particle catalysts for synthesis of 5-hydroxymethylfurfural (HMF), a versatile platform chemical, from fructose dehydration in water. The brush catalysts were prepared by surface-initiated atom transfer radical polymerization of corresponding monomers from initiator-functionalized silica particles in the presence of a free initiator and subsequent acidification. The free polymers that were formed from free initiators in the synthesis of polymer brushes were also purified, acidified, and used as catalysts for HMF synthesis for comparison. It was found that both brush catalysts efficiently catalyzed the dehydration reaction of fructose in water and exhibited a higher catalytic activity than the corresponding free polymer catalysts as evidenced by the higher HMF yields under the same reaction conditions.

5.1. Introduction

Renewable biomass is a promising alternative resource for sustainable supply of industrial chemicals and liquid transportation fuels. Among all intermediate chemicals derived from biomass, 5-hydroxymethylfurfural (HMF) is widely considered as a versatile platform compound that can be used to make fine chemicals, pharmaceuticals, polymers, etc.[1-3] The process of producing HMF from acid-catalyzed dehydration of fructose and other hexoses (glucose, xylose, etc.) has been conducted in many different media, including single-phase systems,[4] biphasic solvent systems,[5,6] and ionic liquids.[7,8] Although high HMF yields can be obtained in some organic solvents (e.g., dimethylsulfoxide[9]) and ionic liquids, separation of HMF is very challenging. From an economic and environmental point of view, water is a desired reaction medium for its zero-toxicity and lower cost. In addition, water can dissolve the majority of sugars in high concentrations, unlike most organic solvents.[10-14] However, it should be noted here that the dehydration reaction of fructose in aqueous media is generally nonselective and many by-products, such as insoluble humins, are produced.[3] To improve the selectivity, biphasic systems of water and organic solvents have been employed to facilitate the extraction of HMF.

Various acids have been employed to catalyze the dehydration of hexoses, particularly fructose, to produce HMF.[15-17] Although small molecule acids are inexpensive and highly active catalysts for dehydration reactions in polar aprotic organic solvents and ionic liquids, it is difficult, if not impossible, to recycle and reuse them. In contrast, heterogeneous solid acids are more advantageous because of the facile recovery and a lower degree of corrosiveness.[18-21] With the use of supported acid catalysts in organic solvents, relatively high HMF yields and selectivity have been reported, and the catalysts can be recycled and reused. For example, Qi et al used DOWEX 50WX8−100 acidic resin as catalyst for fructose dehydration in a solvent mixture of

acetone-DMSO (70:30, w/w), and obtained a HMF yield of 88% at a 98% conversion of fructose after 20 min at 140 ℃.[22] The catalyst was reused multiple times with a negligible decrease in the HMF yield. However, when the dehydration reactions are carried out in aqueous media, the yields and selectivity of HMF are significantly lower because of many side reactions, despite that the catalysts can be recycled.[3]

Polymer brush-supported organocatalysts are a promising class of supported catalysts, which have been shown to exhibit the advantages of both soluble polymer- and insoluble polymer resin-supported catalysts.[23-26] Polymer brushes are an assembly of polymer chains grafted by one end on a solid surface.[23-33] Different from covalently anchored small molecules that are completely fixed on the solid substrate, polymer brushes are a dynamic system with a certain degree of mobility, which has been demonstrated by ^{1}H NMR spectroscopy study of polymer brush-grafted silica particles (hairy particles).[29] Thus, the polymer brush-supported catalysts resemble soluble polymer-supported catalysts and exhibit high catalytic activities. On the other hand, the substrate for polymer brushes can be particles,[23-26] flat substrates,[27] or porous materials,[32,33] allowing facile recovery and reuse. Moreover, the densely grafted polymer brushes create a microenvironment different from bulk media, which can be tailored to further improve the catalytic activity and selectivity of the supported catalyst.

This Chapter presents the synthesis and characterization of acidic poly(3-(3-sulfopropyl)-1-(4-vinylbenzyl)-1H-imidazol-3-ium trifluoromethanesulfonate) brush- and poly(4-vinylbenzenesulfonic acid) brush-grafted silica particles and the use of these hairy particles as catalyst for catalyzing dehydration of fructose to HMF in water (Scheme 5.1). The brushes were synthesized by surface-initiated atom transfer radical polymerization (SI-ATRP) from initiator-functionalized silica particles (initiator particles). The grafted linear polymer chains take

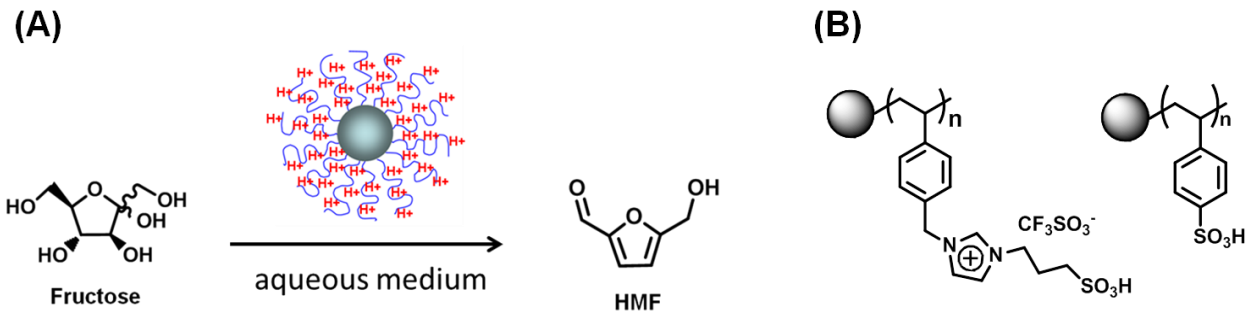

Scheme 5.1 (A) Schematic illustration for the dehydration of fructose to HMF catalyzed by an acidic hairy particle catalyst and (B) molecular structures of two acidic polymer brush catalysts: poly(3-(3-sulfopropyl)-1-(4-vinylbenzyl)-1H-imidazol-3-ium trifluoromethanesulfonate) ($P(VBIm^{+}\text{-}SO_3H/CF_3SO_3^{-})$) brush- and poly(4-vinylbenzenesulfonic acid) (PVBSA) brush-grafted silica particles.

on extended conformations in water due to their hydrophilic nature. When fructose molecules diffuse through the acidic brushes, they experience a microenvironment created by the hydrophobic polymer backbone and the highly concentrated, hydrated organic acid groups, different from the bulk aqueous phase, and undergo a dehydration process to form HMF with the loss of three water molecules. The catalytic activities of two polymer brush acid catalysts in the conversion of fructose to HMF were investigated and compared with those of their corresponding free polymer catalysts.

5.2. Experimental Section

5.2.1 Materials

Tetraethyl orthosilicate (98%), ammonium hydroxide (25% in water), triethoxysilane (95%), 4-vinylbenzyl chloride (tech., 90%), imidazole (99+ %, crystalline), 2,2,2-trifluoroethanol (99.8%), and trifluoromethanesulfonic acid (99%) were purchased from Acros Organics and used as received. Platinum-divinyltetramethyldisiloxane complex in xylene (2.1~2.4% Pt concentration in xylene) was obtained from Gelest, Inc. Sodium 4-vinylbenzenesulfonate (technical, ≥ 90 %), allylamine (98%), 2-bromoisobutyryl bromide (98%), D-(–)-Fructose (> 99%), and 5-hydroxymethylfurfural (analytical standard) were purchased from Aldrich. 1,3-Propanesultone (99 %) was obtained from Alfa Aesar and used as received. CuBr (98%, Aldrich) was stirred in glacial acetic acid overnight, filtered, and washed with absolute ethanol and ethyl ether. The purified CuBr was then collected, dried under vacuum, and stored in a desiccator. CuCl (98%, Aldrich) was purified by using the same procedure as for CuBr. *N*, *N*, *N′*, *N′*, *N″*-Pentamethyldiethylenetriamine (99 %, Aldrich) and ethyl 2-bromoisobutyrate were each dried with calcium hydride, distilled under a reduced pressure, and stored in a desiccator. All other

chemical reagents were obtained from either Aldrich or Fisher and used without further purification.

5.2.2 General Characterization

^{1}H NMR and ^{13}C NMR spectra were recorded on a Varian Mercury 300 MHz NMR spectrometer. Thermogravimetric analysis (TGA) was performed in air at a heating rate of 20 °C/min from room temperature to 800 ℃ or 1000 ℃ using TA Q-series Q50. The particle samples for TGA were dried at 45 ℃ in vacuum for at least 5 h. Dynamic light scattering (DLS) was conducted on a Brookhaven Instruments BI-200SM goniometer equipped with a PCI BI-9000AT digital correlator, a temperature controller, and a solid-state laser (model 25-LHP-928−249, λ = 633 nm) at a scattering angle of 90°. Transmission electron microscopy (TEM) experiments were conducted on a HITACH HD 2000 microscope with an accelerating voltage of 200 kV. The yields of HMF and fructose conversions in the fructose dehydration reactions were determined using a high performance liquid chromatography (HPLC) system (Shimadzu CBM-10AW VP) equipped with an Aminex HPX-87P column (300 mm × 7.8 mm, 9 μm particle size, 8 % cross-linkage, pH range 5-9) and a refractive index detector. The mobile phase was water (HPLC grade) at a flow rate of 0.8 mL/min. Mass spectrometry analysis was performed using a QSTAR Elite quadrupole time-of-flight (QTOF) mass spectrometer equipped with an ESI ion source and an integrated syringe pump (AB Sciex, Forster City, CA, USA)

5.2.3 Synthesis of Bare Silica Particles (SiP-I)

Ammonium hydroxide (25 % in water, 19.907 g) and tetraethyl orthosilicate (TEOS, 10.500 g) were each mixed with 10 mL of ethanol. The two solutions were then added into a 1 L one-necked flask that contained 280 mL of ethanol under the stirring condition. The concentrations of NH_3, TEOS, and water in the solution were 0.43 M, 0.15 M, 2.92 M, respectively. The mixture

was stirred vigorously at room temperature for 20.5 h. The bare silica particles were isolated by centrifugation (Eppendorf 5804 Centrifuge, 8000 rpm), redispersed in ethanol, and centrifuged again. This washing process was repeated with ethanol an additional two times, water four times, and ethanol two times again. The silica particles were dried with a stream of air flow. The yield of bare silica particles (SiP-I) was 3.3 g. The average diameter of SiP-I, measured by dynamic light scattering (DLS) in ethanol, was 189 nm. These particles were used to prepare ATRP-initiator-functionalized silica particles (IP-I).

5.2.4 Synthesis of *N*-Allyl-2-Bromo-2-Methylpropanamide

Allylamine (1.502 g, 26.30 mmol) was dissolved in dry THF (10 mL) in a 100 mL 3-necked flask, followed by the addition of triethylamine (2.815 g, 27.82 mmol). The flask was then placed in an ice/water bath, and a solution of 2-bromo-2-methylpropanoyl bromide (6.581 g, 28.63 mmol) in dry THF (15 mL) was added from an additional funnel into the mixture in a dropwise fashion under N_2. The reaction was allowed to warm to room temperature and to proceed overnight. THF was then removed using a rotavap, followed by the addition of water. The product was extracted with methylene chloride three times. The organic extracts were combined and dried with sodium sulfate overnight. The product was purified by vacuum distillation (1.63 g, 30.1%). ^{1}H NMR ($CDCl_3$) δ (ppm): 6.80 (br, 1H, -CH_2-N*H*-), 5.89 – 5.78 (m, H, CH_2=C*H*-), 5.18 – 5.13 (m, H, C*H*$_2$=CH-), 3.90 – 3.85 (m, 2H, -C*H*$_2$-NH-), 1.95 (s, 6H, -C*H*$_3$); ^{13}C NMR ($CDCl_3$) δ(ppm): 171.87, 133.49, 116.49, 63.03, 42.62, 30.73. Mass spectrum: $[M+H]^+$ at *m/z* 206.018

5.2.5 Synthesis of ATRP Initiator-Functionalized Silica Particles (IP-I) Using 2-Bromo-2-Methyl-*N*-(3-(Triethoxysilyl)propyl)propanamide

N-Allyl-2-bromo-2-methylpropanamide (1.002 g, 4.87 mmol) was added into a 25 mL two-necked flask. Triethoxysilane (3.712 g, 22.60 mmol) was added by a disposable plastic syringe into the flask under the N_2 atmosphere, followed by the injection of Pt complex in xylene (80 μL) using a microsyringe. The mixture was stirred at 45 °C under N_2; the hydrosilylation reaction was monitored by ^{1}H NMR spectroscopy analysis. After the reaction was complete, evidenced by the disappearance of the vinyl peak, excess triethoxysilane was removed under high vacuum at 45 °C, and the product was used directly in the next step for the preparation of 2-bromo-2-methyl-*N*-(3-(triethoxysilyl)propyl)propanamide-functionalized silica particles (IP-I).

Bare silica particles (SiP-I, 1.496 g) were dispersed in ethanol (128 mL) by ultrasonication to form a homogenous, stable dispersion. A solution of ammonium hydroxide (25 % in water, 8.011 g) in ethanol (30 mL) was added dropwise into the particle dispersion. After the mixture was stirred at 40 °C for 2 h, a solution of 2-bromo-2-methyl-*N*-(3-(triethoxysilyl)propyl)propanamide, freshly synthesized from hydrosilylation of 1.002 g of *N*-allyl-2-bromo-2-methylpropanamide, in dry THF (10 mL) was added dropwise into the dispersion. After the reaction mixture was stirred at 40 °C for 19.5 h, the particles were isolated by centrifugation and re-dispersed in ethanol. This process was repeated for a total of five times. The obtained initiator particles (IP-I) were then dried with a stream of N_2 flow (yield: 1.319 g).

5.2.6 Synthesis of 4-Vinylbenzyl Imidazole (VBIm)

Imidazole (10.409 g, 0.1529 mol) was dissolved in dry DMF (6 mL) at 70 °C in a 100 mL three-necked flask first, followed by the addition of 4-vinylbenzyl chloride (8.071 g, 0.0515 mol) in a dropwise fashion. The reaction mixture was stirred in a 70 °C oil bath overnight under N_2 atmosphere, and the reaction progress was monitored by ^{1}H NMR spectroscopy. When the peak of the CH_2 group in 4-vinylbenzyl chloride completely shifted from 4.63 ppm to 5.07 ppm in the

^{1}H NMR spectrum ($CDCl_3$ as solvent), the reaction was stopped, and DMF was removed by vacuum distillation. Diethyl ether (30 mL) was added into the flask. The mixture was transferred into a separatory funnel and washed with 1 M aqueous $NaHCO_3$ three times and then deionized water three times. The aqueous layer were combined and extracted with diethyl ether twice. The diethyl ether layer and extracts were then combined and dried with sodium sulfate overnight. The solvents were removed by a rotavap, and the product, VBIm, was dried under high vacuum, affording a light yellow oil-like liquid (5.001 g, 52.7 %). ^{1}H NMR ($CDCl_3$) δ (ppm): 7.52 (s, 1H, -N-C*H*-N-), 7.37 (d, 2H, CH_2=CH-CC*H*-), 7.09 (d, 2H, CH_2=CH-CCHC*H*-), 7.06 (s, 1H, -C*H*-N-CH-), 6.87 (s, 1H, -N-CH=C*H*-), 6.68 (dd, 1H, -C*H*=CH_2), 5.73 (dd, 1H, C*H*H=CH-), 5.25 (dd, 1H, CH*H*=CH-), 5.07 (s, 2H, -C*H*$_2$-); ^{13}C NMR ($CDCl_3$) δ(ppm): 137.67, 137.35, 136.00, 135.47, 129.74, 127.51, 126.74, 119.22, 114.63, 50.54.

5.2.7 Synthesis of 3-(1-(4-Vinylbenzyl)-1H-imidazol-3-ium-3-yl)propane-1-sulfonate ($VBIm^+$-SO_3^-)

VBIm (3.768 g, 20.48 mmol) was dissolved in dry acetonitrile (CH_3CN, 7 mL) in a 50 mL two-necked flask in an ice/water bath under N_2 atmosphere. 1,3-Propanesultone (2.517 g, 20.61 mmol) was dissolved in dry CH_3CN (3.0 mL), and the solution was added dropwise into the flask that contained the solution of VBIm in CH_3CN. After the reaction proceeded at room temperature for 20.3 h, the reaction mixture was filtered and the white solid were repeatedly washed with diethyl ether and CH_3CN. The final product was dried under high vacuum at 45 °C overnight, yielding a white powder (5.014 g, 79.9 %). ^{1}H NMR (D_2O) δ (ppm): 8.84 (s, 1H, -N-C*H*-N-), 7.51 (s, H, -N-C*H*=CH-N-), 7.50 (d, 2H, CH_2=CH-CC*H*-), 7.45 (s, H, -N-CH=C*H*-N-), 7.35 (d, 2H, CH_2=CH-CCHC*H*-), 6.73 (dd, 1H, CH_2=C*H*-), 5.83 (d, 1H, CH*H*=CH-), 5.32 (d, 2H, -C*H*$_2$-), 5.32 (d, 1H, C*H*H=CH-), 4.31 (t, 2H, -N-C*H*$_2$-CH_2-), 2.88 (t, 2H, -C*H*$_2$-SO_3^-), 2.28

(p, 2H, -CH_2-C*H_2*-CH_2-); ^{13}C NMR (D_2O, one drop of *d*-methanol was added as internal standard at 49.3 ppm) δ(ppm): 139.60, 137.09, 136.85, 134.19, 130.18, 128.18, 123.86, 116.64, 53.89, 49.16, 48.43, 26.32. Mass spectrum: $[M+H]^+$ at *m/z* 307.112.

5.2.8 Surface-Initiated ATRP of $VBIm^+$-SO_3^- from IP-I

IP-I (730 mg) was added into a 25 mL two-necked flask and dried under high vacuum at 40 °C overnight. The initiator particles were then dispersed in trifluoroethanol (11.642 g) by ultrasonication to form a stable dispersion. CuBr (6.3 mg, 0.044 mmol), $VBIm^+$-SO_3^- (4.089 g, 13.32 mmol), *N*,*N*,*N*′,*N*′,*N*″-pentamethyldiethylenetriamine (7.9 mg, 0.045 mmol), and ethyl 2-bromoisobutyrate (EBiB, 7.8 mg, 0.040 mmol) were added into a 50 mL two-necked flask and stirred under a N_2 atmosphere. The initiator particle dispersion was then transferred into the 50 mL flask using a syringe, a sample was taken for ^{1}H NMR analysis (t = 0 min) and the mixture was degassed immediately by three freeze−pump−thaw cycles. The flask was then placed into a 70 ℃ oil bath, and the polymerization was monitored by ^{1}H NMR spectroscopy. After 38 h, the flask was removed from the oil bath and opened to air. A sample was taken for ^{1}H NMR spectroscopy analysis to determine the monomer conversion for the calculation of the degree of polymerization (DP) of the polymer. The monomer conversion was determined from ^{1}H NMR spectra of the t = 0 min sample and the final sample by using the integrals of the peaks at 5.83 ppm, which were from C*H_2*=CH-, in the two samples; the trifluoroethanol peak located at 4.15 ppm was employed as internal standard. The particles were isolated by centrifugation, and the supernatant that contained the free polymer formed from the free initiator was rotavapped to remove trifluoroethanol. The supernatant that contained the free polymer formed from the free initiator in the reaction mixture was dialyzed against pure water for 3 days. The polymer brush-grafted particles were re-dispersed in trifluoroethanol and separated by centrifugation again. This

washing process was repeated with trifluoroethanol four times, followed by drying of the hairy particles with a stream of air flow. The DP of the polymer, P($VBIm^+$-SO_3^-), was 141, which was determined from the monomer-to-initiator ratio and the monomer conversion.

5.2.9 Synthesis of Bare Silica Particles (SiP-II)

Ammonium hydroxide (25% in water, 19.901 g) and tetraethyl orthosilicate (TEOS, 10.512 g) were each mixed with 10 mL of ethanol. The two solutions were then added into a 500 mL one-necked flask that contained 280 mL of ethanol under the stirring condition. The concentrations of NH_3, TEOS, and water in the solution were 0.61 M, 0.22 M, 3.56 M, respectively. The mixture was stirred vigorously at room temperature overnight. The silica particles were isolated by centrifugation (Eppendorf 5804 centrifuge, 8000 rpm), redispersed in ethanol, and centrifugated again. This washing process was repeated with ethanol additional two times, water two times, and ethanol again. The particles were then dried with a stream of air flow (yield: 3.20 g). The average diameter of silica particles, measured by TEM, was 175 nm. This batch of bare silica particles (SiP-II) was used for the preparation of 4-(chloromethyl)phenethyl)triethoxysilane functionalized silica particles (IP-II).

5.2.10 Synthesis of 4-(Chloromethyl)phenethyl)triethoxysilane-Functionalized Silica Particles (IP-II)

The ATRP initiator-functionalized silica particles (IP-II) were prepared by the immobilization of 4-(chloromethyl)phenethyl)triethoxysilane on the surface of bare silica particles (SiP-II) via an ammonia-catalyzed hydrolysis and condensation process. 4-Vinylbenzyl chloride (812 mg, 5.32 mmol) was weighed into a 25 mL two-necked flask, followed by the injection of triethoxysilane (3.0 mL, 27.5 mmol) and the Pt complex in xylene (75 μL). The mixture was stirred at 45 °C under the nitrogen atmosphere, and the hydrosilylation reaction was

monitored by ^{1}H NMR spectroscopy analysis. Once the reaction was complete, excess triethoxysilane was removed under high vacuum at 45 °C. The product, 4-(chloromethyl)phenethyl)triethoxysilane, was purified by column chromatography using dichloromethane as solvent (yield: 0.57 g, 66.0 %). ^{1}H NMR ($CDCl_3$) δ (ppm): 7.28 (d, 2H, $ClCH_2CCH$-), 7.19 (d, 2H, $ClCH_2CCHCH$-), 4.55 (s, 2H, -CH_2Cl), 3.81 (q, 6H, - OCH_2CH_3), 2.73 – 2.70 (m, 2H, -$SiCH_2CH_2$-), 1.21 (t, 9H, -OCH_2CH_3), 0.98 – 0.94 (m, 2H, -Si-CH_2CH_2-); ^{13}C NMR ($CDCl_3$) δ(ppm): 145.06, 134.81, 128.62, 128.19, 58.42, 46.27, 28.64, 18.30, 12.44.

Bare silica particles (SiP-II, 512 mg) were dispersed in a mixed solvent of ethanol (35 mL) and THF (35 mL) by ultrasonication to form a homogenous, stable dispersion. A solution of ammonium hydroxide (25% in water, 5.012 g) in a mixture of ethanol (10 mL) and THF (10 mL) was added dropwise into the particle dispersion. After the reaction mixture was stirred at 40 °C for 2 h, a solution of freshly synthesized 4-(chloromethyl)phenethyl)triethoxysilane (350 mg) in dry THF (5 mL) was added dropwise into the dispersion via a syringe. The mixture was then stirred at 40 °C for 18 h. The particles were separated by centrifugation and re-dispersed in THF. This process was repeated for a total of five times. The obtained 4-(chloromethyl)phenethyl)triethoxysilane-functionalized silica particles (IP-II) were dried with a stream of N_2 flow.

5.2.11 Synthesis of Poly(4-vinylbenzenesulfonic acid) from IP-II

IP-II (422 mg) was dispersed in a mixture of methanol (9.992 g) and water (35.003 g) in a 100 mL three-necked flask by ultrasonication to form a dispersion. CuCl (16.8 mg, 0.170 mmol), sodium 4-vinylbenzenesulfonate (10.413 g, 50.5 mmol), and benzyl chloride (20.7 mg, 0.164 mmol) were then added into the flask and stirred under N_2 atmosphere. After the mixture was degassed by three freeze−pump−thaw cycles, *N*,*N*,*N*′,*N*′,*N*″-pentamethyldiethylenetriamine (29.8

mg, 0.170 mmol) was injected into the solution using a degassed microsyringe. The flask was then placed into a 75 ℃ oil bath, and the polymerization was monitored by ^{1}H NMR spectroscopy analysis. After the monomer conversion reached 100 % (at ~ 5.7 h), the flask was removed from the oil bath and opened to air. Water (~10 mL) was added into the flask to dilute the mixture. The particles were isolated by centrifugation, redispersed in an aqueous HCl solution with pH of ~1, and centrifugated again. This washing process was repeated with acidic water additional five times, followed by drying of the hairy particles under high vacuum at 50 °C overnight for TGA analysis. The free polymer formed from the free initiator, benzyl chloride, was purified by dialysis against an aqueous HCl solution (pH = ~ 1) for 3 days using a regenerated cellulose tubular dialysis membrane with a nominal MWCO of 3500. The HCl aqueous solution with pH of ~ 1 was changed every 2 h in the first two days and then twice in the third day. The water was then rotavapored at 80 °C, and the obtained free polymer was dried at 50 °C under high vacuum overnight. The degree of polymerization (DP) of the free polymer was 309, calculated by using the monomer conversion and the monomer-to-initiator ratio.

5.2.12. Acidic Hairy Particle-Catalyzed Dehydration of Fructose to HMF in Water

A typical dehydration reaction of fructose in water catalyzed by acidic hairy particles is presented in the following. P(VBIm$^+$-SO_3^-) brush-grafted silica particles (750 mg), fructose (1.151 g), triflic acid (0.425 g of a 30.02 wt % aqueous solution, 0.128 g of triflic acid), and deionized water (17.501 g) were added into a 50 mL two-necked flask. The molar ratio of triflic acid and the monomer units in hairy particles was 1 : 1. The reaction mixture was stirred with a magnetic stirrer bar in a 120 ℃ oil bath under N_2 with a slightly positive pressure. Samples (~ 3.5 g each) were taken from the mixture using a degassed syringe at reaction times of 3 h, 6 h, 12 h and 24 h. Each sample was centrifugated to separate the hairy silica particles. The supernatant

liquid was passed through a glass pipet filled with basic aluminum oxide (~ 1 cm high). A pressure, from compressed house air, was applied to force the liquid out of the Al_2O_3 column as completely as possible. The sample was then diluted with HPLC grade water five times and analyzed by HPLC based on the standard curves obtained with pure fructose and HMF (external standard method).

The dehydration reaction of fructose in water catalyzed by free polymer catalyst P($VBIm^+$-SO_3^-)/triflic acid was carried out in a similar fashion as described below. Fructose (1.150 g), P($VBIm^+$-SO_3^-) (260 mg), triflic acid (0.424 g of a 30.02 % aqueous solution), and deionized water (17.492 g) were added into a 50 mL round-bottom flask equipped with a refluxing condenser. The reaction mixture was stirred with a magnetic stirrer bar in a 120 ℃ oil bath under N_2 with a slightly positive pressure than air. Samples were withdrawn from the mixture using a degassed syringe after the reaction proceeded for 3 h, 6 h, 12 h and 24 h. Each sample was also passed through a basic aluminum oxide column, followed by HPLC analysis to determine the HMF yield and fructose conversion.

5.2.13. Determination of HMF Yield and Fructose Conversion

HPLC was used to determine HMF yields and fructose conversions. To make a fructose calibration curve, a series of fructose aqueous solutions with concentrations of 1.000 mg/g, 2.998 mg/g, 4.999 mg/g, 7.001 mg/g, 9.997 mg/g, and 13.001 mg/g were prepared using HPLC grade water and injected into the HPLC system. The peak area of fructose in each sample was integrated, and a plot of area (Y) versus fructose concentration (X) was obtained and used as the calibration curve (Y=181120X-17536**)**. In a similar fashion, a series of HMF aqueous solutions with concentrations of 0.999 mg/g, 2.002 mg/g, 3.977 mg/g, 5.982 mg/g, 7.977 mg/g, and 10.007 mg/g were used to construct the HMF calibration curve (Y=249495X-27451). Note that the

elution time for fructose at a flow rate of 0.8 mL/min using HPLC grade water as eluent was ~ 18 min and the elution time for HMF was ~ 47 min.

A typical sample preparation procedure for HPLC analysis to determine the HMF yield and the fructose conversion is as follows. A sample was taken at a pre-determined time from a fructose dehydration reaction mixture using a pre-weighed degassed syringe. By weighing the syringe plus the sample, the exact amount of the sample withdrawn from the reaction mixture was determined. The sample was centrifuged (VWR Micro 1207 Microcentrifuge, 10000 rpm, 15 min) to isolate the hairy particles, if particles were used as catalyst. The supernatant was passed through a short glass pipet filled with basic aluminum oxide (~ 1 cm in height). A pressure, from compressed house air, was applied to force the liquid out of the Al_2O_3 column as completely as possible. A portion of the filtered supernatant (~ 0.7 g) was diluted with HPLC grade water five times in a small glass vial, and then analyzed by HPLC at room temperature. By integrating the peak areas of fructose and HMF in the HPLC spectrum, the concentrations of fructose and HMF in the diluted sample were determined using the fructose and HMF calibration curves. Thus, the concentrations of fructose and HMF before dilution were obtained. With the mass of the reaction mixture, the yield of HMF was calculated. The fructose conversion was obtained by comparing the calculated initial concentration and the concentration of fructose in the withdrawn sample. For free polymer P($VBIm^+$-SO_3^-)/triflic acid-catalyzed dehydration of fructose, the samples were passed through a basic aluminum oxide column to remove the catalyst before HPLC analysis.

5.3. Results and Discussion

5.3.1 Synthesis and Characterization of Poly(VBIm$^+$-SO$_3^-$) Brush-Grafted Silica Particles

Poly(VBIm$^+$-SO$_3^-$) (P(VBIm$^+$-SO$_3^-$)) brushes were grown from 2-bromo-2-methyl-*N*-(3-(triethoxysilyl)propyl)propanamide-functionalized silica particles by surface-initiated ATRP of VBIm$^+$-SO$_3^-$. The monomer, VBIm$^+$-SO$_3^-$, was prepared through a two-step synthetic process as illustrated in Scheme 5.2, and its molecular structure was confirmed by ^{1}H and ^{13}C NMR spectroscopy and mass spectroscopy. Bare silica particles with an average size of 189 nm, determined by dynamic light scattering in ethanol at 25 °C, were made by the Stöber process. The bare particles were surface functionalized with 2-bromo-2-methyl-*N*-(3-(triethoxysilyl)propyl)propanamide, a triethoxysilane-terminated ATRP initiator, via an ammonia-catalyzed hydrolysis/condensation process, yielding ATRP-initiated functionalized silica particles designated as IP-I (Scheme 5.3). The surface-initiated ATRP of VBIm$^+$-SO$_3^-$ from IP-I was carried out in trifluoroethanol at 70 °C in the presence of a free initiator, ethyl 2-bromoisobutyrate (EBiB). The addition of EBiB facilitated the control of surface-initiated polymerization and also allowed the polymerization to be precisely monitored via ^{1}H NMR. The polymerization was stopped after 38 h. The final monomer conversion was 42.3 %, obtained by comparing the integrals of the peaks at 5.83 ppm, which were from C*H*$_2$=CH-, in the ^{1}H NMR spectra of the t = 0 min sample and the final sample with the trifluoroethanol peak at 4.15 ppm as internal standard. Assuming that the initiator efficiency was 100 %, the DP of P(VBIm$^+$-SO$_3^-$) was 141, which was calculated from the monomer conversion and the monomer-to-initiator ratio.

The P(VBIm$^+$-SO$_3^-$) brush-grafted silica particles were isolated by centrifugation and repeatedly washed with trifluoroethanol. The free polymer in the supernatant was purified by dialysis against deionized water. It should be noted here that free polymer P(VBIm$^+$-SO$_3^-$) was

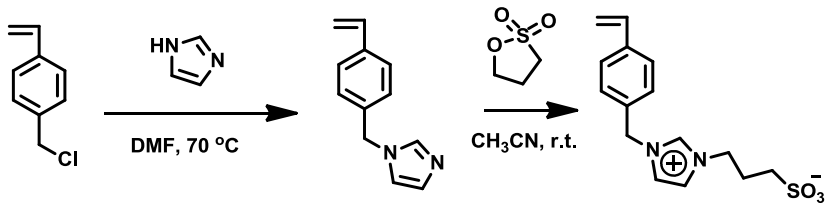

Scheme 5.2 Synthesis of Monomer $VBIm^{+}$-SO_3^{-}

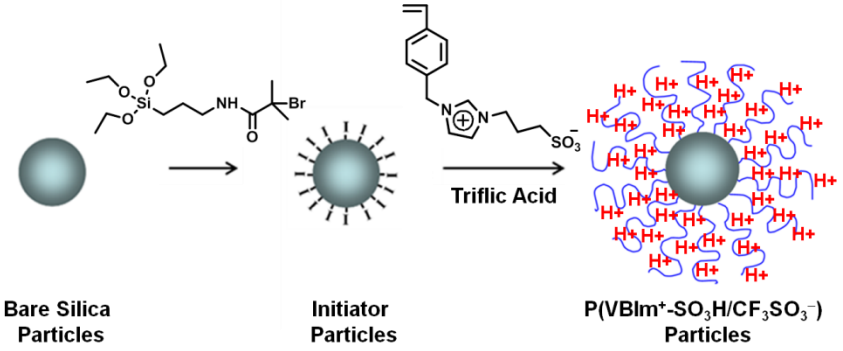

Scheme 5.3 Synthesis of P(VBIm^{+}-SO_3H/$CF_3SO_3^{-}$) brush-grafted silica particles particles from 2-bromo-2-methyl-*N*-(3-(triethoxysilyl)propyl)propanamide-functionalized silica particles by surface-initiated atom transfer radical polymerization and subsequent acidification with trilific acid

insoluble in pure water and precipitated in the dialysis tube during dialysis. The final purified free polymer was dried under high vacuum and characterized with ^{1}H NMR (Figure 5.1). The P(VBIm$^+$-SO$_3^-$) brush-grafted silica particles were dried under high vacuum for over 5 h at 45 °C and the polymer content in hairy particles was determined by TGA (Figure 5.2). It has been commonly observed that the molecular weight and molecular weight distribution of polymer brushes grown on particles by surface-initiated "living"/controlled radical polymerization are essentially identical to those of the free polymer formed from the free initiator. By using the size of bare silica particles (189 nm), TGA data of both IP-I and P(VBIm$^+$-SO$_3^-$) brush-grafted silica particles, DP of P(VBIm$^+$-SO$_3^-$), and assuming that the density of silica particles was identical to that of bulk SiO_2 (2.07 g/cm^3), the grafting density of P(VBIm$^+$-SO$_3^-$) brushes was calculated to be 0.53 chains/nm^2.

5.3.2. Synthesis of HMF from Dehydration of Fructose with Poly(VBIm$^+$-SO$_3$H/CF$_3$SO$_3^-$) Brush-Grafted Silica Particles as Catalyst

The catalytic activity of poly(3-(3-sulfopropyl)-1-(4-vinylbenzyl)-1H-imidazol-3-ium trifluoromethanesulfonate) (P(VBIm$^+$-SO$_3$H/CF$_3$SO$_3^-$)) brush-grafted silica particles for the dehydration of fructose into HMF was examined in pure water at 120 °C. P(VBIm$^+$-SO$_3^-$) is insoluble in pure water; upon addition of one equivalent of triflic acid with respect to the monomer units of P(VBIm$^+$-SO$_3^-$), P(VBIm$^+$-SO$_3$H/CF$_3$SO$_3^-$) was formed and became soluble in water, making it possible to fully disperse P(VBIm$^+$-SO$_3$H/CF$_3$SO$_3^-$) brush-grafted silica particles in pure water for the fructose dehydration reaction. The reaction condition used for the dehydration of fructose with P(VBIm$^+$-SO$_3$H/CF$_3$SO$_3^-$) brush-grafted particles as catalyst was as follows. Fructose (1.151 g), P(VBIm$^+$-SO$_3^-$) brush-grafted silica particles (0.75 g), triflic acid

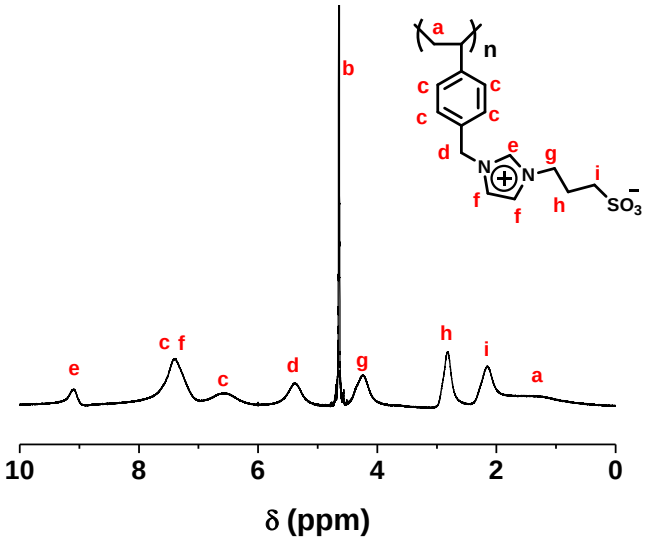

Figure 5.1 ^{1}H NMR spectrum of free polymer P(VBIm^{+}-SO_3^{-}) formed from the free initiator in solution in the synthesis of P(VBIm^{+}-SO_3^{-}) brush-grafted silica particles. D_2O with 25 wt % of NaCl was used as solvent.

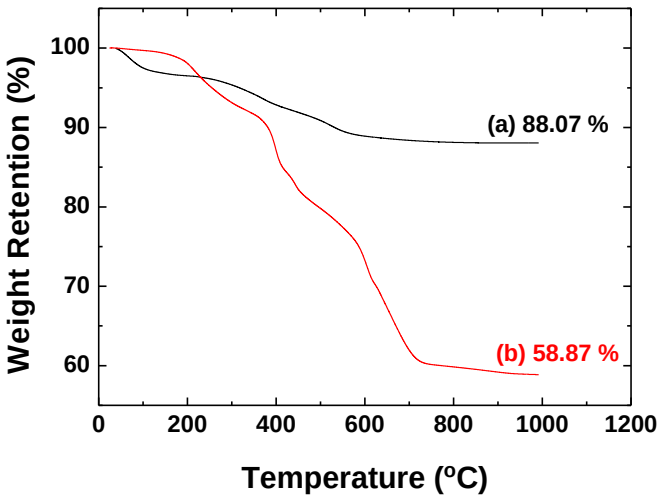

Figure 5.2 Thermogravimetric analysis (TGA) of (a) initiator particles (IP-I) and (b) P(VBIm^{+}-SO_3^{-}) brush-grafted silica particles. TGA was performed in air at a heating rate of 20 °C/min from room temperature to 1000 °C.

(0.128 g), and HPLC-grade water (17.501 g) were added into a flask. After the particles were dispersed in water by ultrasonication, the flask was placed in a 120 ℃ oil bath to start the reaction under N_2 with a slightly positive pressure. All joints were sealed tightly with Teflon tape to prevent water loss. Samples were taken from the reaction mixture at different reaction times (3, 6, 12, and 24 h) for determining HMF yields and fructose conversions by HPLC analysis again the calibration curves to examine the effects of reaction time on HMF yield and fructose conversion. For comparison, the homopolymer analogue, P($VBIm^+$-SO_3H/$CF_3SO_3^-$) from the free polymer formed in the synthesis of hairy particles, was also tested for the dehydration of fructose to HMF in water under the same reaction conditions. The same amount of P($VBIm^+$-SO_3^-) (260 mg) was used for the reaction based on the polymer content of the P($VBIm^+$-SO_3^-) brush-grafted silica particles (34.7 wt%). The results are shown in Figure 5.3.

Clearly, the HMF yield (Figure 5.3A) and the fructose conversion (Figure 5.3B) increased with increasing the reaction time from 3 to 6, to 12, and 24 h for both polymer brush and free polymer catalysts. At 3 h, the HMF yield was only 5.7 % for the hairy particles and 4.7 % for the free polymer catalyst. With increasing the reaction time, the HMF yield for the particle catalyst increased to 8.7 % at 6 h, 17.1 % at 12 h, and eventually 19.9 % at 24 h. For the free polymer catalyst, the HMF yields were 6.8 % at 6 h, 11.9 % at 12 h, and 14.2 % at 24 h, all of which were lower than those with the hairy particles as catalyst under the same conditions. The difference in the HMF yield between the brush catalyst and the free polymer catalyst became larger with the increase of reaction time, with the largest difference, 5.7 %, observed at 24 h. It should also be noted here that the increase in the HMF yield slowed down after 12 h for both catalysts, suggesting that side reactions might have occurred at a longer reaction time. The effect of reaction time on fructose conversion was presented in Figure 5.3B. The fructose conversion with

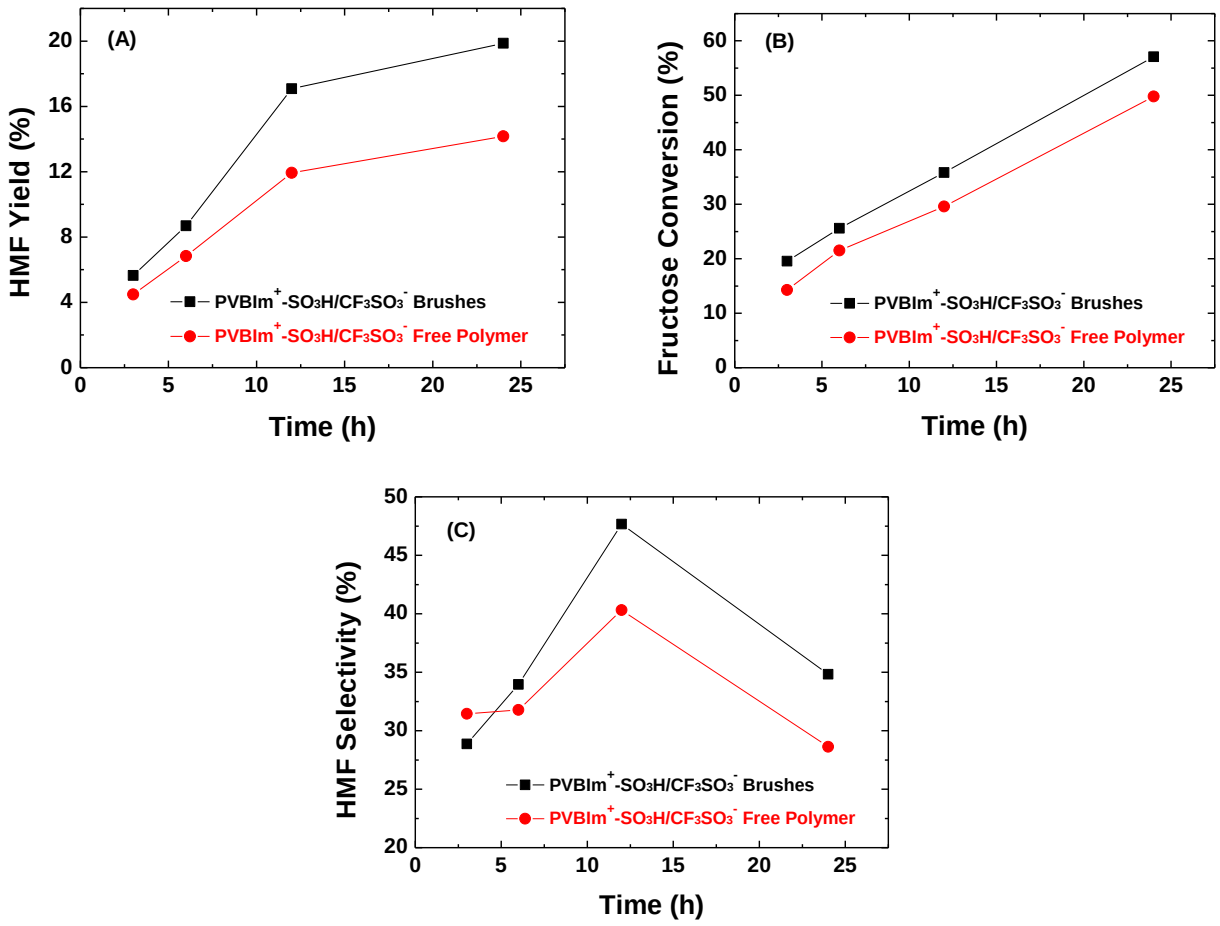

Figure 5.3 Effect of reaction time on (A) HMF yield, (B) fructose conversion, and (C) HMF selectivity in the dehyration of fructose to HMF catalyzed by P(VBIm$^+$-$SO_3H/CF_3SO_3^-$) brush-grafted silica particles (black square) and free polymer P(VBIm$^+$-$SO_3H/CF_3SO_3^-$) acid catalyst (red dot) at 120 ℃ in water.

hairy particles as catalyst was always slightly higher than that for the free polymer catalyst at the same reaction time. For example, the fructose conversion at 24 h was 57.1 % for the particle catalyst and 49.8% for the free polymer. Taking the fructose conversion into consideration, the HMF selectivity (yield/fructose × 100 %) at each reaction time was calculated, and the results are presented in Figure 5.3C. Except the first point, the HMF selectivity was higher for the brush catalyst. At 12 h, the HMF selectivity was 47.7 % for the particle catalyst and 40.3 % for the free polymer catalyst. This is likely caused by the unique microenvironment created by polymer brushes, which may favor the dehydration of fructose to HMF. More experiments are needed to elucidate the effect of polymer brushes on the catalytic activity of the supported catalysts.

5.3.3. Synthesis of Poly(Vinylbenzenesulfonic acid) Brush-Grafted Silica Particles

Poly(4-vinylbenzenesulfonic acid) (PVBSA) brush-grafted silica particles were prepared by surface-initiated of sodium 4-vinylbenzenesulfonate from 4-(chloromethyl)phenethyl)triethoxysilane-functionalized silica particles (IP-II) and subsequent acidification as illustrated in Scheme 5.4. The triethoxysilane-terminated ATRP initiator used in the synthesis of IP-II, 4-(chloromethyl)phenethyl)triethoxysilane, was prepared via hydrosilylation reaction between 4-vinylbenzyl chloride and triethoxysilane catalyzed by a platinum complex at 45 °C. The final product was purified by column chromatography using methylene chloride as solvent. The immobilization reaction was conducted in a mixture of THF/ethanol with a volume ratio of 1 : 1 at 40 °C with ammonia as catalyst. The use of a benzyl chloride initiator-terminated triethoxysilane yielded a linkage that contained only carbon-carbon bonds between the surface of silica particles and the polymer brushes, which would make the grafted polymer chains more stable so that the catalyst can be recycled multiple times without

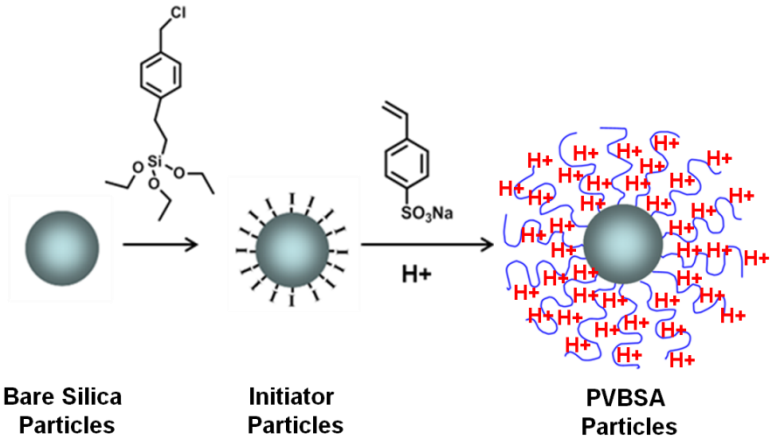

Scheme 5.4 Synthesis of poly(4-vinylbenzenesulfonic acid) (PVBSA) brush-grafted silica particles from 4-(chloromethyl)phenethyl)triethoxysilane-functionalized silica particles by surface initiated atom transfer radical polymerization and subsequent acidification.

significant polymer degradation. The initiator particles, IP-II, were repeatedly washed prior to the use for the synthesis of polymer brushes. The surface-initiated ATRP of sodium 4-vinylbenzenesulfonate was carried out in a mixed solvent of methanol and water with a weight ratio of 1:3.5 at 75 °C using CuCl/*N*,*N*,*N*′,*N*′,*N*′′-pentamethyldiethylenetriamine as catalyst in the presence of a free initiator, benzyl chloride. The polymerization was monitored by ^{1}H NMR spectroscopy analysis and was stopped after the monomer conversion reached 100%. The hairy particles were isolated and redispersed in acidic water with pH of ~ 1 and centrifugated again. This washing process was repeated additional five times, followed by drying of the hairy particles under high vacuum at 50 °C overnight. The degree of polymerization of the free polymer formed from the free initiator was 309, calculated from the monomer conversion and the monomer-to-initiator ratio.

TGA revealed that the weight retentions at 800 °C of initiator particles and hairy particles were significantly different (Figure 5.4). If the weight retention difference at 100 °C between initiator particles and hairy particles is taken into consideration, the polymer content of PVBSA brush-grafted silica particles was 36.6 wt %. Using the TGA data, degree of polymerization of the free polymer, and the size of bare silica particles, we calculated the grafting density of PVBSA brushes on silica particles; it was 0.40 chains/nm^2.

PVBSA hairy particles were also used as catalyst for dehydration of fructose to HMF. The particle catalyst exhibited a higher catalytic activity than the corresponding free polymer catalyst, with the HMF yield of up to 31 %, in contrast to 26 % from the free PVBSA catalyst.[26]

5.4. Conclusions

In summary, two types of acidic polymer brush-grafted silica particles, P($VBIm^+$-$SO_3H/CF_3SO_3^-$) brush- and PVBSA brush-grafted silica particles, were prepared by surface-initiated ATRP and subsequent acidification. The grafting density was 0.53 chains/nm^2 for P($VBIm^+$-$SO_3H/CF_3SO_3^-$) brush-grafted particles and 0.40 chains/nm^2 for PVBSA brush-grafted particles. These hairy particles were used as catalyst for dehydration of fructose in water to synthesize HMF. It was found that the HMF yields with acidic hairy particles were higher than those of the corresponding free acidic homopolymer catalysts under the same conditions, which is believed to result from the unique, favorable microenvironment created by polymer brushes for dehydration of fructose to HMF.

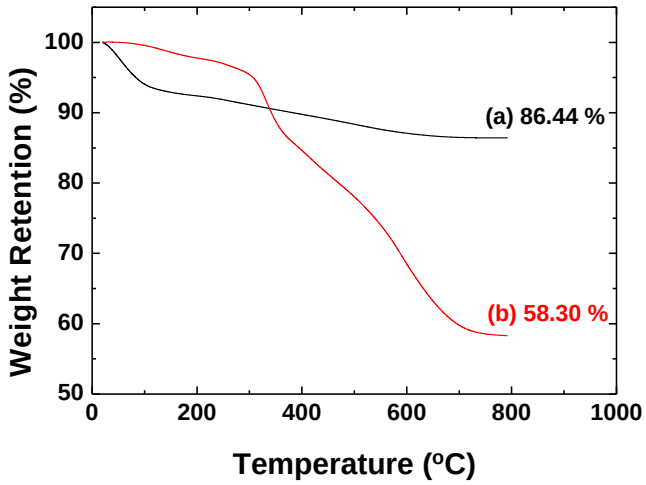

Figure 5.4 Thermogravimetric analysis (TGA) of (a) initiator particles (IP-II), (b) poly(vinylbenzenesulfonic acid) brush-grafted particles. TGA was performed in air at a heating rate of 20 °C/min from room temperature to 800 °C.

References

1. Huber, G. W.; Chheda, J. N.; Barrett, C. J.; Dumesic, J. A. *Science* **2005**, *308*, 1446-1450.
2. Kunkes, E. L.; Simonetti, D. A.; West, R. M.; Serrano-Ruiz, J. C.; Gärtner, C. A.; Dumesic, J. A. *Science* **2008**, *322*, 417-421.
3. van Putten, R.-J.; van der Waal, J. C.; de Jong, E.; Rasrendra, C. B.; Heeres, H. J.; de Vries, J. G. *Chem. Rev.* **2013**, *113*, 1499-1597.
4. Choudhary, V.; Mushrif, S. H.; Ho, C.; Anderko, A.; Nikolakis, V.; Marinkovic, N. S.; Frenkel, A. I.; Sandler, S. I.; Vlachos, D. G. *J. Am. Chem. Soc.* **2013**, *135*, 3997-4006.
5. Roman-Leshkov, Y.; Chheda, J. N.; Dumesic, J. A. *Science* **2006**, *312*, 1933-1937.
6. Ordomsky, V. V.; van der Schaaf, J.; Schouten, J. C.; Nijhuis, T. A. *ChemSusChem* **2012**, *5*, 1812-1819.
7. Zhao, H.; Holladay, J. E.; Brown, H.; Zhang, Z. C. *Science* **2007**, *316*, 1597-1600.
8. Hu, S.; Zhang, Z.; Song, J.; Zhou, Y.; Han, B. *Green Chem.* **2009**, *11*, 1746-1749.
9. Musau, R. M.; Munavu, R. M. *Biomass* **1987**, *13*, 67-74.
10. Asghari, F. S.; Yoshida, H. *Ind. Eng. Chem. Res.* **2006**, *45*, 2163-2173.
11. Carniti, P.; Gervasini, A.; Biella, S.; Auroux, A. *Catal. Today* **2006**, *118*, 373-378.
12. Qi, X. H.; Watanabe, M.; Aida, T. M.; Smith, R. L. *Catal. Commun.* **2008**, *9*, 2244-2249.
13. Daorattanachai, P.; Namuangruk, S.; Viriya-empikul, N.; Laosiripojana, N.; Faungnawakij, K. *J. Ind. Eng. Chem.* **2012**, *18*, 1893-1901.
14. Marzo, M.; Gervasini, A.; Carniti, P. *Catal. Today* **2012**, *192*, 89-95.
15. Nikolla, E.; Román-Leshkov, Y.; Moliner, M.; Davis, M. E. *ACS Catal.* **2011**, *1*, 408-410.
16. Nakajima, K.; Baba, Y.; Noma, R.; Kitano, M.; N. Kondo, J.; Hayashi, S.; Hara, M. *J. Am. Chem. Soc.* **2011**, *133*, 4224-4227.

17. Shi, C.; Zhao, Y.; Xin, J.; Wang, J.; Lu, X.; Zhang, X.; Zhang, S. *Chem Commun* **2012**, *48*, 4103-4105.

18. Moreau, C.; Durand, R.; Peyron, D.; Duhamet, J.; Rivalier, P. *Ind. Crop. Prod.* **1998**, *7*, 95-99.

19. Dias, A. S.; Pillinger, M.; Valente, A. A. *J. Catal.* **2005**, *229*, 414-423.

20. Yang, F. L.; Liu, Q. S.; Bai, X. F.; Du, Y. G. *Bioresour. Technol.* **2011**, *102*, 3424-3429.

21. Khemthong, P.; Daorattanachai, P.; Laosiripojana, N.; Faungnawakij, K. *Catal. Commun.* **2012**, *29*, 96-100.

22. Qi, X. H.; Watanabe, M.; Aida, T. M.; Smith, R. L. *Ind. Eng. Chem. Res.* **2008**, *47*, 9234-9239.

23. Zhao, B.; Jiang, X. M.; Li, D. J.; Jiang, X. G.; O'Lenick, T. G.; Li, B.; Li, C. Y. *J. Polym. Sci., Part A: Poly. Chem.* **2008**, *46*, 3438-3446.

24. Jiang, X.; Wang, B.; Li, C. Y.; Zhao, B., *J. Polym. Sci., Part A: Polym. Chem.* **2009**, *47*, 2853-2870.

25. Long, W.; Jones, C. W. *ACS Catal.* **2011**, *1*, 674-681.

26. Tian, C.; Bao, C.; Binder, A.; Zhu, Z.; Hu, B.; Guo, Y.; Zhao, B.; Dai, S. *Chem Commun* **2013**, *49*, 8668-8670.

27. Husseman, M.; Malmstrom, E. E.; McNamara, M.; Mate, M.; Mecerreyes, D.; Benoit, D. G.; Hedrick, J. L.; Mansky, P.; Huang, E.; Russell, T. P.; Hawker, C. J. *Macromolecules* **1999**, *32*, 1424-1431.

28. Zhao, B.; Brittain, W. J. *Prog. Polym. Sci.* **2000**, *25*, 677-710.

29. Li, D.; Jones, G. L.; Dunlap, J. R.; Hua, F.; Zhao, B. *Langmuir* **2006**, *22*, 3344-3351.

30. Zhao, B.; Zhu, L. *Macromolecules* **2009**, *42*, 9369-9383.

31. Barbey, R.; Lavanant, L.; Paripovic, D.; Schüwer, N.; Sugnaux, C.; Tugulu, S.; Klok, H.-A. *Chem. Rev.* **2009**, *109*, 5437-5527.

32. Sun, J.-T.; Hong, C.-Y.; Pan, C.-Y. *J. Phys. Chem. C* **2010**, *114*, 12481-12486.

33. Huang, X.; Hauptmann, N.; Appelhans, D.; Formanek, P.; Frank, S.; Kaskel, S.; Temme, A.; Voit, B. *Small* **2012**, *8*, 3579-3583.

Chapter 6. Conclusions and Future Work

Well-defined mixed poly(*tert*-butyl acrylate)/polystyrene (P*t*BA/PS) brushes grafted on 170 – 180 nm silica particles were synthesized via sequential surface-initiated atom transfer radical polymerization (ATRP) of *t*BA at 75 °C and nitroxide-mediated radical polymerization (NMRP) of styrene at 120 °C. Transmission electron microscopy (TEM) was used to investigate the nanostrucrures formed by self-assembly of mixed P*t*BA/PS brushes after the particles were cast from dispersion.

Chapters 2 and 3 present systematic studies on the effects of overall grafting density and average molecular weight (MW) of the grafted two homopolymers on microphase separation of mixed P*t*BA/PS brushes. The work was inspired by a theoretical prediction of Zhulina and Balazs that in a nonselective poor solvent, the periodicity of the nanopattern (*D*) formed by symmetric mixed homopolymer brushes scaled with the one-sixth power of the area per chain (s) and half-power of the degree of polymerization (DP) of block A (or block B).[1] To systematically investigate the effect of overall grafting density on phase morphology, a set of mixed P*t*BA/PS brush samples with varying overall grafting densities but comparable individual grafting densities were synthesized and characterized.[2] This was achieved by varying the weight ratio of Y-initiator to silica particles in the initiator immobilization step. The hairy particle samples were cast from chloroform, stained with RuO_4, and studied by TEM. It was discovered that the normalized ripple wavelength (*D*) scaled with $\sigma_{overall}^{-0.47}$ in the $\sigma_{overall}$ range of 1.06 to 0.54 chains/nm^2 and no microphase separation was observed in the sample with $\sigma_{overall}$ of 0.122 chain/nm^2.

The study of the effect of average MW on microphase separation of mixed P*t*BA/PS brushes is presented in Chapter 3.[3] A series of mixed P*t*BA/PS brush-grafted particle samples were made by using the established protocol from our lab, and the MWs of P*t*BA and PS in each sample

were controlled to be similar to each other. TEM samples were prepared by drop casting the dispersions of mixed P*t*BA/PS brush-grafted particles either in $CHCl_3$ or in water (stabilized by a surfactant). The average *D* increased with increasing the MW. For mixed P*t*BA/PS brush samples cast from chloroform, *D* scaled with $MW^{0.70}$ and for uniformly collapsed mixed brushes cast from water, *D* was proportional to $MW^{0.56}$ in the studied MW range. The quantitative relationship between *D* and $\sigma_{overall}$ in Chapter 2 and between *D* and MW in Chapter 3 were close to the theoretical results by Zhulina and Balazs. The difference probably came from the fact that perfect Y-shaped brushes were investigated in the theoretical work while our brushes were not.[1]

Chapter 4 describes the use of surface-initiated ring-opening polymerization and NMRP to synthesize mixed homopolymer brushes grafted on silica particles composed of a degradable polymer, poly(ε-caprolactone) (PCL), and a vinyl polymer (PS). Silica particles with an average size of 157 nm were surface-functionalized with a Y-initiator bearing a hydroxyl group and an NMRP alkoxyamine. The surface-initiated ring-opening polymerization (ROP) of ε-caprolactone was carred out at 75 °C after the system was thoroughly dried, while NMRP of styrene was performed at 120 °C.[4] A corresponding free initiator was added in each polymerization. The overall grafting density of mixed PCL/PS brushes can be tuned by varying the mass ratio of the Y-initiator-terminated triethoxysilane to bare silica particles in the initiator immobilization step.

Chapter 5 presents the synthesis of two polymer brush-supported acid catalysts, poly(3-(3-sulfopropyl)-1-(4-vinylbenzyl)-1H-imidazol-3-ium trifluoromethanesulfonate) brush- and poly(4-vinylbenzenesulfonic acid) brush-grafted silica particles, and the use of these acidic brush catalysts for the synthesis of 5-hydroxymethylfurfural, a versatile platform chemical derived from biomass.[5] Both brush catalysts efficiently catalyzed the dehydration of fructose in water and exhibited a higher catalytic activity than their corresponding free acid polymer catalysts.

A possible research project along this line of research is to systematically investigate the effect of substrate curvature on phase morphology of mixed homopolymer brushes. Horton et al. previously reported the synthesis of mixed P*t*BA/PS brushes with comparable MWs for the two polymers on 67 nm silica particles, and observed distinct truncated wedge-shaped nanostructures formed from lateral microphase separation.[6] It was believed that these interesting nanostructures resulted from the higher substrate curvature of 67 nm silica particles compared with 150-180 nm silica particles. However, more study is needed to elucidate the effect of substrate curvature on morphology of mixed homopolymer brushes, though it is experimentally challenging to synthesize well-defined mixed brushes on nanoparticles. One possible way is to carry out "one-pot" polymerizations for Y-initiator-functionalized silica particles with various sizes. The results will enhance our understanding of how mixed homopolymer brushes pack themselves on a curved substrate surface, which could guide us to design more advanced functional materials.

Reference

1. Zhulina, E.; Balazs, A. C. *Macromolecules* **1996**, *29*, 2667-2673.
2. Bao, C.; Tang, S.; Horton, J. M.; Jiang, X.; Tang, P.; Qiu, F.; Zhu, L.; Zhao, B. *Macromolecules* **2012**, *45*, 8027-8036.
3. Bao, C.; Tang, S.; Wright, R. A. E.; Tang, P.; Qiu, F.; Zhu, L.; Zhao, B. *Macromolecules* **2014**, *47*, 6824-6835.
4. Li, W. [†]; Bao, C. [†]; Wright, R. A. E.; Zhao, B. *RSC Adv.* **2014**, *4*, 18772-18781. [†] Contributed equally to the work.
5. Note that the poly(4-vinylbenzenesulfonic acid) brush catalyst for the dehydration of fructose in water has been reported in a paper published in *Chem. Commun.* (Tian, C.; Bao, C.; Binder, A.; Zhu, Z.; Hu, B.; Guo, Y.; Zhao, B.; Dai, S. *Chem Commun* **2013**, *49*, 8668-8670.)
6. Horton, J. M.; Tang, S.; Bao, C.; Tang, P.; Qiu, F.; Zhu, L.; Zhao, B. *ACS Macro Lett* **2012**, *1*, 1061-1065.

Vita

Chunhui Bao was born in Anhui, China. He attended the University of Science and Technology of China from 2006 to 2010, where he received his B.S. degree in Polymer Chemistry. After graduation, he enrolled as a graduate student in the Department of Chemistry at the University of Tennessee, Knoxville. He joined Professor Bin Zhao's research group in December, 2010, and worked on polymer brush-grafted silica particles (hairy particles). Chunhui Bao received a Doctor of Philosophy Degree in Chemistry from the University of Tennessee, Knoxville in May, 2015.